

UNCLASSIFIED

AD NUMBER
AD912787
NEW LIMITATION CHANGE
TO Approved for public release, distribution unlimited
FROM Distribution authorized to U.S. Gov't. agencies only; Test and Evaluation; JUN 1973. Other requests shall be referred to Air Force Avionics Lab., Wright-Patterson AFB, OH 45433.
AUTHORITY
AFWAL ltr, 20 Sep 1984

THIS PAGE IS UNCLASSIFIED

AD 912782

AUTHORITY:

AFWAL

605 20 Sep 84



AFAL-TR-73-111

Best Available Copy

AD-912 787

THERMAL-OPTIC DISTORTION-FREE SOLID LASER TECHNOLOGY

W. F. HAGEN

*American Optical Corporation
Southbridge, Mass. 01550*

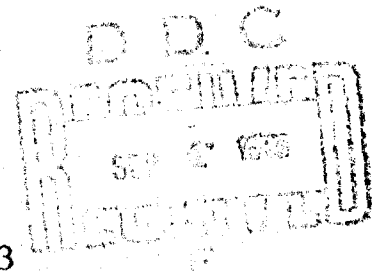
TECHNICAL REPORT AFAL-TR-73-111

July 1973



Distribution is limited to US Government agencies only by reason of inclusion of test and evaluation data; applied June 1973. Other requests for this document must be referred to AFAL / TEO, Wright-Patterson AFB, Ohio 45433.

Air Force Avionics Laboratory
Air Force Systems Command
Wright-Patterson Air Force Base, Ohio 45433



Best Available Copy

NOTICE

When Government drawings, specifications, or other data are used for any purpose other than in connection with a definitely related Government procurement operation, the United States Government thereby incurs no responsibility nor any obligation whatsoever; and the fact that the government may have formulated, furnished, or in any way supplied the said drawings, specifications, or other data, is not to be regarded by implication or otherwise as in any manner licensing the holder or any other person or corporation, or conveying any rights or permission to manufacture, use, or sell any patented invention that may in any way be related thereto.

Copies of this report should not be returned unless return is required by security considerations, contractual obligations, or notice on a specific document.

THERMAL-OPTIC DISTORTION-FREE
SOLID LASER TECHNOLOGY

W. F. Hagen

"Distribution is limited to U.S. Government agencies only by reason of inclusion of test and evaluation data; applied June 1973. Other requests for this document must be referred to AFAL/TEO, Wright Patterson AFB, Ohio 45433."

FOREWORD

This is the final report under Contract No. F33615-71-C-1137, as amended by Modification No. P00003, and titled THERMAL-OPTIC DISTORTION-FREE SOLID LASER TECHNOLOGY. The contract was documented under Project 5237, Task No. 10. The period of performance was 70 November 30 - 72 September 30. The contract scope called for further testing and analysis of two existing segmented laser devices in order to design, construct and evaluate an improved device. The objective of this program was to develop a technology which solves the thermal-optic distortion problem for a broad class of solid state laser types with little or no attendant sacrifice of other desirable qualities, such as efficiency. This present report also summarizes the important results of the two earlier contracts, F33615-68C-1570 and F33615-71-C-1047, as well as compares the final results to those obtained by competing geometries and laser materials.

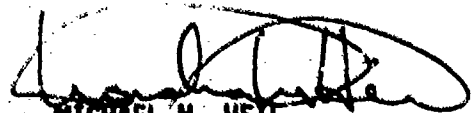
The work described was performed in the Laser Products Department within the Research Division under Dr. C. G. Young, General Manager, and Mr. W. F. Hagen, Manager of Systems Research. Mr. Hagen was Project Engineer on this series of contracts over all but the first few months of the first contract.

Major contributors to the present contract effort were Mr. J. Keefe and Mr. R. Kelley, who carried out most of the experiments.

The development and construction of the 40 kW power supply used in this program was solely for this work, and was entirely funded by American Optical Corporation. The following portions of this report were not funded by these contracts, but were included for completeness: Section II.1 and II.2 were funded by American Optical Corporation, and Sections IV.1, IV.2, and IV.3 were funded by U. S. Army Missile Command, Redstone Arsenal, Huntsville, Alabama under Contract No. DA-AH01-67-C-2343 titled RESEARCH IN GLASS LASER SYSTEM TECHNOLOGY.

This report was submitted by the author in January 1973.

This technical report has been reviewed and is approved for publication.


MICHAEL N. HEIL
E-0 Sources Group
Electro-Optics Device Branch
Electronic Technology Division

ABSTRACT

This report summarizes the design considerations and experimental results obtained from four different disc lasers. These devices were successfully operated as amplifiers and oscillators at high average powers. The results were compared with the performance of solid rods of both circular and rectangular cross section. The thermal lensing, which limits the performance of solid rods, especially under Q-switched operation, was essentially eliminated with the disc approach.

With the disc amplifier, transmission and gain values very close to those of solid rods have been measured. The single pass distortions were reduced by over one order of magnitude, which corresponds to an improvement in amplifier radiance of about two orders of magnitude for the disc laser in comparison to an equivalent solid rod. For Q-switched pulses, an average output power of 110 W was obtained with the disc amplifier operating at 5 pps.

With the disc laser operating as normal mode oscillator, an average output power of 420 W was measured with an improvement in average radiance by a factor of 27 over that of an equivalent solid rod at its fracture point.

The performance of disc lasers is limited by thermal-optic distortions in the coolant and by depolarization losses observed in Brewster disc lasers. The depolarization losses can be avoided with the normal incidence disc approach. To reduce the thermal-optic distortions in the coolant requires careful design of the flow channels and a coolant with a low thermal index coefficient.

Initial problems such as disc holding techniques, mechanical and chemical stability, uniform flashlamp pumping, coolant contamination, solarization protection and uniform flow distribution have been solved, providing reliable performance of the present devices over many hundred thousand shots.

CONTENTS

SECTION		PAGE
I	INTRODUCTION AND SUMMARY	1
II	AVERAGE RADIANCE CAPABILITY OF SOLID RODS	4
	1. CYLINDRICAL LASER RODS	4
	2. RECTANGULAR SLAB LASERS	13
III	GENERAL DESIGN CONSIDERATIONS	18
	1. FLOW DISTRIBUTION IN DISC LASERS	19
	2. THERMAL CHARACTERISTICS OF DISC LASERS	28
	3. THERMAL DISTORTIONS IN DISC LASER ELEMENTS	30
IV	INVESTIGATION OF COOLANTS AND MATERIALS	38
	1. SELECTION OF COOLANTS	38
	2. OPTICAL DISTORTIONS IN COOLANTS	40
	3. DETERMINATION OF dn/dT FOR COOLANTS	41
	4. D ₂ O COOLING UNIT	42
	5. MATERIAL TESTS	43
	6. SOLARIZATION PROTECTION FOR DISC LASERS	44
	7. AR COATINGS FOR NORMAL INCIDENCE DISC LASERS	45
V	DESCRIPTION OF THE DIFFERENT DISC LASERS	48
	1. THE FIRST BREWSTER DISC LASER (B-1)	48
	2. THE FIRST NORMAL INCIDENCE DISC LASER (N-1)	51
	3. THE B-2 AND B-3 BREWSTER DISC LASERS	53
	4. THE N-2 AND N-3 NORMAL INCIDENCE DISC LASERS	57

CONTENTS

SECTION		PAGE
VI	AMPLIFIER PERFORMANCE	59
	1. TRANSMISSION AND GAIN MEASUREMENTS	59
	2. SINGLE PASS BEAM DISTORTIONS	61
	3. ACTIVE TRANSMISSION LOSSES	76
	4. AVERAGE RADIANCE MEASUREMENTS	81
VII	OSCILLATOR PERFORMANCE	83
	1. SINGLE SHOT DATA	83
	2. REPETITIVELY PULSED OPERATION	87
VIII	CONCLUSIONS AND RECOMMENDATIONS	95
	REFERENCES	97

ILLUSTRATIONS

FIGURE		PAGE
1.	Flow distribution for series parallel flow arrangement	20
2.	Localized pressure losses in 10^{-3} psi for one N-2 disc laser section	25
3.	Flow characteristics of disc lasers for D_2O	27
4.	Computed principal stresses for 10 mm thick discs with uniform internal heating at 3.2 W/cm^3 and uniform cooling of all surfaces	34
5.	Change in optical pathlength for radial and tangential polarizations per cm length of laser glass for 10 and 3 mm thick discs with uniform internal heating at 3.2 W/cm^3 and water cooling	35
6.	Dependence of the thermal index coefficient on temperature for different coolants	41
7.	D_2O cooling system	43
8.	Brewster-angled disc laser B-1	49
9.	Conditions for vignette compensation	49
10.	Clad discs for the B-1	49
11.	Normal incidence disc laser N-1	51
12.	Clad disc for N-1	52
13.	Cross-sectional view of segmented Nd glass laser	54
14.	Small signal gain of disc lasers and solid rod	60
15.	Passive single pass distortions of the disc lasers for different diameters of a 6328A probe beam	62

ILLUSTRATIONS

FIGURE		PAGE
16.	Behavior of a 6328A probe beam transmitted through the B-2	63
17.	Behavior of a 6328A probe beam transmitted through the N-2 and B-3	64
18.	Correlation of angular transmission data and photographs of probe beam	66
19.	Beam distortions in the B-2 before, during, and just after the pump pulse for various conditions	68
20.	Photographs of the probe beam before and just after the pump pulse at various distances from the output window of the B-2	69
21.	Photographs of the probe beam for various conditions of the N-2	71
22.	Thermal lensing measured with a 6328A probe beam	72
23.	Behavior of the signal from a probe beam transmitted through the B-2 and focused on an aperture at 8 kJ input and 1 GPM flow rate	73
24.	Increase in single pass beamspread with average input power at 6328A wavelength	74
25.	Dependence of the single pass beamspread of the N-2 on coolant flow rate	76
26.	Change in transmission through the B-1 with parallel and crossed polarizers for 6328A probe beam due to depolarization at 5 and 10 kW average input power	79
27.	Change in transmission of the disc lasers during repetitively pulsed operation	80
28.	Single shot oscillator performance under normal mode operation	83

ILLUSTRATIONS

FIGURE		PAGE
29.	Oscillator performance of the B-2 at 1 pps and 8 kJ input per pulse	88
30.	Oscillator performance of the 3% Nd-doped 18 mm OD solid rod at 1.2 pps and 7 kJ input per pulse	88
31.	Oscillator performance of the N-3 at 3.5 pps and 10 kJ per pulse	89
32.	Repetitively pulsed oscillator performance of the different disc lasers and the solid rod	91
33.	Solid angle beamsread of the disc lasers and the solid rod during repetively pulsed operation	91
34.	Average output radiance for the disc lasers and the solid rod under normal mode operation	92

TABLES

I.	Disc Laser Performance	3
II.	Properties of Laser Materials.	11
III.	Spectral Absorption Characteristics of Coolants	39
IV.	Transmission of Disc Lasers	59

SECTION I

INTRODUCTION AND SUMMARY

One limit to the average power capability of a solid state laser is the cooling of the laser material. The temperature gradients in a solid laser rod generally cause radial index gradients which give rise to optical distortions and finally cause fracture of the laser material due to thermally-induced stress.

One way to increase the cooling surface is to segment the laser rod in a direction perpendicular to the optical axis.* This also has the advantage of having predominantly axial temperature and index-gradients with minimal effect on the beam. The problems most critical are the coolant and the mechanical holding of the discs. A suitable fluid for cooling should be highly transparent and unaffected by laser radiation and pump light. In addition, a low thermal index coefficient of the coolant is essential to avoid thermal-optic distortions in the laser. An ideal coolant should also match the index of the laser material to avoid unreasonably high reflection losses, or the use of coatings would have to be considered.

Another approach is to segment the laser rod at Brewster's angle to avoid the reflection losses, but stress-induced depolarization will then limit the maximum output power.

The objective of this research effort was to investigate these two approaches and determine their characteristics as amplifiers and oscillators. During this program, two different Brewster disc lasers (B-1 and B-2) and an improved device (B-3) were evaluated as well as two different normal incidence disc lasers (N-1 and N-2) and an improved device (N-3).** All these devices were cooled with heavy water, since all other coolants appeared to have excessive thermal-optic distortion, and in many cases high transmission losses as well as poor resistance to deterioration under flashlamp irradiation.

*U.S. Pat. No. 3,311,846, Dated 3-9-71, American Optical Corp.

**These devices were constructed and tested in the following chronological order B-1, N-1, B-2, N-2, B-3 and N-3.

The first Brewster disc laser (B-1) consisted of 30, 3 mm thick discs, mounted in a metal frame at Brewster's angle to the optic axis. The discs had a 25 mm diameter clear aperture and were optically pumped by two 165 mm long flashlamps. An all-parallel flow through the 1.2 mm spacings was chosen, to allow very high flow rates.

The first normal incidence disc laser (N-1) consisted of 46, 10 mm thick discs, mounted in square Pyrex tubing normal to the optic axis. The discs had an 18 mm diameter clear aperture and were pumped by four 457 mm long flashlamps. A series-parallel flow arrangement through the 1 mm spacings of this device was chosen to avoid steering of the beam due to temperature gradients along the coolant path.

All the other disc lasers employ common hardware, consisting of a 22 mm ID square Pyrex tube, surrounded by four 457 mm long flashlamps in a close-wrap configuration. The discs for the B-2, B-3, N-2 and N-3 all have a rectangular clear aperture of 17.2 x 21.7 mm, a thickness of 4.65 mm and are spaced 0.4 mm apart. The discs were made from 3% Nd doped glass and are held by slots in four stainless steel rails mounted in the corners of the square Pyrex tube. These devices require 67 Brewster-angled discs or 91 normal-incidence discs. Series-parallel flow is used in all devices. The flow channels in this design are almost as wide as the discs, which allows uniform flow and cooling across the disc surfaces.

All these devices were evaluated, measuring passive and active transmission, gain, threshold energy, slope efficiency, and passive and active single-pass distortions for variable flow rates, repetition rates, coolant temperatures and beam diameters. Data are presented on average output power, beams spread, average radiance and thermal lensing, as a function of average input power, and compared to like properties of comparable solid rods.

Theoretical analyses were made of the average radiance capability of solid rods, the flow distribution in disc lasers, as well as the thermal distortions in disc laser elements, which all agreed reasonably well with the experimental results.

Design considerations for disc lasers are outlined and the results of tests on materials and components to improve system life and performance are reported. The advantages and limitations of the disc lasers are compared to other approaches and recommendations are made for further improvements.

The following table summarizes the actual performance of the B-3 and N-3 in comparison to our goals, which shows in general, close agreement between the predicted and actual performance values. Because of time limitations, the performance of the N-3 as a Q-switched oscillator could not be evaluated.

Table I							
DISC LASER PERFORMANCE							
				B-3		N-3	
				Goal	Actual	Goal	Actual
OSCILLATOR	Normal Mode	Output Power	W	300	300	360	420
		Input Power	kW	20	30	30	35
		Overall Efficiency	%	1.5	1.0	1.2	1.2
		Repetition Rate	pps	3	3	3	3.5
	Q-switched	Output Power	W	50	60	100	--
		Output Energy	J	10	10	10	--
		Input Energy	kJ	3	3.8	3	--
		Repetition Rate	pps	5	6	10	--
		Input Power	kW	15	24	30	--
	AMPLIFIER	Q-switched	Output Power	W	90	90	90
Output Energy			J	30	23	30	22
Input Signal			J	5	5	5	5
Input Energy			kJ	10	6	10	6
Repetition Rate			pps	3	4	3	5
Input Power			kW	30	24	30	30

SECTION II

AVERAGE RADIANCE CAPABILITY OF SOLID RODS

The advantage of a laser over a conventional light source is its high spectral radiance, which allows focusing of its output beam to a small spot, generating extremely high power densities and temperatures on a target or workpiece.

The average radiance of a solid rod laser is limited due to an increase in beamspread with input power, which is caused by induced thermal lensing in the rod. Experimental results on cylindrical Nd glass laser rods show about a linear increase in solid angle beamspread and thermal lensing with average input power. In this analysis the laser cavity is treated as an infinitely long lens-like medium which allows correlation of the induced thermal lensing to the solid angle beamspread. From the experimental results available on thermal lensing of different laser materials, the expected solid angle beamspread of an oscillator cavity can be estimated.

The average radiance N of a laser is approximated by [1].

$$N = \frac{P}{2A\Omega} \quad (1)$$

where P = the average output power,

A = the cross-sectional area of the laser beam,

and Ω = the solid angle beamspread (full angle containing $P/2$).

For typical pump and overall efficiencies obtained with different lasers and for known laser material properties, the described model provides a rough estimate of the average radiance capability of solid rod lasers under CW or normal mode operation for different laser materials and geometries.

1. CYLINDRICAL LASER RODS

The radial temperature distribution of a cylindrical laser rod, assuming uniform volumetric heating and uniform cooling at the rod surface is given by [2].

$$T = T_0 - \Delta T (r/R)^2 \quad (2)$$

with $\Delta T = \frac{R^2}{4k} \dot{q} = \frac{\epsilon_p P_i}{4\pi k \ell}$ (3)

and $\dot{q} = \frac{\epsilon_p P_i}{\pi R^2 \ell}$

where T_0 = temperature in the center of the rod

r = radial position in the rod

R = radius of the laser rod

ℓ = pump length of the laser rod

ΔT = temperature difference from rod center to surface

\dot{q} = volumetric heating rate

k = thermal conductivity

ϵ_p = pumping efficiency

P_i = average input power

The tangential stress σ at the surface of such a heated laser rod is given by [3]

$$\sigma = \frac{\alpha E}{2(1-\nu)} \Delta T \quad (5)$$

where E = Young's modulus

α = linear thermal expansion coefficient

ν = Poisson's ratio

The maximum output power \hat{P} of a solid laser rod can then be estimated by

$$\hat{P} = \epsilon_o \hat{P}_i = \frac{\epsilon_o}{\epsilon_p} \frac{1-\nu}{\alpha E} 8\pi k \ell \sigma \quad (6)$$

where ϵ_0 = overall efficiency of the laser

$\hat{\sigma}$ = tensile strength of the laser material.

To determine the average radiance of a laser requires an estimate of the angular beam divergence as a function of geometry and input power. The parabolic temperature distribution in the laser rod will result in the first approximation in a parabolic index distribution of the form

$$n = n_0 - \Delta n (r/R)^2 \quad (7)$$

with $\Delta n = \frac{dn}{dT} \Delta T + \sum B \sigma = C \Delta T \quad (8)$

where n_0 = refractive index in the center of the rod

Δn = index difference from rod center to surface

B = stress optic coefficients

C = material constant, combining the effects of the index change due to temperature, strain, and expansion in cylindrical rods.

A medium with such an index distribution is considered an ideal lens-like medium. A paraxial ray will pass through such a medium in a sinusoidal path. The radial position r of a ray entering the medium parallel to the axis at the radial position r_0 is given by [4]

$$r = r_0 \cos \sqrt{2\Delta n/n} \frac{z}{R} \quad (9)$$

where z is the axial distance from the entrance face.

An initially parallel beam entering this medium will be focused inside the medium at a distance

$$f = \frac{\pi}{2} \frac{R}{\sqrt{2\Delta n/n}} \quad (10)$$

and refocused at axial distances of $3f$, $5f$, etc.

An oscillator cavity with the mirrors very close to the rod can essentially be considered as a folded infinite long lens-like medium. At the output mirror, rays are incident with slopes given by

$$\psi \approx -n \frac{dr}{dz} = \frac{r_0}{R} \sqrt{2n\Delta n} \sin \sqrt{2n\Delta n} \frac{z}{R} \quad (11)$$

which range from 0 to $\hat{\psi} = \sqrt{2n\Delta n}$.

Since the beamspread of a laser is measured as the full angle containing one half of the output power, an averaging of the above range of beam angles over the focusing length f and the cross-sectional area A has to be taken in the form of

$$\bar{\psi} = \frac{1}{fA} \int_0^f \int_0^R \psi \, 2\pi r_0 \, dr_0 \, dz = \frac{4}{3\pi} \sqrt{2n\Delta n} = \frac{4}{3\pi} \hat{\psi} \quad (12)$$

which essentially assumes that every volume element of the rod contributes equally to the output.

The solid angle beamspread can then be approximated by

$$\Omega = \pi \bar{\psi}^2 = \frac{32}{9\pi} n\Delta n = \frac{8}{9\pi^2} \frac{nC}{kl} \epsilon_p P_i \quad (13)$$

This equation is only valid where the beamspread is mainly determined by the lensing in the rod. At low input powers the beamspread is determined by the ratio of beam diameter to cavity length and the optical quality of the cavity, while at high input powers, the beamspread becomes independent of the rod diameter.

With this model, the average radiance for different laser materials and laser rod dimension can be estimated by

$$N = \frac{\epsilon_0 P_i}{2A\Omega} = \frac{9\pi^2}{16} \frac{k}{nC} \frac{\epsilon_0 l}{\epsilon_p A} \quad (14)$$

The average radiance for CW or repetitively pulsed normal mode operation is in the first approximation independent of the average

input power as was found experimentally. Since the overall efficiency ϵ_0 is proportional to the pump efficiency ϵ_p , the ratio ϵ_0/ϵ_p can be replaced by a conversion efficiency ϵ which takes into account the cavity and quantum efficiency as well as the losses due to off-axis radiation, threshold, etc.

The term k/nC depends only on the laser material and can be used as a figure of merit, assuming laser rods of the same geometry can be fabricated.

The constant C has been calculated for different laser materials, and approaches the dn/dT value for crystalline materials, where the effects due to strain and expansion are subordinate. However, this constant can also be determined experimentally measuring the effective focal length of the laser rod as a function of input power. This effective focal length f_0 is given by

$$f_0 = \frac{r_0}{\psi_{z=l}} \approx \frac{R^2}{2\Delta n l} \quad (15)$$

which is only valid for $l \ll f_0$.

Substituting (8), (3) and (4) in (15) results in

$$C \approx \frac{2kA}{f_0 \epsilon_p P_i} \quad (16)$$

with quantities which can be measured quite accurately.

Substituting (15) or (16) in (13) results in

$$\Omega = \frac{16}{\pi} \frac{nR^2}{lf_0} \quad (17)$$

which provides a close correlation of the effective focal length to the solid angle beamsread.

a. Experimental Results

The effective focal length of different laser materials as a function of input power has been measured by several investigators [5,8]. Data about the change in solid angle beamsread

with input power, however, are scarce. We have measured the effective focal length and the solid angle beamsread as a function of input power for Nd-doped laser glass and find good agreement of our results with our estimates, which supports the validity of this model, correlating the effective focal length of a laser rod to its beam divergence as an oscillator. Most measurements were taken with a 18 mm OD laser rod of 3% Nd-doped AO C1020 laser glass, pumped by four linear flashlamps with an arc length of 457 mm in a close-wrap configuration. The solid angle beamsread of this device was found to increase linearly with input power at a rate of 1.1×10^{-4} sr/kW. The induced thermal lens power of this rod was also measured using a 6328Å He-Ne probe beam. The optical power was also measured to increase linearly with input power, at a rate of 0.73 diopter/kW. Calculations of the C value for this laser glass indicate a lower thermal lensing than for OI ED-2 laser glass. This difference is mainly due to the negative dn/dT value for AO glass, which partially compensates for the stress-optic effects and makes this glass semi-athermal. For ED-2 glass, the dn/dT value is positive, which does not compensate but adds to the stress-optic lensing.

Measurements taken with 12.7 mm diameter rods at 1.15 μ m wavelength resulted in a linear increase in thermal lensing with input power at rates of 0.8 and 1.3 diopter/kW for AO and OI glass, respectively.

To determine the C values for AO and OI laser glass, the pump efficiency was measured from the heat dissipated by the laser rod in the cooling system.

For the 18 mm OD rod, a pump efficiency of 15% was measured, while the cavity used for the 12.7 mm diameter rods was only about one half as efficient. From these measurements C values of 2.0 and $2.2 \times 10^{-6} \text{ } ^\circ\text{C}^{-1}$ were determined for AO glass at 6328Å and 1.15 μ m wavelength, respectively. Calculations of the change in optical pathlength at 1.06 μ m due to thermal index change, strain and thermal elongation yield C values of 1.4 and $2.5 \times 10^{-6} \text{ } ^\circ\text{C}^{-1}$ for tangential and radial polarized light, respectively. The average calculated C value of $2 \times 10^{-6} \text{ } ^\circ\text{C}^{-1}$ agrees well with our measured values.

The measured C value for OI glass is about $5 \times 10^{-6} \text{ } ^\circ\text{C}^{-1}$ or 2.5 times larger than for AO glass, which also agrees well with our estimates.

The thermal lensing of 6.3 mm OD YAG and YAlO₃ rods was measured in cavities with about 5% pump efficiency by several

investigators using 6328Å probe beams. The results average to about 0.5 and 0.7 diopters/kW, which corresponds to C-values of 7 and $10 \times 10^{-6} \text{ }^{\circ}\text{C}^{-1}$ for YAG and YAlO_3 , respectively. For YAG, C-values of 6.9 and $9.7 \times 10^{-6} \text{ }^{\circ}\text{C}^{-1}$ were calculated for tangentially and radially polarized light, respectively, which is within the accuracy of the measured value.

The data available on beam divergence of YAG oscillators are difficult to compare with the lensing data, because the thermal lensing was only measured at 6328Å and the beamsread was taken with the mirrors of the cavity relatively far removed from the ends of the rod in comparison to the length of the rod. For extended cavities, the beamsread is probably somewhat lower than for very short cavities, assumed in this model, because of some spatial mode selection.

From data available on 102 mm YAG rods, the measured solid angle beamsread is about 30 μsr per kW input power. With Eq. (13) the C value for YAG at 1.06 μm can be estimated at $4 \times 10^{-6} \text{ }^{\circ}\text{C}^{-1}$, which is reasonably close to the value obtained from the thermal lensing measurement at 6328Å.

For calcium tungstate only very limited performance data are available. For a 76 mm long crystal in a pump cavity with about 5% pump efficiency, a solid angle beamsread of 60 μsr per kW input power was estimated, which corresponds to a C value of approximately $2.1 \times 10^{-6} \text{ }^{\circ}\text{C}^{-1}$. This value is low in comparison to the dn/dT value of 4.6 and $7.7 \times 10^{-6} \text{ }^{\circ}\text{C}^{-1}$ for the ordinary and extraordinary ray, respectively.

For 102 mm long ruby crystals, a solid-angle beamsread of about 30 μsr per kW input power was measured in pump cavities with about 8% efficiency. The resulting C value of $10 \times 10^{-6} \text{ }^{\circ}\text{C}^{-1}$ is reasonably close to the dn/dT value of $15 \times 10^{-6} \text{ }^{\circ}\text{C}^{-1}$.

In Table II, properties of different laser materials are summarized, as well as average C values and typical efficiencies. To compare the average radiance for the different materials, practical values for the cross-sectional area and length of the laser rods have to be determined. Since the radiance is proportional to l/A , the longest but thinnest possible rods should be used. However, there are practical limitations. The pump efficiency falls off about linearly with diameter for rods of less than 6.3 mm OD because the rods become optically too thin even at maximum doping levels. In order to maintain a high overall efficiency, rods with 6.3 mm diameter were chosen for this comparison.

Table II

PROPERTIES OF LASER MATERIALS

*at 6328 Å

	Sym.	Units	AO Glass	OI Glass	YAG	YAlO ₃	CaWO ₄	Ruby
Index of Refraction	n_o		1.51	1.56	1.82	~ 1.96	~ 1.90	1.76
Center Wavelength	λ	μm	1.060	1.062	1.0641	{ 1.0645 1.0795	1.058	0.6943
Fluorescence Linewidth	$\Delta\lambda$	nm	26	26	0.8	0.8	2	0.5
Fluorescence Decay Time	τ	ms	0.57	0.30	0.23	0.16	0.17	3
Thermal Conductivity	k	$\text{W/m}^\circ\text{C}$	0.84	1.25	11	11	4	40
Thermal Expansion	α	$\times 10^{-6} \text{ }^\circ\text{C}^{-1}$	10.3	10.0	7	~ 10	~ 15	6
Young's Modulus	E	$\times 10^6 \text{ psi}$	9.9	13.07	45	32		90
Tensile Strength	σ	$\times 10^3 \text{ psi}$	12	13.6	32	56		45
Poisson's Ratio	ν		0.225	0.242	0.3			~ 0.2
ΔT at Fracture Level	ΔT	$^\circ\text{C}$	180	160	130	240	100	130
Max. Thermal Loading	$\epsilon_p P_i$	W/cm	19	25	180	330	47	670
Thermal Index Change	dn/dT	$10^{-6} \text{ }^\circ\text{C}^{-1}$	- 3.3	+ 2.8*	7.3*	~ 10*	{ 4.6 o 7.1 e	15
Average C Values	C	$\times 10^{-6} \text{ }^\circ\text{C}^{-1}$	2	5	5	7	3	12
Figure of Merit	k/nC	kW/cm	2.8	1.6	12	8	7	19
Typ. Pump Efficiency	ϵ_p	%	15	15	5	5	5	8
Typ. Overall Efficiency	ϵ_o	%	2.5	3	2.5	2.5	1.5	1.2
Typ. Conversion Efficiency ϵ_o/ϵ_p	ϵ	%	17	20	50	50	30	15
Typ. Length for 6.3 mm Rods	l	cm	30	30	10	10	10	10
Max. Output Power	\bar{P}	W	100	150	900	1700	150	1000
Typ. Output Power	\bar{P}	W	20	25	200	200	~ 50	100
Thermal Lensing at \bar{P}	f	cm	33	25	22	18	26	21
Average Radiance	N	$\text{MW/cm}^2 \text{ sr}$	0.25	0.17	1.0	0.7	0.4	0.5

Glass laser rods can be fabricated with lengths of several meters. However, the overall efficiency was found to have a maximum for glass rods with an aspect ratio of about 40:1. Here again, rods with about 30 cm pump length were chosen for maximum overall efficiency. For crystalline materials, it is difficult to produce rods of this length, or at least very expensive. However, rods with 10 cm length can be produced economically.

With these considerations, the maximum output power at the fracture point of the rod can be estimated as well as the expected average radiance. The maximum output power can usually not be realized for long-term operation. For laser glass the maximum power is limited to about 20% of the fracture level because at higher thermal loadings, permanent optical inhomogeneities are induced, which reduce the efficiency. For crystalline materials, the maximum output power is usually limited by the lamps. For arc lamps of about 1 cm bore diameter, long lifetimes can be expected for input powers below 1 kW per 25.4 mm arc length. In double elliptical pump cavities with 102 mm arc length lamps, an average input power of 8 kW is available, which corresponds to an output power of about 200 W for YAG and YAlO_3 , and about 100 W for ruby. These estimates agree well with measured performance levels.

At these typical output levels, the thermal focusing length is about equal to the length of the glass laser rods, but about twice the length of the crystalline rods.

The average radiance obtainable from 6.3 mm diameter rods of different laser materials is well within one order of magnitude, ranging from 0.17 to 1 MW/cm²sr. The experimental results are all within a factor of 2 of the estimated values given in the table, which could be caused by an error of $\pm\sqrt{2}$ in the available beamsread data alone. Uncertainties also arise from the use of data taken with extended cavities, which tend to reduce the beamsread and increase the radiance. However, the cavities can only be extended to a length equal to twice the thermal focusing length of the rod. Beyond this point, the cavity becomes unstable and off-axis losses reduce the overall efficiency.

The average radiance can also be increased by compensation for the induced thermal lensing. This is most effective, where the thermal focusing length is long in comparison to the length of the laser rod. However, at typical output levels, the focusing length is close to the length of the laser rod, which requires compensation at both ends of the rod. This approach

allows increase of the average radiance by up to one order of magnitude.

Another approach to increase the average radiance is to pump many thin rods in a single pump cavity. Such a "fagot" laser allows reduction of the diameter of the individual rods to less than 6.3 mm OD while still maintaining a high pump efficiency. The average radiance for the total output beam of the fagot laser is usually about one half or at best equal to the average radiance of the individual rods, because the area of the total output beam is larger than the total cross-sectional area of all rods. The full advantage of a fagot laser can only be realized if the individual output beams are also used individually, for example, for multiple spot welding or drilling applications. However, to obtain equal output from each rod requires individual mirror adjustments for each rod, which makes this approach less attractive.

2. RECTANGULAR SLAB LASERS

This approach provides a larger cooling surface and essentially a one-dimensional temperature gradient across the thickness s of the slab. The temperature over the width w of the slab is approximately constant up to about one half thickness from the edge. Since the resulting index gradients are also one dimensional, efficient operation with a polarizer in the laser cavity is possible, since the birefringence of this geometry is much lower than for a cylindrical rod. Compensation for thermal lensing is also easier since only one cylindrical focus exists, while for the rod the thermal focusing length is different for radially and tangentially polarized light.

The temperature distribution across the thickness of a uniformly heated and surface cooled slab is parabolic with a temperature difference from the center to the surface given by

$$\Delta T_s = \frac{s^2}{8k} \dot{q} = \frac{s \epsilon_p P_i}{8k w l} \quad (18)$$

The tangential stress σ_s at the surface of a heated slab is

$$\sigma_s = \frac{2\alpha E}{3(1-\nu)} \Delta T_s \quad (19)$$

which allows estimation of the maximum output power at the fracture

point of the slab to

$$\hat{P}_s = \epsilon_0 \hat{P}_{is} = \frac{\epsilon_0}{\epsilon_p} \frac{1-\nu}{\alpha E} 12 \text{ kl } \frac{w}{s} \hat{\sigma} = \frac{1.5}{\pi} \frac{w}{s} \hat{P} \quad (20)$$

A slab with a width-to-thickness ratio of greater than $\pi/1.5 \approx 2.1$ has superior output power capabilities in comparison to a rod of the same length.

The temperature distribution in the laser slab results approximately in a parabolic index distribution which gives rise to a cylindrical lens power in the slab with a focusing length of

$$f_s = \frac{\pi}{4} \frac{s}{\sqrt{2\Delta n_s/n}} \quad (21)$$

$$\text{where } \Delta n_s = C_s \Delta T_s \quad (22)$$

For an infinite slab of isotropic material

$$C_s \approx \frac{dn}{dT} + (B_{\parallel} + B_{\perp}) \frac{\alpha E}{1-\nu} \quad (23)$$

For a rod of isotropic material the C values for radial and tangential polarized light are

$$C_r \approx \frac{dn}{dT} + (B_{\parallel} + 7 B_{\perp}) \frac{\alpha E}{4(1-\nu)} \quad (24)$$

$$\text{and } C_t \approx \frac{dn}{dT} + (3 B_{\parallel} + 5 B_{\perp}) \frac{\alpha E}{4(1-\nu)} \quad (25)$$

Only for AO glass is the C_s and the average C value appreciably different (3.3 versus $2 \times 10^{-6} \text{ } ^\circ\text{C}^{-1}$) because of the athermalization of this glass. For crystalline materials, the C_s and C values are essentially equal to the dn/dT value of the material.

A slab oscillator exhibits an increase in beamspread mainly in the direction across the slab thickness. To estimate this beamspread requires averaging of the beam angles incident on the output mirror by

$$\bar{\psi}_s = \frac{1}{fA} \int_0^f \int_0^{s/2} \psi_s \, 2w \, dy \, dz = \frac{1}{\pi} \hat{\psi}_s \quad (26)$$

with $\psi_s \approx -n \frac{dy}{dz} = \frac{2y}{s} \sqrt{2n\Delta n_s} \sin \sqrt{2n\Delta n_s} \frac{2z}{s} \quad (27)$

and $\hat{\psi}_s = \sqrt{2n\Delta n_s} \quad , \quad (28)$

where y is the distance from the central plane of the slab.

The solid angle beamspread can be approximated by

$$\Omega_s \approx 2\psi_w \bar{\psi}_s = \frac{\psi_w}{\pi} \sqrt{\frac{nC_s}{kw\ell} \epsilon_p P_i} \quad (29)$$

where ψ_w is the beamspread in the direction of the width of the slab, measured with a slit containing one half of the output energy. Since a rectangular aperture with an acceptance angle of $\psi_w \times \psi_s$ would only transmit about one quarter of the output energy, the solid angle beamspread Ω_s , which is defined as containing one half of the output energy, is about twice the product of ψ_w and $\bar{\psi}_s$. This equation is again only valid where the beamspread is mainly determined by the lensing in the slab.

The average radiance of a slab laser under CW or repetitively pulsed operation can then be estimated by

$$N_s = \frac{\epsilon_0 P_i}{2A\Omega_s} = \frac{\pi \epsilon_0}{2s\psi_w} \sqrt{\frac{k}{nC_s} \frac{\ell}{A} \frac{P_i}{\epsilon_p}} \quad (30)$$

To compare the performance of slab lasers to cylindrical rods, practical dimensions for the slab have to be determined. The thickness of the slab is again chosen to maintain a high overall efficiency. Slabs with a thickness of 3 mm were found to be

as efficiently pumped as 6.3 mm rods in the same pump cavity. In order to compare 3 mm slabs with 6.3 mm rods, the cross-sectional area and length for the slabs and rods were kept equal, which resulted in a width for the slab of 10 mm. For a 3 x 10 mm slab, the maximum input power capability is 1.5 times higher than for a 6.3 mm OD rod.

The ratio in average radiance of the 3 x 10 mm slab to the 6.3 mm rod is

$$\frac{N_s}{N} \approx \frac{0.55}{\psi_w} \sqrt{\frac{nC^2}{\ell k C_s}} \epsilon_p P_i \quad (31)$$

assuming the same overall and pump efficiencies are obtained.

For crystalline materials, where the maximum input power is limited by the lamps to about 8 kW, as discussed earlier and $C_s \approx C$, an order of magnitude improvement in radiance of 3 x 10 x 100 mm slabs over 6.3 mm OD by 100 mm long rods can be expected, assuming the beams spread ψ_w remains below 3 mrad.

From measurements taken on 2 x 6 x 75 mm glass slabs, the beams spread ψ_w was found to increase only slightly with input power from about 2 to 3 mrad, while the beams spread across the thickness of the slab increased from 2 to 8 mrad, at 1.5 kW input power. With a pump efficiency of about 6% for this cavity, the calculated beams spread $\bar{\psi}_s$ agrees well with the measured values. Good agreement of the calculated and measured beams spread $\bar{\psi}_s$ was also found on 3 x 10 x 230 mm and 5 x 20 x 165 mm glass slabs.

With the 3 x 10 x 230 mm slab, a larger increase in the beams spread ψ_w with input power was measured than observed on the 2 x 6 x 75 mm slab. Some increase of the beams spread ψ_w with input power is expected, since the width-to-thickness ratio of these slabs is only about 3:1. This means that 1/3 of the slab cross section is influenced by the edges, similar to a rod, and only 2/3 of the slab cross section can be approximated by an infinite slab. It is desirable to increase the width-to-thickness ratio to at least 5:1 in order to reduce the edge effects.

For 3 x 10 x 300 mm slabs made from AO laser glass, an order of magnitude improvement in radiance over 6.3 mm OD by 300 mm long AO laser glass rod can be expected at an input power of 1.2 kW. Higher input powers would again result in induced permanent optical distortions, as discussed earlier. At 0.5 kW

input power an average radiance of $1.2 \text{ MW/cm}^2\text{-sr}$ was measured, which agrees well with a calculated radiance of $1.5 \text{ MW/cm}^2\text{-sr}$ assuming ψ_w remains constant at 2 mrad. The somewhat lower experimental results are due to the edge effects.

Since the input power for laser glass is limited to about 20% of the fracture level, the maximum radiance for a glass slab can be estimated by

$$N_s = \frac{2.4}{\psi_w} \frac{k\ell}{s^2} \frac{\epsilon_o}{\epsilon_p} \sqrt{\frac{\sigma}{nC_s} \frac{1-\nu}{\alpha E}} \quad (32)$$

which is independent of the width of the slab as long as the edge effects can be neglected. Since ℓ and s are limited to about 300 and 3 mm, respectively, to insure efficient operation, the maximum radiance for a slab of AO glass is about $2.5 \text{ MW/cm}^2\text{-sr}$.

This value could again be improved by compensation for the induced thermal lensing or by the use of thinner multiple slabs.

This analysis allows a rough prediction of the average radiance capability of solid rods under CW or normal mode operation. However, under Q-switched operation, limitations due to damage of the laser material caused by focusing of the laser beam within the cavity, reduces greatly the average output power capability of solid rods.

Since the cylindrical rod and the rectangular slab laser are both limited in average radiance by index gradients transverse to the beam, the performance limits of disc or axial gradient lasers were investigated.

SECTION III

GENERAL DESIGN CONSIDERATIONS

To overcome the limitations of solid rod lasers as described in the previous section, the axial-gradient or disc laser provides an alternative solution. A disc array is a logical design approach for high average radiance or high average power, Q-switched lasers.

The thermal-optic distortions in the laser material of a disc laser will certainly be greatly reduced, because of the better cooling capabilities. However, the coolant itself can introduce thermal-optic distortions, which are greater than those eliminated in the solid laser discs. This is due to the high thermal index coefficients for most liquids, which are in general about two orders of magnitude larger than for solids. The design of the coolant flow channels is therefore most important, in order to minimize the thermal gradients in the coolant. A high coolant flow rate and a uniform flow distribution in the disc array without generating excessive pressure losses, is most desirable.

The methods of holding the discs should allow a uniform flow distribution between the discs without compromising pumping efficiency, pump uniformity, ease in assembly and manufacture of the components. Maximum efficiency will result by using holding materials which are transparent to, or at least vignette a minimum of, the pump light and a design which allows close coupling of the disc array with the flashlamps.

In the design of a disc laser, several conflicting requirements have to be satisfied, to arrive at a reasonable compromise.

To avoid thermal-optic distortions and fracture of the discs at maximum input power, the discs should be as thin as possible. However, this would require more discs for a given active pump length and more disc surfaces, which would increase the interfacial losses and the beam distortions due to surface imperfections.

The flow channels should be as narrow as possible to reduce absorption losses in the coolant between discs and to keep the inactive volume within the pump cavity small. However, narrow flow channels would reduce the coolant flow rate for a given safe operating pressure and increase the thermal-optic distortions in the coolant.

To avoid steering of the beam due to thermal gradients along the coolant path requires alternating flow directions across the disc surfaces. An all-alternating flow arrangement would provide a uniform flow distribution but requires an excessive high pressure drop. A series-parallel flow arrangement requires a much lower pressure drop, but provides also a less uniform flow distribution.

During this development program, several different disc lasers were investigated to determine the relative importance of these requirements in order to optimize the overall performance in a well-balanced design.

1. FLOW DISTRIBUTION IN DISC LASERS

Since a uniform flow distribution was found to be most important in disc laser design, a more detailed analysis of the flow distribution for the final disc design became essential. This analysis was derived in general for series-parallel flow arrangements as shown in Fig. 1, but in particular carried out for the N-2 design as outlined in Section V.2. This model was used to obtain some correlation between the pressure drop, flow rate and uniformity of the flow distribution for different geometries of the flow channels.

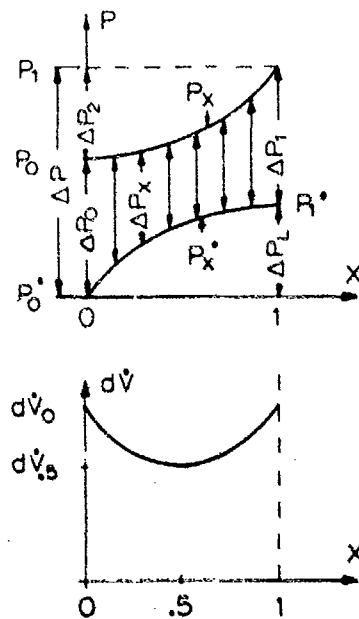
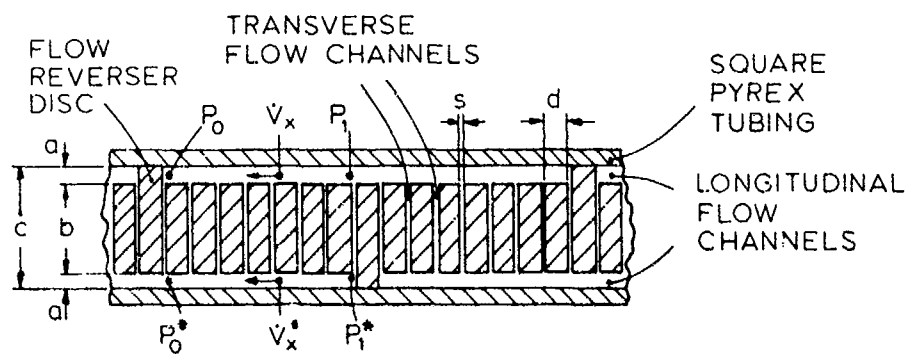
This approximation does not take into account acceleration and deceleration losses of the fluid as well as pressure losses caused by the right angle turns of the flow between the longitudinal and transverse flow channels.

Assuming a parabolic flow distribution with z being a measure of the uniformity of flow, the localized flow rate \dot{V}_x can be calculated by

$$\dot{V}_x = \int_0^x d\dot{V}_x = \dot{V} (x - 2zx^2 + \frac{4}{3} z x^3) / (1 - \frac{2}{3} z) \quad (33)$$

where \dot{V} is the total flow rate.

Since the flow distribution is symmetrical with minimum flow in the center and maximum flow at the ends of each section, the flow and pressure drop ratio of the center disc in respect to the end disc will determine the maximum nonuniformity. The pressure drop for the center disc is



$$P_x = P_0 + \int_0^x dP_L$$

$$P_x^* = P_1^* - \int_x^1 dP_L^*$$

$$\Delta P_x = P_x - P_x^*$$

SYMMETRY:

$$\dot{V}_x = \dot{V}_{1-x}^*$$

$$\Delta P_x = \Delta P_{1-x}^*$$

$$\int_x^1 dP_L^* = \int_0^x dP_L$$

FOR PARABOLIC FLOW DISTRIBUTION:

$$d\dot{V}_x = d\dot{V}_0 (1 - 4Zx + 4Zx^2)$$

$$\text{WITH } Z = 1 - d\dot{V}_s/d\dot{V}_0$$

Fig. 1 Flow distribution for series parallel flow arrangement

$$\Delta P_{0.5} = \Delta P_0 - \Delta P_L + 2(P_{0.5} - P_0) \quad (34)$$

The pressure drop along a flow channel of length L , cross-sectional area A and effective diameter D is given by [6].

$$\Delta P = \phi \rho \frac{L}{2D} v^2 \text{ with } D = \frac{4A}{u} \text{ and } v = \frac{\dot{V}}{A} \quad (35)$$

where ϕ represents a coefficient of flow resistance, ρ the density of the fluid, v the mean flow velocity and u the circumference of the channel. For laminar flow with Reynolds numbers of less than 10^3 the value for

$$\phi = \frac{64}{Re} \text{ with } Re = \frac{D}{\nu} v \quad (36)$$

where ν is the kinematic viscosity. For turbulent flow close to the transition region with Reynolds numbers from 10^3 to 10^4 , an average value of $\phi \approx 0.05$ was applied for these estimates. For heavy water, and converting from the cgs system to psi, GPM and mm, the pressure drop for laminar flow is

$$\Delta P_{lam} = K^* \frac{L}{D^3 A} \dot{V} \text{ with } K^* = 0.29 \frac{\text{psi}}{\text{GPM}} \text{ mm}^3 \quad (37)$$

and for turbulent flow from $10^3 < Re < 10^4$ about

$$\Delta P_{turb} \approx K \frac{L}{DA^5} \dot{V}^3 \text{ with } K \approx 15 \frac{\text{psi}}{\text{GPM}^3} \text{ mm}^4 \quad (38)$$

For the case of all turbulent flow in the disc laser, the pressure drop along the longitudinal flow channel can be approximated by

$$dP_L \approx K \frac{dx}{D_L A_L} \dot{V}_x^3 \quad (39)$$

The ratio of pressure drop from center to end is then

$$\frac{\Delta P_{0.5}}{\Delta P_0} = \left(\frac{d\dot{V}_{0.5}}{d\dot{V}_0} \right)^2 = (1-z)^2 = 1 - \left(1-2 \frac{P_{0.5}-P_0}{\Delta P_L} \right) \frac{\Delta P_L}{\Delta P_0} \quad (40)$$

with

$$\frac{P_{0.5}-P_0}{\Delta P_L} = \frac{\int_0^{0.5} \dot{V}_x^2 dx}{\int_0^1 \dot{V}_x^2 dx} = \frac{1}{8} \left[\frac{1 - 1.1z + 0.3z^2}{1 - 1.4z + 0.5z^2} \right] \quad (41)$$

Evaluating $\Delta P_L/\Delta P_0$ as a function of z allows a close approximation in the form of $\Delta P_L/\Delta P_0 \approx 2z$ which relates the ratio of pressure drop along the longitudinal and first transverse flow channel to the uniformity of flow. For $\Delta P_L \ll \Delta P_0$ the flow is uniform with $z \approx 0$. In order to obtain a flow distribution uniform to within 25%, requires $\Delta P_L \approx 1/2 \Delta P_0$, which was used as a design criterion.

For m sections with n transverse channels each, the pressure drop along the longitudinal and first transverse flow channel can be estimated by

$$\Delta P_L = \frac{K_L}{m} \dot{V}^2 (1 - 1.4z + 0.5z^2)/(3-2z) \quad (42)$$

$$\Delta P_0 = K_T \Delta \dot{V}_0^2 \approx K_T \left[\frac{\dot{V}}{n(1-2z/3)} \right]^2 \text{ for } x = \frac{1}{n} \ll 1 \quad (43)$$

$$\text{with } K_L = K \frac{L}{D_L A_L^3} \approx K \frac{L}{2a^3 c^3} \quad (44)$$

$$\text{and } K_T = K \frac{b}{D_T A_T^3} \approx K \frac{b}{2s^3 c^3} \quad (45)$$

where L is the pump length of the disc laser.

From this we can relate the dimension and number of flow channels to the flow uniformity by

$$\frac{\Delta P_L}{\Delta P_0} = \frac{n^2 L s^3}{3m b a^3} (1 - 1.4z + 0.5z^2) \left(1 - \frac{2}{3} z\right) \approx 2z \quad (46)$$

For $L = 460$ mm, $s = 0.4$ mm, $b \approx 20$ mm, $n \cdot m = 90$ and $z = 0.25$, we obtain

$$m = \frac{16 \text{ mm}}{a} \approx 7 \quad (47)$$

which determines the number of sections required for a given width of the longitudinal flow channel, to obtain a flow distribution uniform within 25%.

So far, only all-turbulent flow was considered, which was actually not obtained because of relatively high pressure losses in the cooling system.

For the more typical flow rates of 1 GPM through the N-2, the flow in the transverse flow channels is laminar and in the longitudinal flow channels turbulent. A similar analysis can be made for this case, which results in a better flow uniformity than estimated from the all-turbulent case, because the ratio $\Delta P_L / \Delta P_0$ becomes smaller. However, the flow uniformity is no longer independent of the flow rate. The number of sections required for the N-2 design with $z = 25\%$ and $\dot{V} = 1$ GPM is for this case,

$$m = \sqrt{115 \frac{\text{mm}^3}{\text{GPM}} \frac{\dot{V}}{a^3}} \approx 3 \quad (48)$$

For the case of all laminar flow, the flow uniformity is again independent of flow rate and is related to the geometry of the flow channels by

$$\frac{z}{1-z} = \frac{nLs^3}{mba^3} \quad (49)$$

The number of sections required for the N-2 design with $z = 25\%$ is for the all laminar case,

$$m \approx \sqrt{\frac{400 \text{ mm}^3}{a^3}} \approx 6 \quad (50)$$

which again indicates a better flow uniformity than estimated from the all-turbulent case.

From this analysis, the total pressure drop for the all-turbulent case can be estimated by

$$\Delta P_t = m(\Delta P_L + \Delta P_o) = m(1 + \frac{1}{2z}) \Delta P_L = f(z) K_L \dot{V}^2 \quad (51)$$

with $f(z) = (1 - 1.4z + 0.5z^2) \frac{1 + 1/2z}{3 - 2z}$.

For the N-2 with 8 sections as described in Section V.2, the estimated total pressure drop is then

$$\Delta P \approx 1 \frac{\text{psi}}{\text{GPM}^2} \dot{V}^2 \quad (52)$$

From the flow characteristic of the N-2 as shown in Fig. 3, a value of 1.6 psi/GPM² was measured, which is in reasonable agreement with our estimate. The difference in these values might be explained by the pressure losses caused by acceleration and deceleration of the fluid.

For a better understanding of the magnitude of these pressure losses, one section of the N-2 design with n = 11 was evaluated for a flow rate of 1 GPM, assuming a uniform flow distribution.

The acceleration losses were approximated by [7]

$$\Delta P_A = \frac{\rho}{2} K_C v^2 \approx 3.6 \times 10^{-6} \text{ psi} \left(\frac{\text{s}}{\text{cm}} \right)^2 v \Delta v \quad (53)$$

with $K_C \approx \frac{1}{2} \frac{\Delta v}{v}$

where v is the higher flow velocity and Δv the velocity difference.

The deceleration losses are given by

$$\Delta P_D = \frac{\rho}{2} \Delta v^2 \approx 7.2 \times 10^{-6} \text{ psi} \left(\frac{\text{s}}{\text{cm}} \right)^2 \Delta v^2 \quad (54)$$

The pressure loss in the transverse flow channel for laminar flow was estimated at

$$\Delta P_T \approx 0.75 \frac{\text{psi}}{\text{GPM}} \frac{\dot{V}}{n} \approx 0.07 \text{ psi} , \quad (55)$$

and the pressure loss along the longitudinal flow channel at the i th disc by

$$\Delta P_{\Delta L} \approx 0.009 \frac{\text{psi}}{\text{GPM}^2} \dot{V}^2 \left(\frac{i}{n} \right)^2 . \quad (56)$$

Figure 2 shows the calculated pressure losses at different locations in the N-2 disc laser section in 10^{-3} psi values. The total pressure losses per N-2 section for the different coolant pathways are also given. The average of these values is 0.186 psi, which agrees well with the measured pressure loss of about 0.2 psi per N-2 section. This analysis results in a non-symmetrical flow distribution, which has a maximum flow rate approximately in the center of each section and a minimum flow rate through the first spacing following the flow entrance.

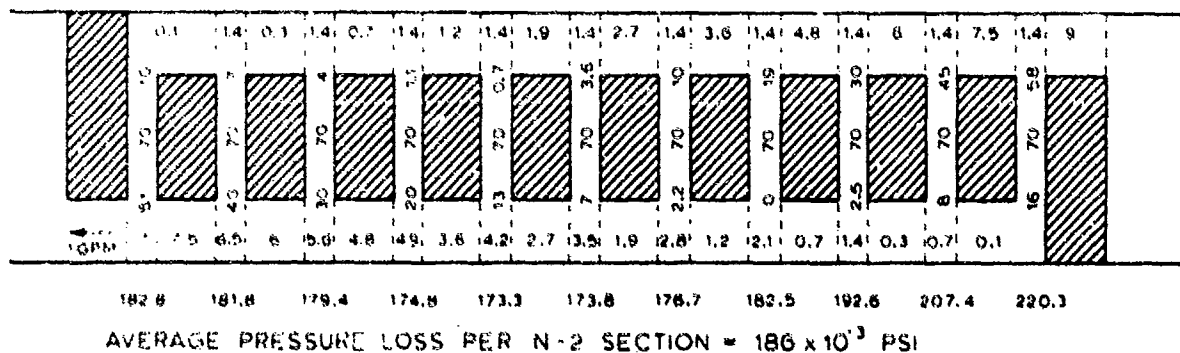


Fig. 2 Localized pressure losses in 10^{-3} psi for one N-2 disc laser section

To reduce the acceleration and deceleration losses as shown in Fig. 2, the coolant flow velocities should be equalized by graduating the longitudinal cooling channels as shown in

Fig. 13 for the N-1 design. With this approach a well-balanced flow distribution can be obtained.

Since the recovery time for the thermal-optical distortions was found to be about equal to the time τ required to exchange the coolant in the device, as described in Section VI.2, the repetition rate will be limited by the maximum flow rate, which in turn is limited by the safe operating pressure of about 10 psi in the square Pyrex tubing.

An estimate for the bursting pressure of the square Pyrex tubing indicates failure at 56 psi, primarily due to bending stresses in the corners of the tubing. This estimate is in reasonable agreement with the experimental results on several tubes, considering the variations due to surface imperfections and annealing conditions.

To reduce the recovery time for the thermal-optic distortions, the time to exchange the coolant in the device has to be reduced, which can be approximated for reasonably uniform flow by

$$\tau \approx \frac{2A_L L}{\dot{V}} \approx 10^{-3} \text{ sec} \sqrt{f(z) \frac{L^3}{a\Delta P_t} \frac{\text{psi}}{\text{cm}^3}} \quad (57)$$

For the N-2 and for $\Delta P_t \approx 10$ psi, this results in a minimum recovery time of about 0.2 sec. The most effective way to increase the repetition rate would be to reduce the pump length L of the device. However, Nd glass lasers with a low aspect ratio are less efficient because of a lower pump- and cavity efficiency. A high gain material like Nd-YAG would be ideal for a short pump length, allowing an increase in repetition rate of over an order of magnitude, up to 50 pps.

The flow characteristics for other disc lasers are also shown in Fig. 3. The measured pressure drop for the Brewster disc laser B-2 and the normal incidence disc laser N-2 were about the same for the same number of sections. For the B-2 the pressure drop was found to be approximately proportional to the number of sections and could be expressed in an empirical form by

$$\Delta P_t \approx 0.18 \frac{\text{psi}}{\text{GPM}^2} \dot{V}^2, \quad (58)$$

which agrees in general well with Eq. (51), since an evaluation

of $f(z)$ as a function of m results in an approximately linear relationship.

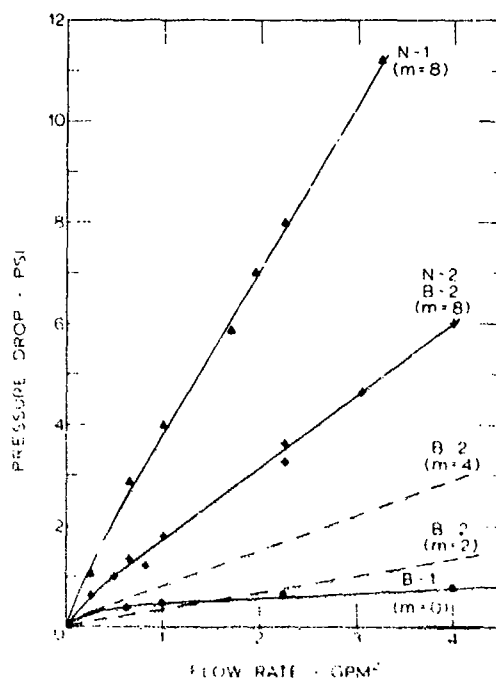


Fig. 3 Flow characteristics of disc lasers for D_2O

In order to obtain some experimental information about flow uniformity of the B-2, a small amount of ink was suddenly introduced at the flow entrance and the change in transmission through the device recorded.

This test is very sensitive to non-uniformities in flow since a very small amount of ink remaining in the disc laser keeps the device essentially opaque. The recovery time with the ink test was again found to be inversely proportional to the flow rate but about three times longer than the recovery time for the thermally induced optical distortions. For different flow configurations but constant flow rate, the recovery time was measured to be about inversely proportional to the square root of the number of sections in the B-2. However, the recovery time was found to be almost independent of the numbers of sections in the B-2 for constant pressure drop across the device.

From these measurements, the recovery time for the ink test can be approximated by

$$\tau_i \approx \frac{7.5 \text{ sec GPM}}{\sqrt{m} \dot{V}} \approx 3.2 \text{ sec} \sqrt{\frac{\text{psi}}{\Delta p_t}}, \quad (59)$$

in reasonable agreement with equation (57), which is only valid for relatively uniform flow distributions.

2. THERMAL CHARACTERISTICS OF DISC LASERS

For a better understanding of the behavior of the disc laser under single and repetitively pulsed operation, the thermal decay rate of the discs and the time required to reach thermal equilibrium were estimated and compared to experimental results.

The temperature profile during cooling at the surfaces of an initially uniform heated infinite plate of thickness d can be calculated from Eq. (13-35) given by [6].

$$\theta = \frac{4}{\pi} \theta_0 e^{-t/T} \left(\cos \psi - \frac{1}{3} e^{-8t/T} \cos 3\psi + \frac{1}{5} e^{-24t/T} \cos 5\psi - \dots \right) \quad (60)$$

with θ_0 = initial temperature difference

$$T = \frac{d^2}{\pi^2 \alpha} = \text{thermal decay rate}$$

$$\alpha = 0.54 \times 10^{-8} \frac{\text{cm}^2}{\text{s}} = \text{thermal diffusivity of glass}$$

and $\psi = \frac{\pi x}{d}$

with $x = 0$ at the center of the plate.

The thermal decay rate for the discs of the B-2 and N-2 is $T \approx 4$ seconds.

For repetitively-pulsed operation a uniform temperature increase of θ_0 is added to the remaining temperature profile of

the previous pulses. The temperature at the center of the disc just after the second pulse is

$$\theta_2 = \theta_1 + \theta_0 \text{ with } \theta_1 = \frac{4}{\pi} e^{-t/T} \left(1 - \frac{1}{3} e^{-8t/T} + \dots \right) \theta_0 = q \theta_0 \quad (61)$$

For n pulses the center temperature θ_n can be approximated by

$$\theta_n = \theta_0 \sum_{i=0}^{n-1} q^i = \theta_0 \frac{1 - q^{n-1}}{1 - q} \quad (62)$$

with the final temperature

$$\theta_{\infty} = \theta_0 / 1 - q \quad (63)$$

The number of pulses required to reach 90% of the final temperature is then

$$n_{0.9} = 1 + \frac{\ln 0.1}{\ln q} \quad (64)$$

For a repetition rate of 1 pps we obtain $q = 0.95$ and $n_{0.9} \approx 46$, which corresponds to a time required to reach 90% of thermal equilibrium of 46 seconds.

This estimate results in an upper limit for the thermal equilibrium time since only the temperature at the center of the disc is considered instead of the complete temperature profile.

For a closer approximation, the average temperature across the disc is used which can be determined by

$$\bar{\theta} = \frac{2}{\pi} \int_0^{\pi/2} \theta \, d\psi = \frac{8}{\pi^2} \theta_0 e^{-t/T} \left(1 + \frac{1}{9} e^{-8t/T} + \frac{1}{25} e^{-24t/T} + \dots \right) \quad (65)$$

For a repetition rate of 1 pps we obtain $\bar{q} = \bar{\theta}_1/\theta_0 = 0.64$ and $\bar{n}_{0.9} \approx 6.2$, which corresponds to a time required to reach 90% of thermal equilibrium of 6.2 seconds.

This estimate provides a lower limit for the thermal equilibration time, since the heat in the center of the disc is transferred to the edge of the disc by the averaging process of this model.

A temperature ratio between these two extremes is probably the best approximation. With $q \approx 0.85$ the time required to reach 90% of thermal equilibrium is about 15 seconds.

The time required to reach 50% of thermal equilibrium at 1 pps ranges from 2.5 to 14 seconds with an average of 5 seconds, which is in reasonable agreement with the experimental results.

To estimate the dissipated heat in the disc laser devices, the temperature difference between coolant inlet and outlet was measured, when the devices were repetitively pulsed. At a flow rate of 5.5 l/min, this differential temperature increased by 0.4°C per kW average input power for both the B-1 and N-1. With the specific heat for heavy water of 4.2 Ws/g°C, the ratio of dissipated heat output to electrical power input is about 15%. Since these results were the same for both devices, it was assumed that 15% of the input energy was absorbed in the laser glass. This implies that either the fraction of pump light absorbed in other parts of the device compensates the heat loss from the device other than through the coolant, or that these effects are negligible.

3. THERMAL DISTORTION IN DISC LASER ELEMENTS

The subject of thermal distortion from radial temperature variation in long glass laser rods has been studied extensively heretofore [8,9]. Also, as a special problem, the more complicating effects in a finite region from the end which do not submit to a generalized plane strain solution have been investigated for both unclad [10] and clad [11] configurations. It appears though, there has been no previous attempt to examine carefully the thermelastic behavior of the disc and accompanying optical effects that result under typical conditions of temperature. Evidently, the disc constitutes only a special case of a finite length rod in which the geometric parameter of length to diameter ratio is much less than one. If conditions of axisymmetric temperature exist in the disc, then, the stress-strain distribution may be obtained from the same expressions that were derived for the ends.

The computer program solution developed previously using a finite difference technique for solving the representative stress functions in the short cylinder was again used in the present work. An example of thermal loading has been employed in which the temperature function corresponds to steady-state behavior. This behavior is typical only under high repetition rate conditions wherein the thermal decay time is long compared to the time between successive pulses. The analyses are also based on assumptions whereby the heat is deposited uniformly over the volume of the disc and the cooled surfaces maintained at nearly constant temperature. Heat flow, in turn, will be symmetrical with respect to the axis of the disc. In practice, these conditions are virtually achieved if the convective heat transfer film coefficient is maintained sufficiently high at the solid-liquid interfaces.

Of primary interest have been solutions to the optical distortion effects in discs with a cooling environment which stimulates existing or anticipated conditions during operation of the laser. Evaluations have been performed, therefore, on 20 mm diameter by 3 mm and 10 mm thick segments, which although simplified from the actual square cornered geometry of the B-1 and N-1 discs, represent approximately the configuration on which experimental data would be obtained. Construction of the actual system provides for some coolant flow on all sides of the discs thus establishing both radial and axial heat flow. By analytical means, the two-dimensional temperature pattern was determined making first the following assumptions:

- (1) Fifteen percent of the energy input to the device would be deposited uniformly throughout the discs.
- (2) The cooled surface of the disc would be maintained at a reference temperature of zero.

The following expression, then, given by Carslaw and Jaeger [12] provides a solution for temperature distribution in the disc:

$$T(r, z) = \frac{\dot{q} z(d-z)}{2k} - \frac{4d^2 \dot{q}}{k\pi^2} \sum_{n=0}^{\infty} \frac{I_0 \left[(2n+1) \frac{\pi r}{d} \right]}{(2n+1)^2 I_0 \left[(2n+1) \frac{\pi R}{d} \right]} \frac{\sin (2n+1) \pi z}{d} \quad (66)$$

where \dot{q} , the volumetric thermal loading, has been based on total electrical input into the segmented device, d is the thickness,

R, the radius of the disc, and K, its thermal conductivity. I_0 is the modified Bessel function of order zero.

Having computed the temperature distribution for a representative axial cross section, the value of temperature at regularly spaced intervals, constituting a finite difference mesh, was subsequently introduced into the stress program to obtain the complete stress-strain distribution. These results were employed finally in determining the optical pathlength changes at radial stations across the disc by numerically integrating the following expressions from 0 to $d/2$.

$$\Delta P_r^*(r) = (n-n') \int_0^{d/2} \epsilon_z(r,z) dz - \int_0^{d/2} [\sigma_r(r,z)B_{\parallel} + (\sigma_{\theta}(r,z) + \sigma_z(r,z))B_{\perp}] dz + n\alpha_n \int_0^{d/2} T(r,z) dz \quad (67)$$

$$\Delta P_{\theta}^*(r) = (n-n') \int_0^{d/2} \epsilon_z(r,z) dz - \int_0^{d/2} [\sigma_{\theta}(r,z)B_{\parallel} + (\sigma_r(r,z) + \sigma_z(r,z))B_{\perp}] dz + n\alpha_n \int_0^{d/2} T(r,z) dz \quad (68)$$

ΔP_r^* and ΔP_{θ}^* are the pathlength changes for radial and tangential polarization over a half thickness of the disc. σ_r , σ_{θ} , σ_z and ϵ_z are radial, tangential, and axial stresses and axial strain, respectively. B_{\parallel} and B_{\perp} are stress optic coefficients. T , α_n , n and n' are temperature, thermal index coefficient, index of the disc and index of the immersion medium, respectively. The first integral will be referred to as the axial surface displacement, $w(z)$.

When the results are plotted for various radial positions, r , the curves produced will identify the wavefront forms for the two polarizations. The effects of discs immersed in air will be

different from discs immersed in water and this is accounted for by proper assignment of the index value, n' , in reducing Eqs. (67) and (68). To find the total distortion in a full array of discs, one must simply multiply the values obtained by the proper number of half-sections which constitute the complete system.

The single disc results are described in Figs. 4 and 5. In Fig. 4, the stress distribution is given for 10 mm discs along the cross-sectional planes $z/L = 0$, $z/L = 0.4$, $z/L = 0.8$ and $z/L = 1$, where $L = d/2$ and assuming all surfaces are cooled. These results depict the non-uniform state of stress which exists. Maxima in the tensile stresses occur, as one would expect, at central locations of the surfaces coincident with the quadrant reference axes, r and z . The stresses also appear to be of approximately equal and opposite magnitude at the center of the disc where the field is strongly compressive. The maximum surface tensile stress exhibited of about 3,000 psi shows, at a loading of 3.2 W/cm^2 , the disc to be near 30 percent of its fracture level assuming 10,000 psi the limit of the glass. Lowering the stress level becomes significant when the thickness of the disc can be reduced. The maximum stress occurring in a 3 mm disc (computed, but not shown) at 3.2 W/cm^2 loading is only 300 psi or about 3 percent of its fracture limit. The results for a 10 mm disc in which only axial cooling is effective, the circumferential surface being insulated to heat flow, showed that a maximum tensile stress would be developed of 3600 psi. The one-dimensional axial cooled disc exhibits somewhat higher stresses because overall temperatures increase due to diminished surface area for the cooling, and consequently greater internal expansion of the material occurs. At a thermal loading of 3.2 W/cm^2 , the temperature difference between center and edge of the 10 mm thick discs is 51 and 42°C for the cases of axial cooling and axial and radial cooling respectively. For the 3 mm thick disc this temperature difference is only 4.6°C for both cases of cooling.

Plots describing the optical pathlength change in typical AO 3835 laser glass for radial and tangential beam polarizations for 10 mm and 3 mm water immersed discs appear in Fig. 5.

Since the optical distortions in the N-1 were measured at $0.63 \text{ } \mu\text{m}$ wavelength and the thermal index coefficient $\alpha_n = 1/n(dn/dt)$ varies from -0.86 to $-2.2 \times 10^{-4} \text{ } ^\circ\text{C}^{-1}$ for wavelength of $0.63 \text{ } \mu\text{m}$ and $1.06 \text{ } \mu\text{m}$ respectively, the change in optical pathlength was calculated for both wavelengths. Fig. 5 shows how the mode of cooling introduces characteristic patterns which influence the birefringence as well as degree of optical power. When radial and axial cooling are both effective on surfaces of

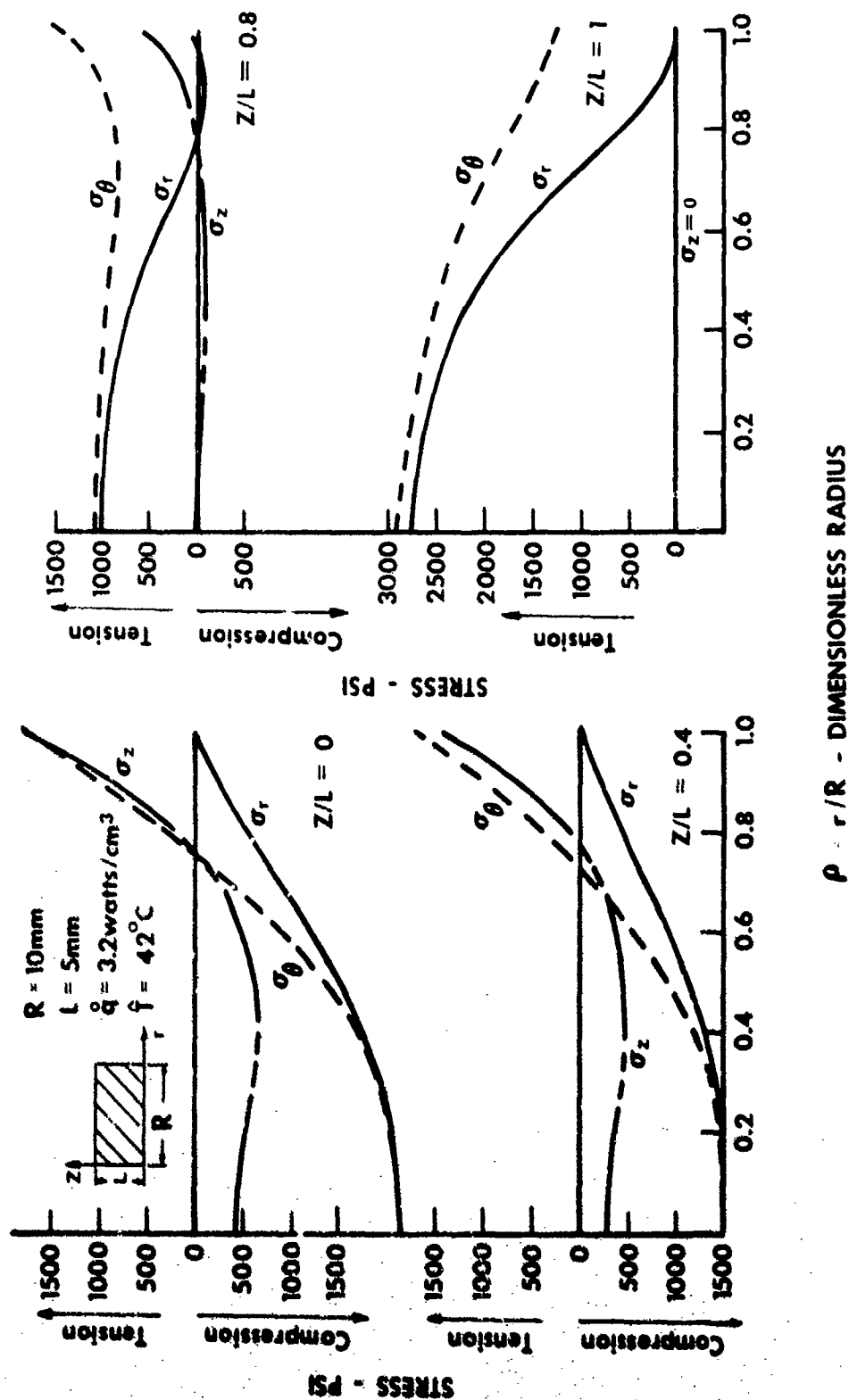


Fig. 4 Computed principal stresses for 10 mm thick discs with uniform internal heating at 3.2 W/cm³ and uniform cooling of all surfaces

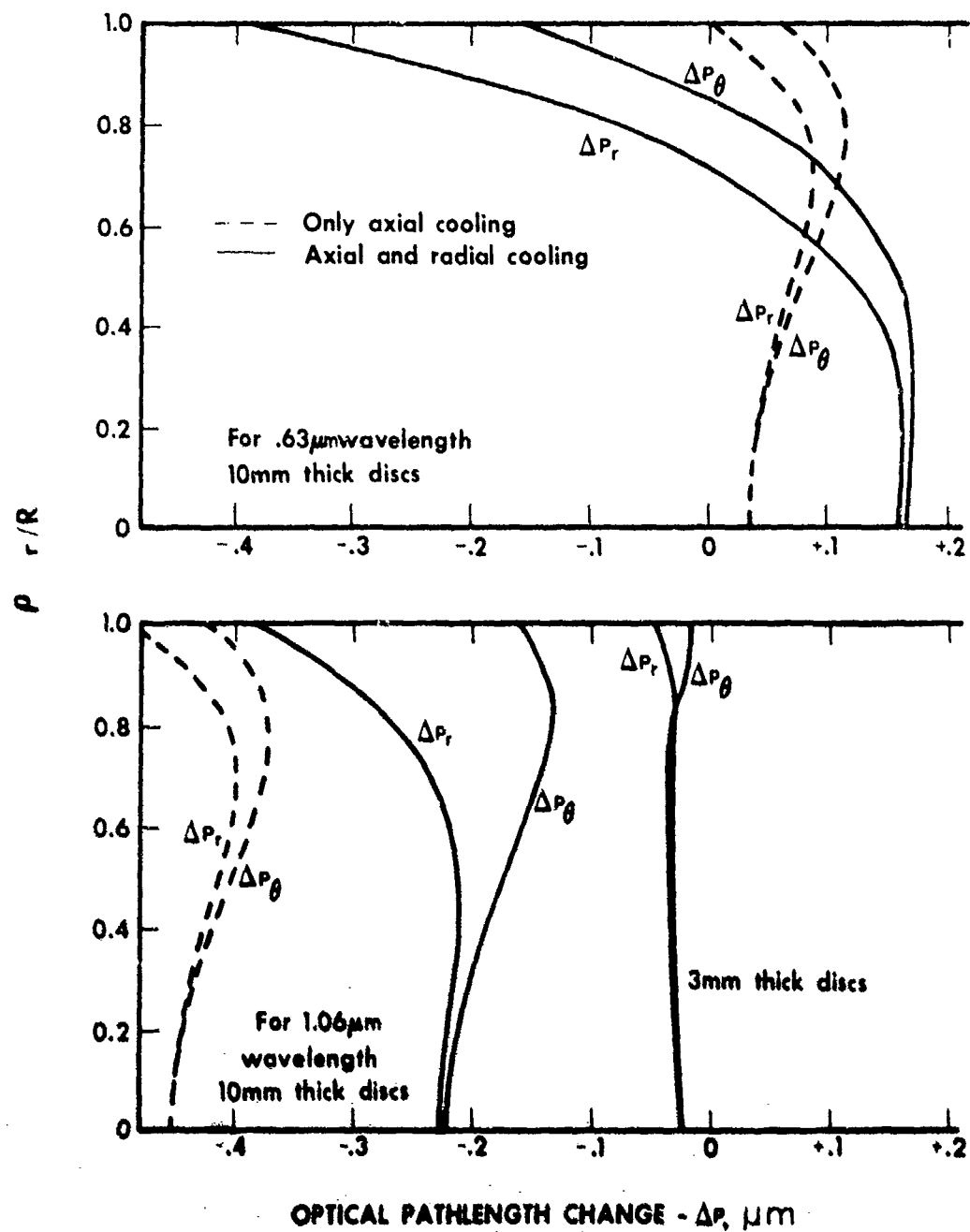


Fig. 5 Change in optical pathlength for radial and tangential polarizations per cm length of laser glass for 10 and 3 mm thick discs with uniform internal heating at 3.2 W/cm^3 and water cooling

the disc, the predominant lensing behavior will be positive at 0.63 μm wavelength. When no cooling takes place at the radial boundary, the optical power produced by the axial cooling alone will be negative for the central part of the discs and positive for the outer zones. In this case, the radial distortions are the same for 0.63 and 1.06 μm wavelength. For the case of axial and radial cooling of the 10 mm thick discs and for 1.06 μm wavelength, the induced optical power will be predominately positive or negative, respectively, for the radial or tangential beam polarization. However, the average induced optical power for AO 3835 laser glass at 1.06 μm wavelength for both beam polarizations and both modes of cooling is well compensated and practically zero because of its large negative thermal index coefficient.

In order to make a comparison of the analytical results derived in this section with experimental measurements, the cumulative change in optical pathlength ΔP was related to diopter power D using the following relationship

$$D = 2\Delta P / R^2 \quad (69)$$

Using a linearly polarized gas laser beam in the experiments, both components of change in pathlength for radial and tangential polarization contributed equally to the optical power. From the values plotted in Fig. 5, the cumulative pathlength change through 42 cm of laser glass in the array becomes, to a first approximation, additive, considering each element constitutes a simple lens. The total pathlength difference, then, between center and edge amounts to about 17 μm for the case of axial and radial cooling of the 10 mm thick discs with uniform internal heating at 3.2 W/cm³. This corresponds to an induced optical power of +0.34 diopter at an electrical input of 2.2 kW into the N-1. However, with no radial cooling, the average induced optical power is practically zero for 0.63 μm radiation as shown in Fig. 5. In the experiment an induced optical power of about +0.07 diopter was observed as shown in Fig. 22, indicating a situation of principal axial cooling with partial radial cooling, which seems reasonable. Fig. 5 shows also the change in optical pathlength for 1.06 μm radiation for 10 mm and 3 mm thick discs respectively. The results obtained for axial and radial cooling are shown in solid lines and for only axial cooling in dashed lines. All these curves show induced optical distortions but practically no average spherical power. The optical distortions in the 3 mm thick discs are more than an order of magnitude less than for the 10 mm thick discs. The magnitude of optical distortions can therefore be lowered for a given thermal loading by reducing the thickness and increasing the number of discs in the array.

Calculations for different volumetric thermal loadings shown a linear relationship between change in optical pathlength and loading of the discs. The calculations also show the contribution of the axial surface displacement $w(z)$ to the induced optical distortions could be adjusted by the index of the immersion medium. Taking these factors into account, there seems to be some possibility to design an optimum geometry and cooling scheme to effectively limit the thermo-optical effects even further.

SECTION IV

INVESTIGATION OF COOLANTS AND MATERIALS

1. SELECTION OF COOLANTS

In previous work with disc systems, heavy water was found to be a usable coolant because of its apparent inertness to high intensity flashlamp and improved transmission qualities over ordinary water at the neodymium wavelength, $1.06\ \mu\text{m}$. A prime drawback is that water has an index of refraction considerably lower than that of glass. Its use requires either that the array of discs be positioned at Brewster's angle, which allows the stimulated radiation to propagate in a preferred plane of polarization, or that the discs be antireflection (AR) coated, to eliminate Fresnel losses from the surfaces. In addition, heavy water still exhibits a finite absorption of about $0.85\%/cm$ for $1.06\ \mu\text{m}$ laser light in our measurements.

A program was therefore initiated to find liquids which displayed little or no absorption through the principal laser pumping wavelengths and at the principal neodymium fluorescence line. These candidates were submitted to appropriate irradiation tests to establish a measure of their resistance to degradation under such conditions.

Table III lists the various compounds that were examined. Transmission characteristics were measured from 0.58 to $1.2\ \mu\text{m}$ through a 10 cm length cell on the Cary Model 14 recording spectrophotometer for the "as supplied" condition of the samples. In addition, differential measurements were taken on 1 cm cells after irradiation tests were conducted. Liquids having refractive index values both lower and higher than that of typical laser glass at $n_d = 1.52$ were looked at with the intent of possibly compounding an acceptable high and low value candidate. This would be done by employing the Clausius-Mosotti relationship and proportioning the molar polarization of each to achieve the index desired. Liquids which belong to the same family of compounds would in general be miscible in one another.

To evaluate the durability of the liquids, a 10 cm^3 sample was placed in the center of a helical flashlamp and exposed to UV filtered flashlight for 120 consecutive shots with 1 kJ input per pulse. This corresponds to a higher volumetric radiation intensity than anticipated in the disc laser.

Table III. SPECTRAL ABSORPTION CHARACTERISTICS OF COOLANTS

Liquid	Grade*	n _d	As Supplied**				Increase after irradiating with flashlamp at 100 J/cm ³ liquid (120 shots)**				Increase after irradiating with 1.06 μm laser source at 30 J/cm ² Long Pulse (50 shots)**			
			0.59μm	0.81μm	1.06μm	0.59μm	0.81μm	1.06μm	0.59μm	0.81μm	1.06μm	0.59μm	0.81μm	1.06μm
Heavy Water														
Perchloroethylene	R	1.33	N	0.2	0.85	0.2	0.1	0.1	N .5 kJ	N .5 kJ	0.1			
FC-104		1.49	N	N	0.05	N	N	N	N	N	N			
Pentachloroethane	T	1.28												
Tetrachloroethane	R	1.50	0.15	0.1	0.4	0.2	N	N						
Tetrabromoethane	R	1.5	0.4	0.22	1.0									
Pentachloropropane	R	1.63	0.55	0.15	0.2	3.5	1.5	1.2						
Hexachloropropane	T	1.51	0.6	0.21	0.8									
Heptafluorotrichloro-butane	T	3.8		2.1	1.75									
Heptafluorotrichloro-butane	R	1.35	N	0.02	0.05	N	N	N	2.0	1.1	1.7			
Heptachloropropane	T	1.54	0.4	0.86	1.6									
Freon '214'	D	1.395	0.2	0.18	0.23	2.0	1.2	0.5	4.5	0.6	N			
After Filtration														
Heptachloropropane	T	1.54	0.2	0.05	0.27	1.2	1.1	1.0	N	N	N			
Freon '214'	D	1.395	N	N	0.05	(a) N	N	N	N	N	N			

* Grade: R - reagent, T - technical, D - developmental

** Units: %/cm, N = no absorption detectable - less than 0.1%/cm

Filtration: Through activated alumina column and 0.22 μm Millipore filter
(a) 5% potassium chromate solution for UV filtering.

Durability against long-pulse laser irradiation was tested by exposing a 4 cm³ sample to a 6 mm diameter, 8 joule laser beam for 50 consecutive shots.

Only heptachloropropane was tested with Q-switched pulses of 40 nsec duration and an energy density of 20 J/cm². After 45 shots, a loss of 5%/cm was observed in the visible as well as in the near infrared. After filtration through a 0.22 μ m Millipore filter this greyness was reduced to 1%/cm.

A summary of results appears in Table III. The spectral absorption changes are reported here for two important wavelengths associated with the neodymium absorption spectrum and one at the laser emission line. A more detailed description of this test is reported in reference 13.

2. OPTICAL DISTORTIONS IN COOLANTS

The most promising fluids for cooling the B-1 and the N-1 were Freon 214 and heptachloropropane. However, when Freon 214 was installed in the B-1, attempts to measure the gain of this device revealed induced losses instead of gain. These induced losses were also observed when the discs were removed and the cavity filled only with Freon 214. The magnitude of this induced loss varied from shot to shot, which made it difficult to investigate this behavior.

Similar problems were encountered when heptachloropropane was used as coolant for the N-1. With the N-1 set up as a long pulse oscillator, threshold was found to be at 4 kJ input. Above this input level laser oscillations have been observed, but the output was very low and not reproducible, compared to the results obtained with D₂O as coolant.

During these tests, the coolants were well protected from UV radiation, using yellow filter tubing which absorbs strongly below 500 nm wavelength. The coolants were not circulating; however, enough time was allowed between shots to reach thermal equilibrium. More detailed measurements to determine if thermal gradients in the fluids could cause this behavior are also reported in Ref. [13].

The tentative conclusion drawn from these experiments is that optical distortions, due to the relative high dn/dT values for Freon 214 and heptachloropropane cause the problems mentioned.

3. DETERMINATION OF dn/dT FOR COOLANTS

Due to a lack of published data of the dn/dT value for specific coolants, the refractive index change as a function of temperature was measured at 6328 and 10,790Å, using a heated hollow prism, as described in reference 13.

The results of the experiment are shown in Fig. 6.

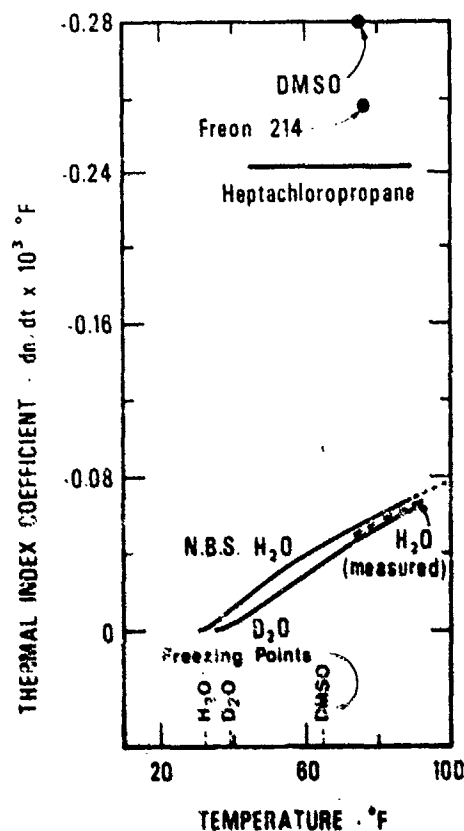


Fig. 6 Dependence of the thermal index coefficient on temperature for different coolants

The curve for ordinary water has been taken from precise refractive index measurements [14] by the National Bureau of Standards for the wavelength 5850Å. Within the accuracy of the present experiment, heptachloropropane and heavy water behaved essentially the same for the two wavelengths, 6328Å and 10,790Å, used. Also, as depicted in Fig. 6, the dn/dT obtained for heptachloropropane was constant over the temperature range investigated yielding a value of $-0.24 \times 10^{-3}/^{\circ}\text{F}$. Upon comparison with other experimental

results reported [15], another halogenated compound, Freon 214, is found to have a value of $-0.256 \times 10^{-3}/^{\circ}\text{F}$. DMSO, sometimes suggested as coolant because of the closer index of 1.477 in respect to glass, has a dn/dT value of $-0.28 \times 10^{-6}/^{\circ}\text{F}$ at room temperature. DMSO has also the disadvantage of a high freezing point of 18.5°C and a relatively low convective heat transfer coefficient. The measurements for heavy water, on the other hand, show that dn/dT diminishes in magnitude with decreasing temperature and becomes zero near the freezing point at 3.8°C . In these respects, the thermal-optic characteristics of ordinary water and heavy water appear the same.

A few experimental points for ordinary water were also obtained between 70 and 90°F to compare with the National Bureau of Standards data presented. These data are represented by a dashed curve in Fig. 6. The results suggest that operation of a heavy water immersed disc laser device near the freezing point may prove a way of minimizing thermal distortion caused by temperature gradients in the coolant.

4. D_2O COOLING UNIT

After evaluating other liquids, D_2O seemed to be the only fluid suitable for use in disc lasers. Its primary advantages are a low value of dn/dT , stability in the disc laser environment, safety, low transmission loss at $1.06 \mu\text{m}$, non-toxicity and reasonably low cost.

A major disadvantage of D_2O is its hygroscopic nature. A special D_2O circulation system was constructed which is completely sealed from the atmosphere to prevent moisture contamination. A block diagram is shown in Fig. 7.

All system components were stainless steel or some form of plastic compatible with the D_2O , which seems to be about as corrosive as H_2O . A pressurized reservoir consisting of a piston and spring was used to hold a constant pressure with respect to the surrounding atmosphere as well as replace D_2O losses due to seepage. A 293 mm diameter Millipore filter was installed in line using a $0.22 \mu\text{m}$ filter, which eliminated the greyness in the D_2O below $0.7 \mu\text{m}$ wavelength, observed during preliminary tests.

Pressure gages, electrically-insulated thermocouples, and bubble traps were placed as close as practical to the inlet and outlet of the laser. To remove any residual moisture, the entire system was purged with N_2 before installing the D_2O . The total volume of about 4.5 liters of coolant required to fill the

cooling unit was kept low to reduce cost. The D_2O to water heat exchanger dissipates 2 kW at flow rates of 1 GPM with a temperature difference of about $10^\circ C$.

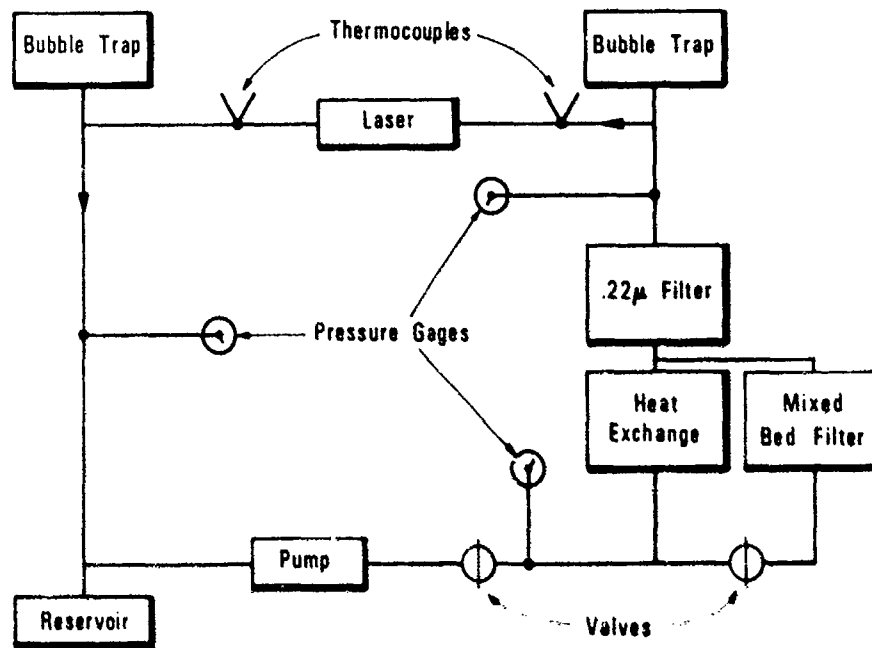


Fig. 7 D_2O cooling system

After several months of use of this cooling system, parts of the stainless steel heat exchanger were found to rust. This problem was corrected by use of an epoxy coating.

Over long periods of time, the transmission of the disc lasers still deteriorated, which was probably caused by bacterial growth on the disc faces evidenced in the form of a brown deposit. A bacteria filter and deionizer was installed which corrected this problem. This mixed bed filter had to be deuterized in order to remove any normal water. After three fillings of the filter with 98 +% D_2O , the normal water in the filter was essentially removed as indicated by the transmission curves of the D_2O used in the filter.

5. MATERIAL TESTS

For the design of disc lasers, optically clear plastics or silicon rubbers for mounting or holding of the discs would be

useful, to avoid losses due to absorption or vignette. These materials could also provide a strain-free cladding to control radial heat flow.

Thirty-two transparent samples from different manufacturers as listed in Ref. [14] were submersed in water and subjected to flashlamp light without UV protection. The flashlamps were operated at 1 pps with an input energy of 1.4 kJ in a 0.6 msec pulse.

Virtually all samples developed damage sites within the material after only a few shots, except for Plexiglas UVA, and CR-39. The damage seemed to occur due to pockets of uncured resin scattered throughout the sample and particulate contaminants. Several rails for the B-2 design as described in Section V.3 were machined out of Plexiglas. However, the fingers of the rails were weak because of surface imperfections introduced during the milling operation. These imperfections might be overcome by molding. CR-39 requires a special mold which is inert to its chemical components and will not retard curing while Plexiglas requires a special mold for high pressure injection molding. Because of cost and time considerations, opaque materials were tested to determine possible degradation of these materials or the coolant in a flashlamp pumped environment.

Stainless steel, Teflon, aluminum, brass, and nickel were submersed in D_2O and exposed to flashlamp light with 4 kJ input energy per pulse. The Teflon was burned on the surface by the pump light which made this material unacceptable. The aluminum and brass withstood the pump light without changing the absorption coefficient of the D_2O at $1.06 \mu m$; however, these materials did cause greyness in the UV and visible portions of the spectrum. Stainless steel and nickel were the two most promising materials; stainless steel was the first choice because of easier machining.

6. SOLARIZATION PROTECTION FOR DISC LASERS

Wavelengths shorter than about 400 nm do not significantly contribute to pumping neodymium in glass. They do contribute to solarization in all known useful laser glass hosts. Wavelengths shorter than 400 nm must therefore be kept out of the laser glass by filtering at some point. This can be done by introducing a material in the laser glass which absorbs strongly below 400 nm, but this puts excess heat and strain in the laser glass pieces. A better approach appears to be one in which these unwanted shorter wavelengths are retained in the flashlamp cooling system, since other elements such as the reflective wraps and the square Pyrex tube also suffer degradation due to these shorter wavelengths.

A search was therefore initiated to obtain a sharp cutoff filter glass at 400 nm, shaped into tubing, which could be used as flashlamp water jackets. Unfortunately, no manufacturer contacted would supply their filter glass in tubing form of any size. Schott and others would supply billets which could be cored and drawn at great expense.

As an interim solution, Schott's Supremex tubing, which is a sharp cutoff UV filter at 350 nm, was utilized. It has been used as an effective solarization protection filter for smaller devices developed at AO despite the low UV cutoff point. However, in the disc application, Supremex was found to be unsatisfactory because the discs became solarized after a few thousand shots causing the slope efficiency to drop by about 15%.

It has long been established that an aqueous 10% sodium nitrite solution is an excellent UV absorber, cutting off at 400 nm, and showing no effect on the performance of the laser. However, it does have the drawback of being very corrosive and highly conducting electrically. The advantage of using a liquid UV absorber is that the heat generated by the UV emitted from the flashlamp may be easily removed with heat exchangers.

Two different versions of sodium nitrite-cooled flashlamps were constructed and tested as reported in [16]. However, these approaches, using a three-section coolant jacket or graded glass seal, were not found reliable for high power and long-term operation. The most reliable solution was a flashlamp design with an inner coolant jacket for distilled water and an outer tubing for the sodium nitrite solution. Standard FXG-47C-18 flashlamps with standard EG&G hardware to make the water-tight seal and electrical connections were used in this design. A set of four of these flashlamps was successfully operated up to 35 kW average input power and used for all tests on the B-3 and N-3 disc lasers.

7. AR COATINGS FOR NORMAL INCIDENCE DISC LASERS

Since no suitable index matching fluid was found, the discs for the normal incidence disc laser had to be AR coated to avoid excessive reflection losses of the glass-coolant interfaces. A material with an index of 1.41 at 1.06 μm wavelength would be ideal to match the index for AO laser glass of 1.508 to heavy water which has an index of 1.32 at 1.06 μm . Magnesium fluoride and quartz with an index of 1.37 and 1.45 respectively, come closest to this requirement. For a quarter-wave coating with a material having an index difference Δn in respect to the ideal index n , the resulting reflectivity can be approximated by

$$R \approx \left(\frac{\Delta n}{n} \right)^2 \approx 0.08\% \quad (70)$$

for MgF_2 and quartz coatings on AO laser glass.

Without coating, a reflection loss of 0.45% per surface would be encountered. The relative transmission, taking into account the reflection losses through a disc array with N surfaces, is

$$T_R = (1 - R)^N \approx 66\% \quad (71)$$

for the N-1 with 46 uncoated discs. With MgF_2 coatings, this relative transmission could be increased to 93%, which agrees well with the measured increase in transmission of the N-1 from 49% to 72% as discussed in Section VI.1. However, the MgF_2 coatings were found to deteriorate during several months of testing of the N-1. The greatest deterioration was observed in the active area of the discs. This would suggest that in addition to being dissolved by the water and damaged by pump radiation, the coatings were also damaged by $1.06 \mu\text{m}$ radiation.

Realizing the need for a suitable antireflection coating for the normal incidence discs, sputtered quartz coatings were investigated for damage resistance during disc laser operation. A sputtered quartz coating on an undoped laser glass substrate was damage tested and found to be as durable to long pulse $1.06 \mu\text{m}$ radiation as MgF_2 on the same substrate. As a final test, alternate discs throughout the stack were coated with sputtered quartz and MgF_2 . H_2O was used as the coolant because it has the same physical properties as D_2O with the advantage of easier handling. The N-1 was operated at 2.0 kW average input power, which damaged the original MgF_2 coatings. After about the same number of flash-lamp pulses and three times more exposure to flowing water as the original MgF_2 coatings, the coated discs were removed and inspected. The MgF_2 was again severely damaged while the quartz coatings appeared undamaged.

A set of 91 discs for the N-2 disc laser was coated with quartz. The transmission of the N-2 was measured at $1.06 \mu\text{m}$ and found to be 46% instead of about 68% as estimated.

Assuming an absorption loss in the coolant and laser glass of about 20% results in an actual reflection loss of 42%, which corresponds to a reflectivity of 0.23% per surface.

Monitoring of the thickness is difficult with our present facilities because the reflectivity of the disc in air varies only from 8% without coating to 6.7% with the coating. A second coating was done at a different facility, which resulted in a transmission through the N-2 device of 55%. The actual reflection loss of about 30% was still twice as high as expected for the 192 surfaces of the N-2.

In order to overcome this problem, discs were fabricated from OI laser glass, which has an index of 1.556 and provides a better index match to the quartz coating and the heavy water. With a quarter-wave quartz coating, the reflectivity per surface would be reduced to about 0.01%, which corresponds to an expected total reflection loss through the N-3 device of only 2%. The measured transmission through the N-3 was 71%, which was quite an improvement over the previous results but was still 11% lower than expected for a perfect coating. Better monitoring of the coating process could still provide some improvement in transmission and performance of the N-3 disc laser.

SECTION V

DESCRIPTION OF THE DIFFERENT DISC LASERS

1. THE FIRST BREWSTER DISC LASER (B-1)

The mechanical assembly of the B-1 as shown in Fig. 8 consists of 30 discs mounted in a rectangular metal frame with the faces of the discs parallel to each other, but at nearly Brewster's angle to the optic axis, provided coolants with an index of refraction of about 1.35 are used. In such an array, a beam parallel to the geometrical axis will be displaced sideways, causing vignette. To eliminate vignetting, the angles of the beam in the coolant, $(\alpha_1 - \theta)$ and the discs $(\theta - \alpha_2)$ with respect to the geometrical axis are chosen to compensate for this displacement as shown in Fig. 9. The required angles for the discs and the windows are determined by the indices of refraction n , the spacing between the discs s , the thickness of the discs d and the conditions for:

$$\begin{aligned} \text{I. Brewster's angle: } \alpha_1 + \alpha_2 &= 90^\circ \text{ and} \\ \tan \alpha_1 &= n_2/n_1 \end{aligned} \quad (71)$$

$$\begin{aligned} \text{II. No vignette: } l_1 \sin (\alpha_1 - \theta) \\ = l_2 \sin (\theta - \alpha_2) \end{aligned} \quad (72)$$

$$\begin{aligned} \text{III. Refraction at} \quad n_0 \sin \phi &= n_1 \sin \beta \\ \text{the windows:} \quad &= n_1 \sin (\phi + \alpha_1 - \theta) \end{aligned} \quad (73)$$

with the results:

$$\tan \theta = \frac{s_1 n_2/n_1 + s_2 n_1/n_2}{s_1 + s_2} \quad (74)$$

and

$$\tan \phi = \frac{n_1 \sin (\alpha_1 - \theta)}{n_0 - n_1 \cos (\alpha_1 - \theta)} \quad (75)$$

For 3 mm thick discs, a spacing of 1.2 mm and the indices of refraction $n_0 = n_2 = 1.50$ and $n_1 = 1.35$, the angle for the disc is $\theta \approx 44^\circ$ and the angle for the window is $\phi \approx 33^\circ$. The discs were made from a clad piece of 2 % Nd-doped glass. The dimensions of each disc are shown in Fig. 10. The

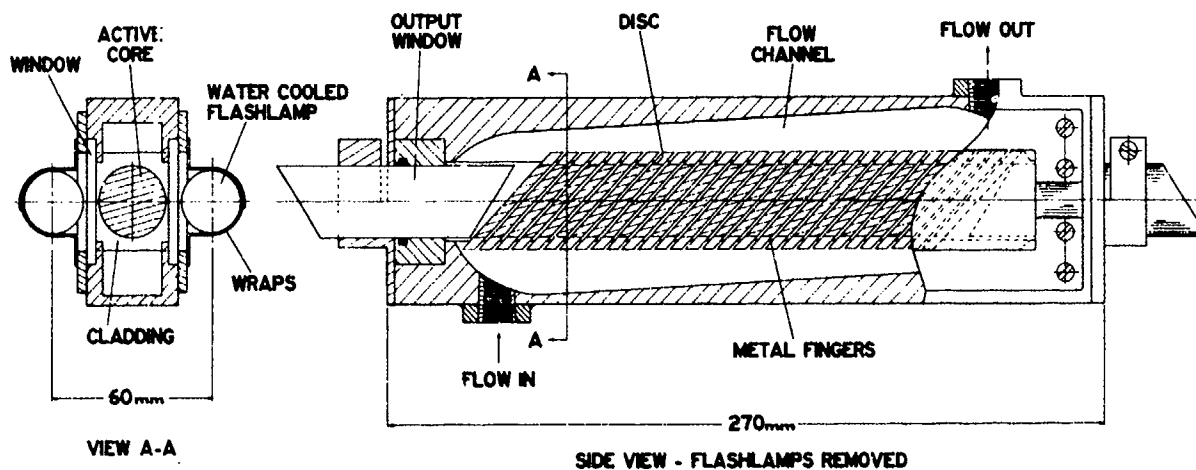


Fig. 8 Brewster-angled disc laser B-1

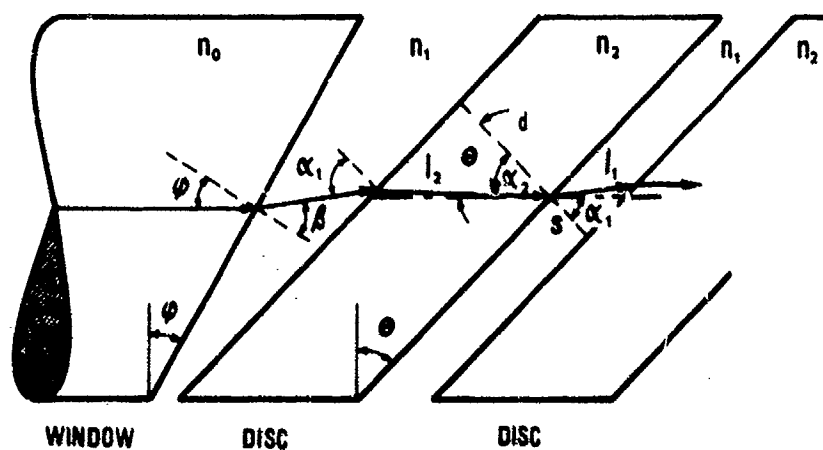


Fig. 9 Conditions for vignette compensation

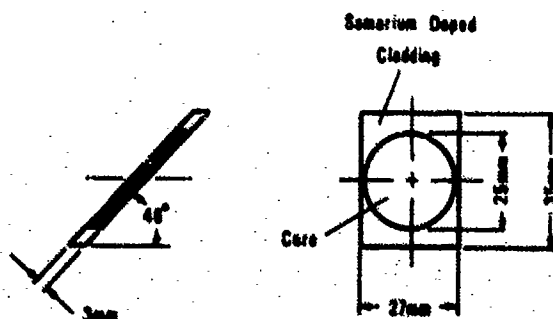


Fig. 10 Clad discs for the B-1

center active core, when viewed along the optic axis, was 25 mm in diameter. The windows were of laser glass with the outside faces cut at Brewster's angle to the optic axis, and the inside faces cut at the vignette compensating angle ϕ . The glass discs had inherent core-cladding strain and were only flat to a few fringes. At room temperature, the cladding was in compression and the core in tension, which increases the average power capability. The discs were polished in two sets of 17 discs each, which does not allow a better flatness. To obtain a flatness of a fraction of a wave, the discs would have to be polished individually. Since this device was built only for preliminary tests, individual figuring was considered too time consuming as well as too expensive. When all 30 discs were assembled, some static cylindrical power of about +0.2 diopter and spherical power of about +0.1 diopter was observed.

The coolant flow between discs was all-parallel to allow very high flow rates in order to reduce the thermal gradient along the coolant flow path and reduce beam steering to a negligible amount. However, due to pressure losses in the cooling system and a pressure limit of about 5 psi due to leakage at the window seals, a flow rate of only 1.5 GPM was possible, despite the good flow characteristics of the B-1 as shown in Fig. 3. The 3.5 mm thick Pyrex side windows were sealed with RTV silicone rubber, after an attempt to use O-ring seals failed. The entire assembly was mounted with the discs vertical to reduce bubble problems.

Two water-cooled EG&G FX 47-6.5 flashtubes were positioned perpendicular to the edges of the discs with wraps terminated at the side windows. The flashlamps were connected in series to a 40 kW power supply which consisted of an energy storage bank with 640 μ F capacitance and 250 μ H inductance. The flashlamps were triggered, using an EG&G TR-136A injection trigger transformer in series with the lamps. The flashlamp pulse duration was measured at 0.83 msec, which was about optimum for the B-1 disc laser.

For UV protection, a yellow filter tubing was planned to be used as water jacket for the flashlamps. This filter tubing absorbs strongly below 500 nm wavelength, but also reduces the effective pumping of the device by about 20%. Most tests were therefore taken with Pyrex tubes around the flashlamps, which caused a slow deterioration of the B-1 performance due to solari-
zation.

2. THE FIRST NORMAL INCIDENCE DISC LASER (N-1)

The N-1 design utilized a quantity of generally-square cross sectioned discs closely fitted in a precision-bore tube, providing support and alignment for the discs. The mechanical assembly of the N-1 consisted of 46 discs with optically-polished faces perpendicular to the optic axis, installed in a square Pyrex tube as shown in Fig. 11. Each disc consists of an 18 mm diameter core of 2% Nd-doped AO 1838 laser glass fused into a samarium-doped cladding glass. The thickness of each disc was 10 mm while the sides are 22 mm as shown in Fig. 12. Two opposite corners of each disc are relieved in various amounts for coolant flow. The two other corners have steps cut out to receive Teflon balls as spacers. The spacing between each disc was 1 mm, which resulted in a glass-coolant spacing ratio of 10:1. Since the cooling fluid proposed for the N-1 was index matching, no effort was taken to polish the discs better than a few fringes in flatness.

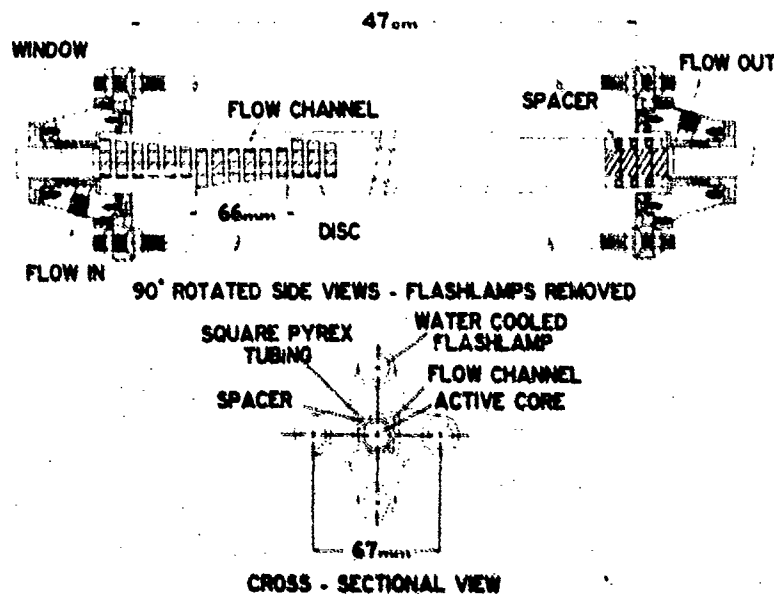


Fig. 11 Normal incidence disc laser N-1

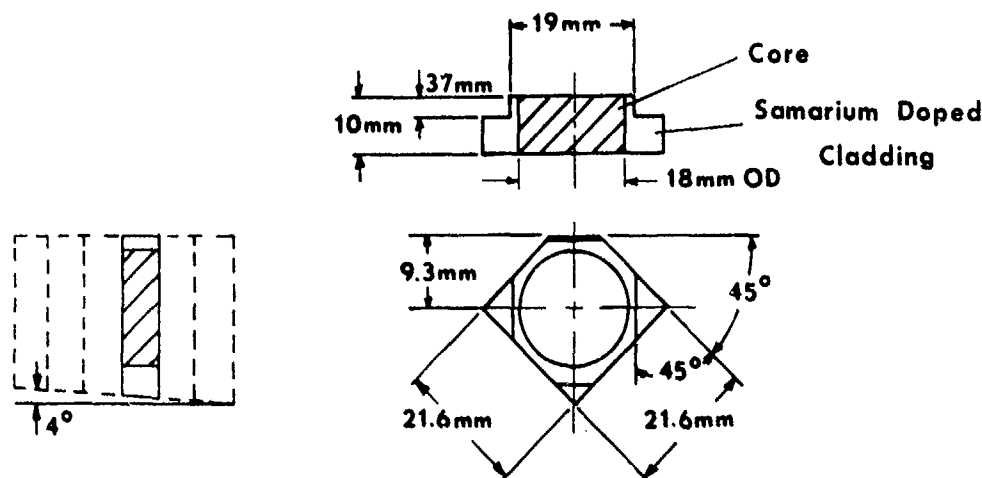


Fig. 12 Clad disc for N-1

The coolant flow was a series-parallel arrangement consisting of 8 groups of 6 discs in series with each other, with each group of 6 discs having parallel flow. At a pressure of 10 psi at the entrance part of the N-1, a flow rate of 1.4 GPM was measured, which was sufficient for adequate cooling of the discs. Higher flow rates would be desirable to reduce the thermal-optic distortion in the coolant, but pressure losses in the cooling system raised the pressure in the N-1 appreciably. A pressure loss of 1.7 psi/GPM^2 was estimated, which is about one half of the measured value. Since the flow path changes continuously in direction, fully developed flow conditions are never actually attained in this design. Loss in fluid momentum and friction because of vortices add to the flow resistance, especially for the case where the flow direction was reversed after each disc, as in the initial N-1 disc arrangement.

Nylon bulkheads support the flashlamps and the square Pyrex tube with the discs. The device was optically pumped with four EG&G FX 47-18 flashlamps surrounded by Pyrex tubing to prevent darkening of the silver wraps. The flashlamps were connected to the two energy storage banks of the 40 kW power supply in two sets of 2 lamps in series. Since the yellow filter tubing was found to reduce the effective pumping to about 80%, no UV protection other than Pyrex tubing was used for most measurements, which also resulted in a slow deterioration of the N-1 performance

due to solarization. In addition, difficulties in maintaining the coolant free of contamination were experienced during the evaluation of this device.

3. THE B-2 AND B-3 BREWSTER DISC LASERS

The new disc laser was designed, combining the advantages of the two previous disc devices in a single unit.

The advantage of the N-1 design was the more uniform and more efficient pumping geometry. With four flashlamps in a close-wrap configuration, uniform pumping could be obtained within ± 1 dB at a 20 dB gain level, provided the correct Nd concentration is chosen. However, the N-1 discs were too thick, because one disc fractured at 6 kW input to the device and thermal lensing was observed. In addition, the coatings required for the N-1 discs deteriorated. The clear advantage of a Brewster disc laser is the elimination of reflection losses. The B-1 had also a more uniform flow distribution over the disc surfaces than the N-1. The holding of the discs in the B-1 allowed the exchange of a single disc, while in the N-1, a whole array of discs had to be removed.

In order to allow a close comparison between the new disc laser and the N-1, the same pump geometry was chosen, utilizing the same square Pyrex tubing, surrounded by four linear water-cooled flashlamps in a close-wrap configuration. An active pump length of 457 mm and heavy water as coolant was maintained, since all other coolants previously tested had shown excessive thermal-optic distortions. To avoid coatings required in the normal incidence approach without index matching coolant, discs at Brewster's angle were chosen.

In the new disc laser design, the discs were held by four rails which were mounted on an end piece to form a self-supporting cage, allowing immediate access to each individual disc. The rails were placed in the corners of the square Pyrex tubing as shown in Fig. 13. This design provided longitudinal flow channels, which were almost as wide as the discs, allowing uniform flow and cooling across the disc surfaces. This design did not require clad discs, since only a negligible amount of active volume was obstructed by the fingers of the rails. Discs clad with a $1.06 \mu\text{m}$ absorbing glass would be desirable from the standpoint of ease of holding the discs mechanically and suppressing off-axis depletion. However, these advantages are offset by the strain induced in the core-cladding interface at some operating point, as the disc is heated by pump radiation due to the difference

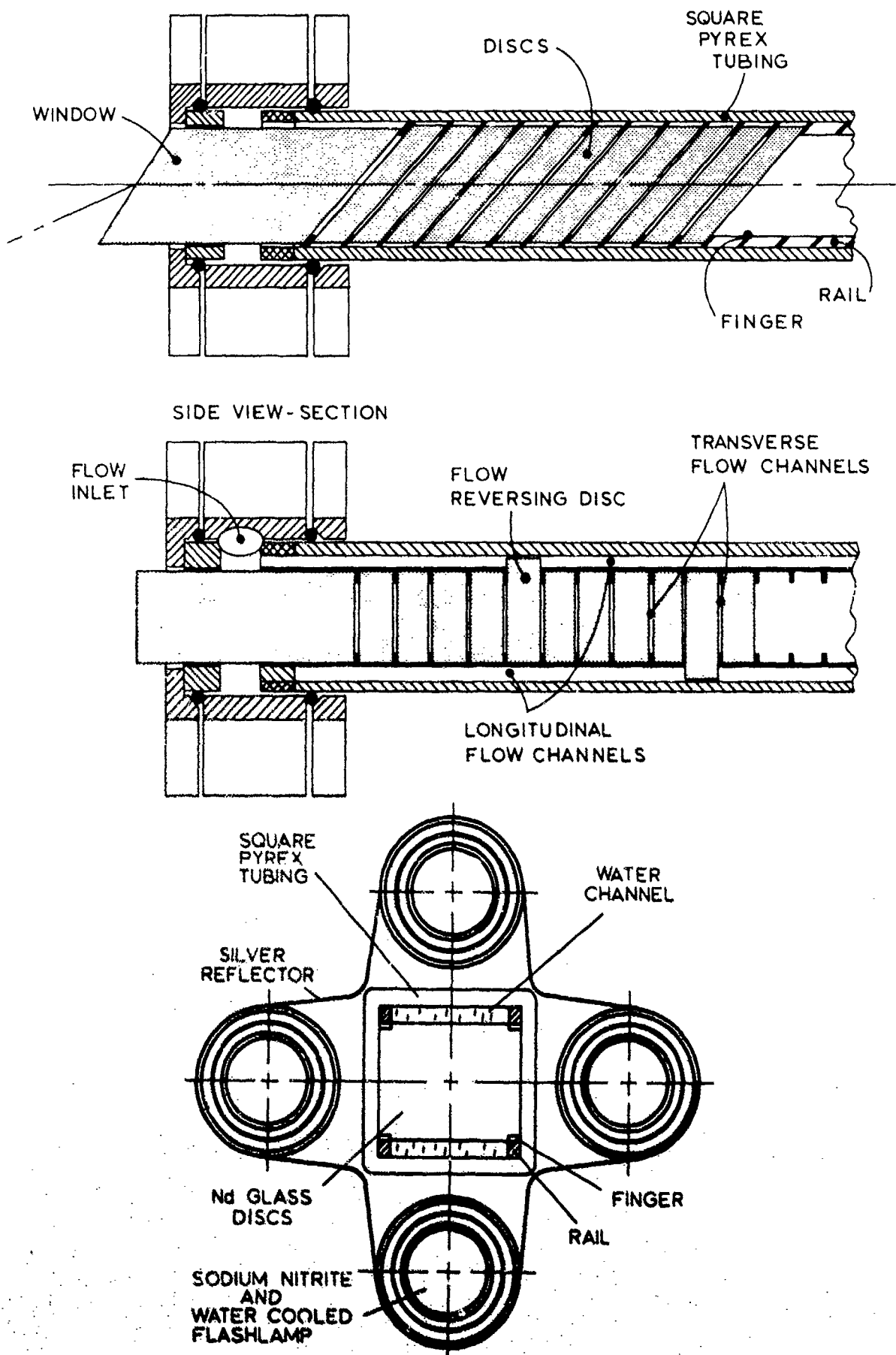


Fig. 13 Cross-sectional view of segmented Nd glass laser

in the Nd-doped glass core and the cladding glass absorption curves, and the increased cost of cladding the discs.

To determine optimum dimensions for the thickness of the discs d , the spacing between discs s and the width of the longitudinal flow channels a , the analysis of the flow distribution and the thermal distortions in disc elements as outlined in Section II were utilized. The thickness of the discs was determined from theoretical calculations on 3 mm and 10 mm thick discs. The maximum surface tensile stress was found to be proportional to the square of the disc thickness and linear with volumetric thermal loading. From previous experiments, a 10 mm thick N-1 disc fractured at 6 kW input. Since the volume of laser glass in the new disc laser could be increased by about 50%, eliminating the cladding, about 5 mm thick discs should allow a maximum input power of 40 kW without fracture.

A glass-to-coolant ratio of greater than 10:1 was found desirable from our previous measurements, which means a spacing of less than 0.5 mm for the new disc laser. A lower limit for the spacing, set by the strength of the fingers on the rails, was determined to be about 0.3 mm. Thinner fingers were difficult to machine. To reduce errors in machining of the rails, the fingers on the rails were spaced even steps of 0.200 inches apart, which determined the final thickness of the disc to be 4.65 mm, allowing for the thickness of the finger of 0.3 mm and 0.1 mm clearance. The spacing between discs was 0.4 mm which allowed also sufficient flow in a series-parallel flow arrangement without excessive pressure drop. With these dimensions, 67 Brewster angled discs were required for an active pump length of 457 mm.

From our analysis of the flow distribution, the pressure drop along the longitudinal flow channel ΔP_L should be about one half or less than the pressure drop across the first disc ΔP_0 to keep the flow distribution uniform to within 25% or less. Evaluation of Eq. (46) for the Brewster disc laser with $n \cdot m = 67$ and $A_T \approx \sqrt{2} \text{ sc}$ because of the Brewster angle, results in

$$a \approx \frac{17 \text{ mm}}{m} \quad (76)$$

where m is a number of sections. For a single flow reverser disc ($m = 2$) the longitudinal flow channels would have had to be about 8 mm wide, which is certainly not tolerable in this design. To maintain a close-coupled system and high efficiency, an active volume of about 80% of the total volume or more is desirable

which corresponds to a width of about 2.2 mm for the longitudinal flow channels. For ease of machining the rails, a final width of 2.4 mm for the longitudinal flow channels was chosen, which requires 8 sections of about 8 discs each to maintain a uniform flow distribution.

The discs for the B-2 were made from 3% Nd-doped C1020 laser glass and provide a rectangular clear aperture of 17.2 by 21.7 mm, which increased the available beam cross-sectional area by almost 50% over the N-1 design, using the same square Pyrex tubing and same close coupling of the flashlamps. This increase in beam cross-sectional area allowed 50% more Q-switched output energy than for the N-1.

The edges of these discs were initially polished. The optical finish on the 134 surfaces was limited due to economics of fabrication. An autocollimator return from a flat mirror with the beam passing twice through the array, consisted of two almost distinct returns with an angular divergence of 1.5 mrad. The divergence and the polarization of both returns was in the low-loss plane of the B-2. The discs were inspected for flatness with the results of 127 surfaces being flat to one fringe and 7 surfaces flat to two fringes. The strain pattern produced by the discs showed that all but the corners extinguished between crossed polarizers, which is comparable to that of the best solid rod we have observed. The input and output was coupled by means of 0.5% Nd-doped solid windows with external faces cut at Brewster's angle and internal faces cut for minimum vignette as described in Section V.1.

The coolant flow path through the device consisted of eight individual sections in series, with each section composed of eight discs in parallel. The pressure drop across the entire array of discs was about 2 psi at 1.0 GPM. From the flow characteristic as shown in Fig. 3, an appreciable reduction in pressure drop was obtained for the B-2 design in comparison to the N-1.

The entire array was mounted on Micarta blocks for electrical insulation with the flow moving in the vertical plane to facilitate the removal of trapped air.

The device was close-coupled with four EG&G FX47-18 water-cooled flashlamps using water jackets of Supremex tubing. Supremex tubing absorbs strongly at wavelengths below 350 nm, but was found to be not sufficient to protect the B-2 from solarization.

During testing of the B-2 several design improvements were made, which were all incorporated in the improved B-3 device.

The final B-3 disc laser consisted essentially of the same components as the B-2 device except for discs which were made from ED-2 laser glass. A flow arrangement with only 3 flow reverser discs was chosen in order to determine if there is any appreciable difference in the single-pass beam distortions. In addition, the following improvements were incorporated:

(1) Sodium nitrite cooled lamps as described in Section IV.6 were used, which provided UV protection and less heating of the discs.

(2) A bacteria filter was installed in the D₂O cooling system which eliminated the brown deposit previously observed on the discs.

(3) The flow channeling around the entrance and exit window was redesigned, to eliminate stagnant flow conditions observed with the ink-test.

(4) The internal angle of the window was modified, to eliminate the coolant wedge between the window and the first disc. This coolant wedge did not allow the full beam from the window to enter the first disc. To reduce this vignette, the spacing between the window and disc was made the same as between the discs, which also improved the flow distribution. The beam was slightly realigned for minimum vignette

(5) The entrance and exit windows were mounted more rigidly, using high melting point materials and additional mechanical supports for the end plates, to avoid movement of the windows.

(6) The 40 kW power supply was modified to provide an energy storage bank and injection trigger transformer for each lamp. Previously two lamps were operated in series, which required high trigger voltages to ionize the lamps and resulted occasionally in electrical breakdown and damage to the device. The new arrangement with 340 μ F capacitance and 250 μ H inductance per lamp provides also a shorter and more efficient pump pulse of 0.66 msec duration.

4. THE N-2 AND N-3 NORMAL INCIDENCE DISC LASERS

Because of the depolarization losses observed with the Brewster disc lasers as described in Section VI.3, and the encouraging results obtained with the quartz coatings as described in Section IV.7, the performance capability of the normal incidence approach was again investigated.

In order to have a side-by-side comparison between the Brewster and normal incidence approach, the pump geometry and the hardware used was essentially the same as for the B-2 and B-3 described in the previous section. The thickness of the discs and the spacing between discs was maintained at 4.65 and 0.4 mm, respectively. The discs for the N-2 were again made from 3% Nd-doped C1020 laser glass, while the discs for the N-3 were fabricated from ED-2 glass. The clear aperture of these discs was maintained at 17.2 by 21.7 mm, which corresponds to a pumped cross section of 3.7 cm^2 .

For the N-3 all the improvements as outlined in the previous section were incorporated, while for the N-2 the bacteria filter was not yet installed in the D_2O cooling system. For the N-2 and N-3, a flow arrangement with 7 flow reverser discs was chosen because of the better results in single pass beams spread of the B-2 with 7 flow reversers in comparison to the B-3 with only 3 flow reversers.

The discs for the N-2 were again polished in two sets with about 50 discs each, which results usually in a flatness of the individual disc surfaces of about one fringe. The cumulative distortions of such an array of discs can be quite well determined and compensated for by figuring the surface of a single disc. The observed optical distortions through the N-2 with 196 surfaces corresponded to about $+1/8$ diopter cylindrical power, which was corrected with an appropriately figured disc.

All discs for the N-2 and N-3 were coated with quartz, which provided a good AR coating for the N-3, but did not meet the expectations for the N-2 as described in Section IV.7. In addition, deterioration of the N-2 was observed, because of contamination of the coolant, which was later eliminated with a mixed bed filter.

SECTION VI
AMPLIFIER PERFORMANCE

1. TRANSMISSION AND GAIN MEASUREMENTS

The passive transmissions of the disc lasers at 1.06 μm were measured on an instrument which provides an accuracy of about $\pm 1\%$ and is insensitive to changes in beam direction, size and quality. The measured transmission values are summarized in chronological order in Table IV.

Table IV TRANSMISSION OF DISC LASERS					
Device	Measured 1.06 μm Transmission	Estimated losses due to Glass Coolant Reflections			Remarks
B-1	84%	8%	8%	0%	Contaminated D ₂
N-1	49%	16%	7%	38%	No coating
N-1	72%	16%	7%	7%	MgF ₂ coatings
B-2	78%	16%	5%	0%	
N-2	46%	16%	5%	15%	First quartz coating
N-2	55%	16%	5%	15%	Second quartz coating
B-3	84%	12%	5%	0%	
N-3	71%	12%	5%	2%	Quartz coating

The transmission of the Brewster disc lasers was measured with a linearly polarized beam in the low-loss plane of polarization. The estimated transmission values in general agreed well with the measured transmission except for the N-2 and N-3 results, where difficulties of monitoring the thickness of the coatings were encountered, as described in Section IV.7.

A loss coefficient of about 0.3%/cm, which is typical for AO C-1020 laser glass, was used for the estimated absorption loss in the laser glass and windows, while for ED-2 glass a somewhat lower value was assumed. For the D₂O from the cooling system, a loss coefficient of about 1 to 1.5%/cm was measured, depending on the degree of contamination.

The transmission of the B-3 and N-3 was maintained at its initial value over a long period of time, which indicates that the problems due to solarization and coolant contamination have been solved. With all the other devices, a slow deterioration in performance and transmission was observed.

The small signal gain of the different disc lasers was measured as the ratio of output signal of the pumped and unpumped disc amplifier, for a constant input signal from an oscillator. Both normal mode and Q-switched oscillators were used which resulted in the same measured gain as long as the pump pulse of the oscillator was shorter than for the disc amplifier and the output energy density was kept well below saturation. The results of these measurements are shown in Fig. 14. The gain for the B-1 was taken without the yellow filter tubing. With the yellow filter tubing for UV protection, the effective input was reduced by about 23%, which resulted in still lower gain for the B-1. Comparing the area weighted gain for the B-1 of about 5 dB cm²/kJ to typical results for close-wrapped solid rod amplifiers of 7 dB cm²/kJ indicates about 40% more pump light is required for the B-1 to obtain the same small signal gain as for a solid rod. In other words, about 30% of the pump light was lost in the B-1 fixture.

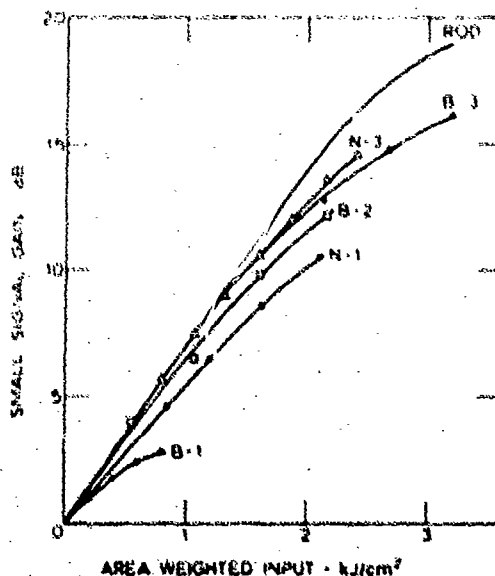


Fig. 14 Small signal gain of disc lasers and solid rod

For the N-1, the area weighted gain of $5.6 \text{ dB cm}^2/\text{kJ}$ indicates a coupling efficiency of about 80% in comparison to the solid rod, which is probably due to the reduced active volume in this device due to the claddings of the discs.

The gain of the B-2 compares favorably with the results for the solid rod. The active volume in the B-2 is about 50% higher than in the N-1 design, which is probably the reason for this improvement in comparison to the N-1 results.

The gain of the B-3 and N-3 is still higher, which is due to the higher gain coefficient of ED-2 glass in comparison to C-1020 Glass. At high input energies, the small signal gain is no longer linear with input energy, because of increased amplified spontaneous emission and the UV shift of the flashlamp output. Because the B-3 discs are not coated, the increased amplified spontaneous emission perpendicular to the disc faces could cause the lower gain for the B-3 in comparison to the N-3.

2. SINGLE PASS BEAM DISTORTIONS

The optical quality of a passive disc laser cavity will certainly be lower than for an equivalent solid rod, because of surface imperfections. This can cause some loss in efficiency and an increase in beamspread for single-shot operation of a disc laser. However, under repetitively pulsed operation, induced thermal optic distortions dominate the performance of disc and solid rod lasers.

(a) Passive Beam Distortions

The passive distortions were measured with an expanded 6328\AA He-Ne gas laser beam passing through the disc laser. The probe beam was then focused on a small aperture and the transmitted beam intensity recorded. The beamspread, which is the full angle containing 50% of the total beam intensity, was measured for different probe beam diameters as shown in Fig. 15. For small beam diameters, the diffraction limit can be approached; however, with increasing diameter of the probe beam, the optical distortions become more noticeable. The quality of the optical arrangement was measured without a disc device present and found to depart from the theoretical curve for a diffraction limited beam as shown in Fig. 15.

The optical distortions observed in the B-1 are caused by the limited flatness of the discs, which resulted in about +0.2 diopter cylindrical power and +0.1 diopter spherical power.

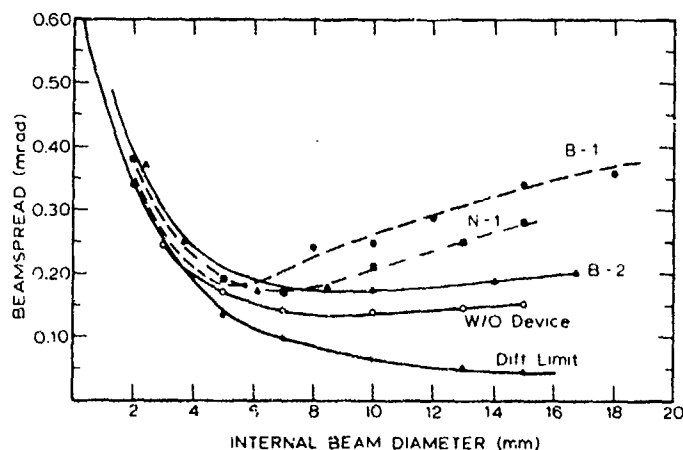


Fig. 15 Passive single pass distortions of the disc lasers for different diameters of a 6328A probe beam

The flatness of the N-1 discs was appreciably better than for the B-1 discs because of the better surface area to thickness ratio. The resulting optical distortions from the 92 disc surfaces in the N-1 were lower than for the 60 disc surfaces in the B-1.

The measured optical distortions in the B-2 are much reduced in comparison to the B-1 and N-1 despite the larger number of disc surfaces. This improvement was obtained by optical correction of the cumulative distortions in the disc array with an appropriately figured disc. The optical distortions in the N-2 and B-3 were also reduced by this method to 0.1 and 0.2 mrad, respectively, for the full aperture of these devices. This approach allows improvement of the optical quality of disc lasers without polishing the discs individually to very close tolerances at great expense.

(b) Active Beam Distortions

The beam distortions during and after a single pump pulse were also measured with the probe beam focused on an aperture after passing through the disc laser. The intensity of the probe beam transmitted through this aperture was recorded on an oscilloscope.

The results for the B-2 under various conditions are shown in Fig. 16. For this measurement parallel oriented polarizers were

installed before and after the B-2. The beam distortions are most noticeable at high input energies and high coolant temperatures as expected. For high flow rates, the distortions are more pronounced, but also recover faster. This is probably caused by thermal gradients in the coolant due to mixing of heated and unheated fluid. For zero flow, the thermal gradients probably remain predominantly axial with little influence on the beam, but exist for a very long time. The recovery time of the distortions was found to be independent of input energy and coolant temperature, but about inversely proportional to the flow rate. At 1 GPM, the recovery time is about 1 second, which is approximately equal to the time required to exchange the coolant in the B-2 cavity.

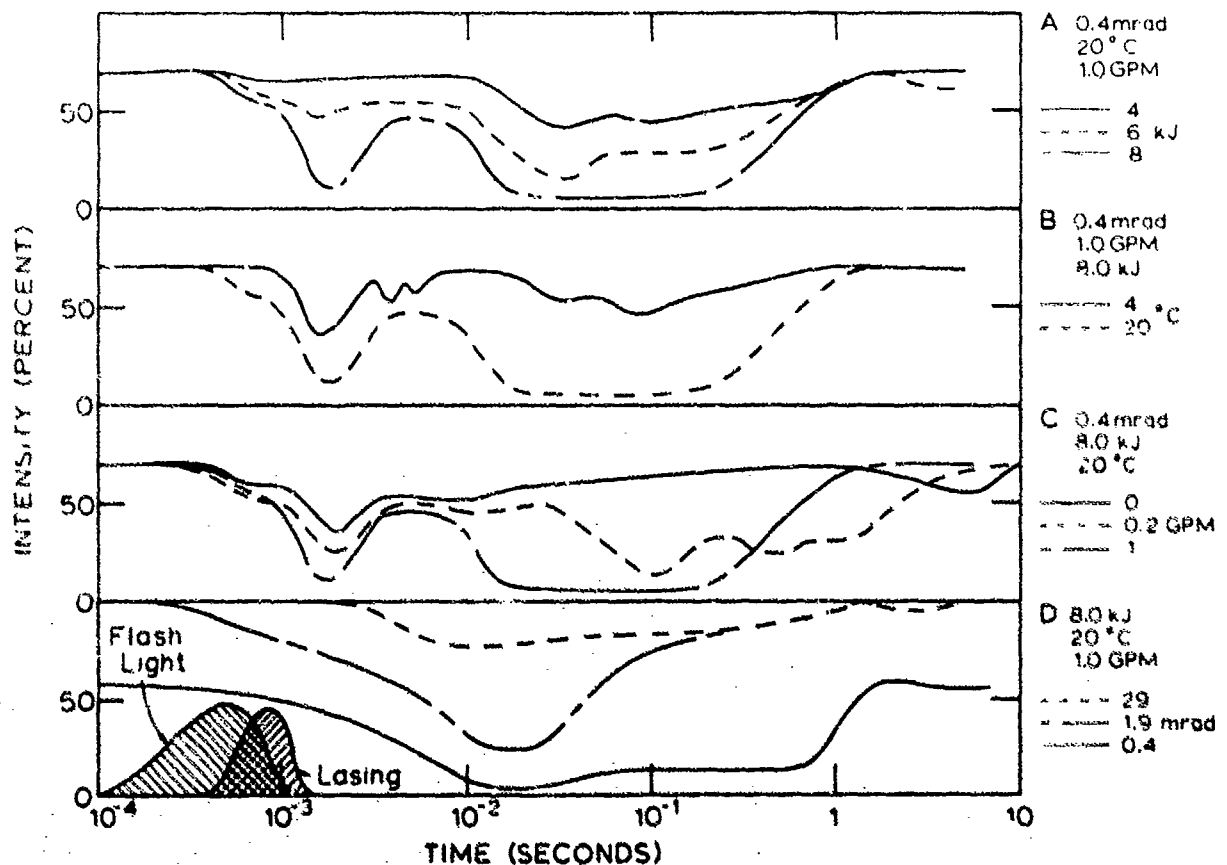


Fig. 16 Behavior of a 6328 Å probe beam transmitted through the B-2

The first minimum just after the pump pulse as shown in Trace 16 A, B and C was found to be caused by beamsteering due to movement of the windows. Trace 16 D shows the results obtained with the more rigidly mounted windows, which reduced the observed steering to a negligible amount.

The second minimum is due largely to severe index gradients in the coolant caused by temperature gradients as the discs cool. This was supported by photographs taken of the probe beam as discussed in the next section.

With the coolant temperature lowered from 20°C to 4°C, the beams spread during the cooling cycle was reduced from about 2 mrad to 0.4 mrad. This also indicates that most of the distortions are caused by the coolant, since the thermal distortions in the discs are negligible for a single shot and would not vary significantly with coolant temperature and flow rate.

Trace 16 D shows also the transmitted signal for larger angles of acceptance and indicates losses in the B-3, possible due to depolarization, vignette, bubbles, etc.

The results obtained for the N-2 and B-3 are shown in Fig. 17.

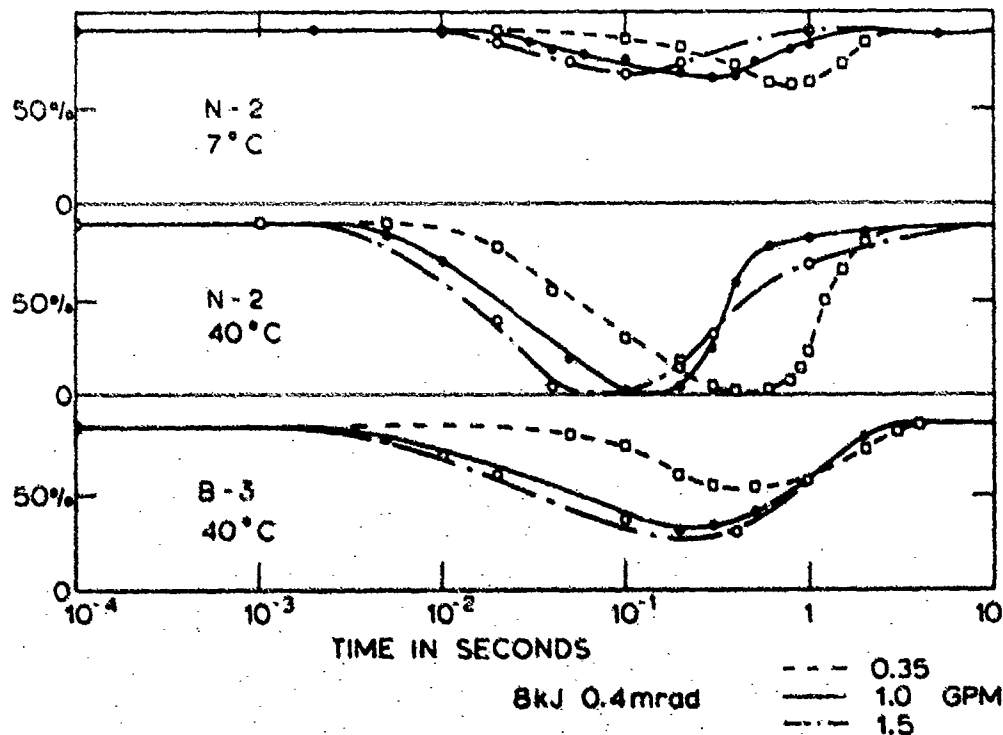


Fig. 17 Behavior of a 6328Å probe beam transmitted through the N-2 and B-3

For the N-2, the observed beam distortions are again greatly reduced at low coolant temperatures. For the B-3, the observed beam distortions were not as pronounced as observed for the B-2, despite the higher coolant temperature. In addition, the recovery time for the B-3 was about 2 seconds and almost independent of flow rate. This could be caused by the different flow arrangement of the B-3 with only 3 flow reverser discs in comparison to the B-2 and N-2 with 7 flow reversers. In addition, all the improvements as outlined in Section V.2 were installed in the B-3 including the sodium nitrite cooled lamps, which would greatly reduce the amount of UV light absorbed in the B-3.

(c) Photographic Data

To explain the beam distortions observed after a single pulse as described in the previous section, the probe beam was photographed using a high-speed movie camera and a still Polaroid camera. Initially, the high-speed camera was utilized to gain an understanding of the problem and to gain a key as to which areas of time needed further investigation. The still camera was then used to take photographs in the desired time domain while varying critical parameters. The input energy for each shot was kept constant at 8 kJ.

Using a Hycam movie camera at 1000 frames per second with an exposure time of 0.4 msec, the transmitted probe beam was photographed during and just after the 8 kJ pump pulse at a distance of 2 m from the exit window of the B-2 to capture both near and far field distortions with respect to time with the coolant flow rate of 1 GPM. Exerpts from the movie are shown alongside the angular transmission data for the B-2 in Fig. 18. Just after the pump pulse, the beam converged in both planes by about 20% neglecting the two side bands appearing parallel to the direction of the coolant flow. The pictures during the pump pulse were overexposed, which did not allow us to ascertain the exact time when this distortion occurred. A few milliseconds later, when sufficient heat was transferred into the coolant, causing large index gradients due to mixing of still cold and warm coolant, the image became extremely distorted as shown in the next pictures. The observed asymmetrical distortions were caused by using only one side of the coolant inlet and outlet on the B-2 bulkheads. This asymmetry was greatly reduced by using both inlets and outlets. The relaxation time for these most-severe distortions of about 1 second seems to be equal to the exchange time of the exposed coolant in the B-2 cavity.

Similar pictures were obtained for the B-3 and are also shown in Fig. 18 for comparison. These pictures were taken with

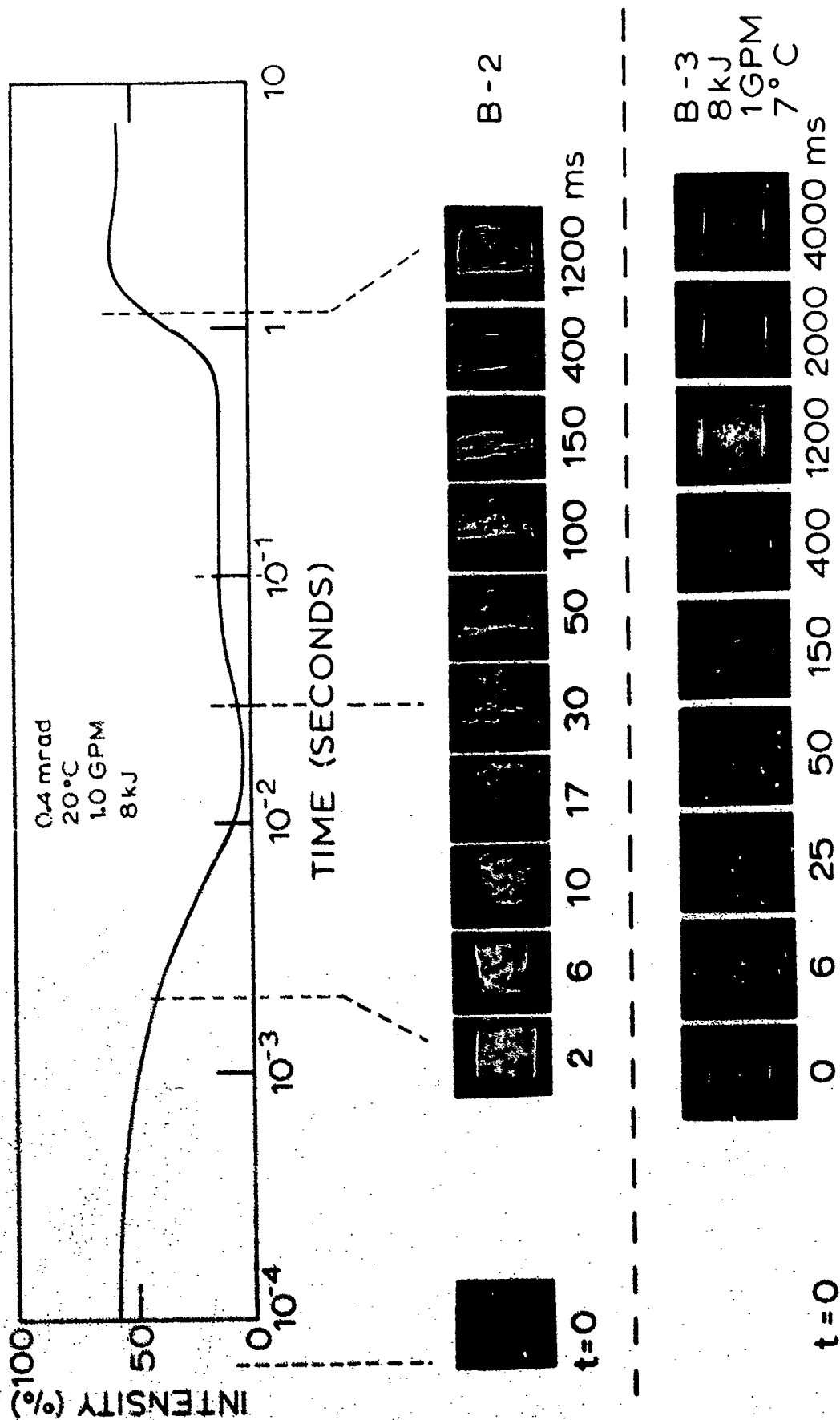


Fig. 18 Correlation of angular transmission data and photographs of probe beam

a Polaroid still camera synchronized to the flashlamp pulse to open at variable delay times after the 8 kJ pump pulse. The exposure time was 12 msec, which did not allow taking pictures closer than an average of about 6 msec after the pump pulse. The pictures were also taken 2 m from the exit window of the B-3. The flow rate in the B-3 was again 1 GPM, however, the coolant temperature was lowered to 7°C. The observed beam distortions are greatly reduced in comparison to the B-2. This improvement is probably due to the difference in coolant temperature, the UV filtering of the flashlamps and the different flow arrangement.

In order to investigate the beam distortions of the B-2 during and just after the pump pulse, the speed of the Hycam movie camera was increased to 7700 frames per second and the camera placed 3 m from the exit window of the B-2 to increase the visibility of angular distortions. Excerpts from the movies in the time domain of interest are shown in Fig. 19. The distortions are developing during the pump pulse, which agrees well with the angular transmission vs time data of Fig. 16. The flow rate had little or no influence on the distortions just after the pump pulse as expected. The difference in the shape of the beam at 4°C for 0 GPM in comparison to 1 GPM flow rate might be caused by temperature gradients due to heat transfer between the initially cooled-down B-2 cavity and the room temperature environment. With the 4°C coolant flowing, these temperature gradients are removed and the distortions eliminated. Reducing the temperature of the coolant close to its freezing point reduces also the observed distortions, especially the side bands.

From the movies, it seems likely that bubbles are generated during the pump pulse, which can be observed in the form of circular diffraction patterns moving across the probe beam in the direction of the coolant flow. These diffraction patterns have not been observed before the pump pulse, but appear frequently thereafter. These bubbles could reduce the transmission as discussed in the previous section and shown in Fig. 16 D.

To determine which areas within the clear aperture of the B-2 contribute most of the distortions, the emerging probe beam was photographed at various distances from the output window just after the pump pulse, as shown in Fig. 20. From these pictures, the useful aperture of the B-2, which remained undistorted just after the pump pulse, was found to be only about one half of the total pumped cross section. A more detailed description of the results for the B-2 is given in Ref. 16.

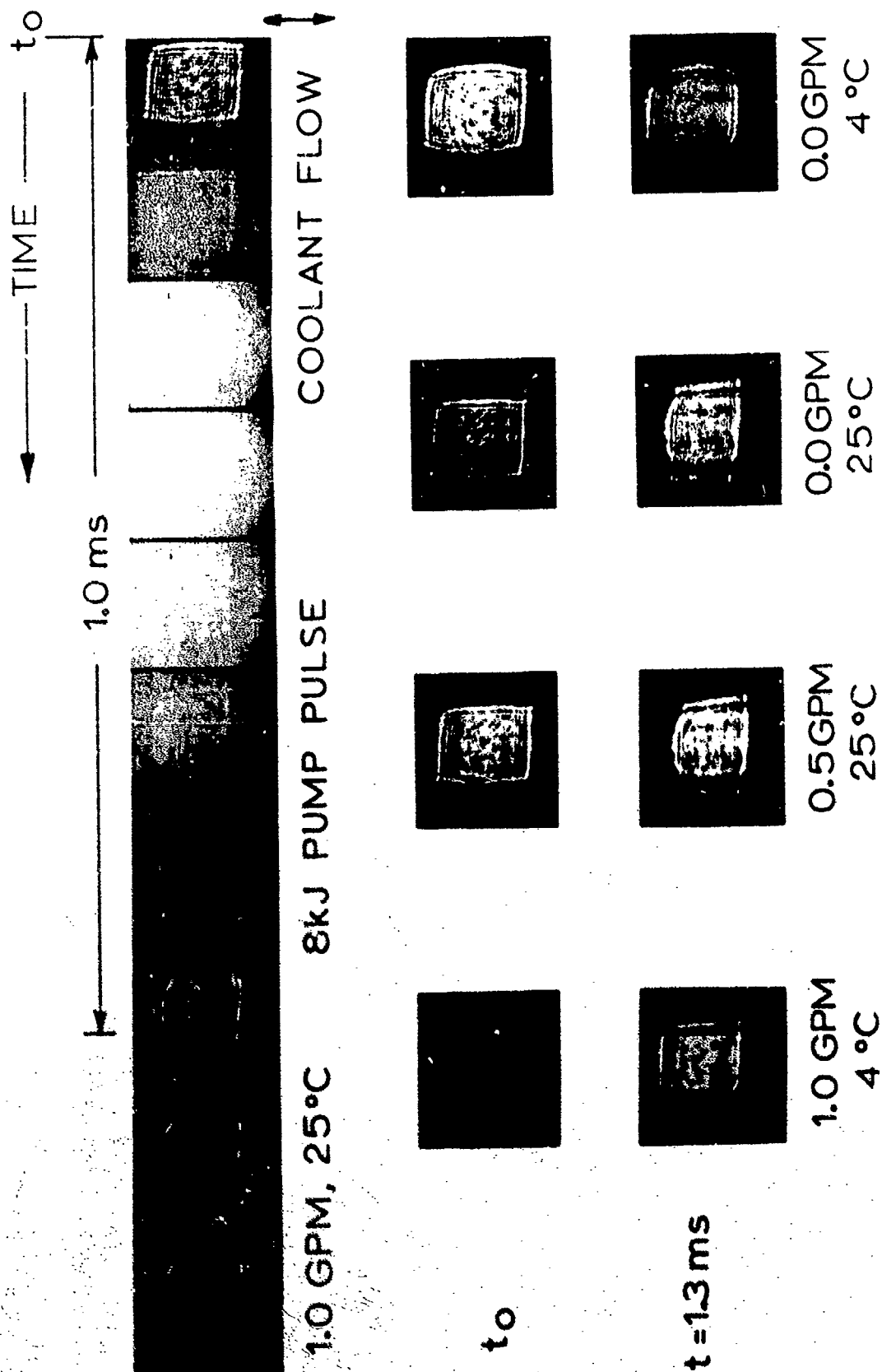


Fig. 19 Beam distortions in the B-2 before, during, and just after the pump pulse for various conditions

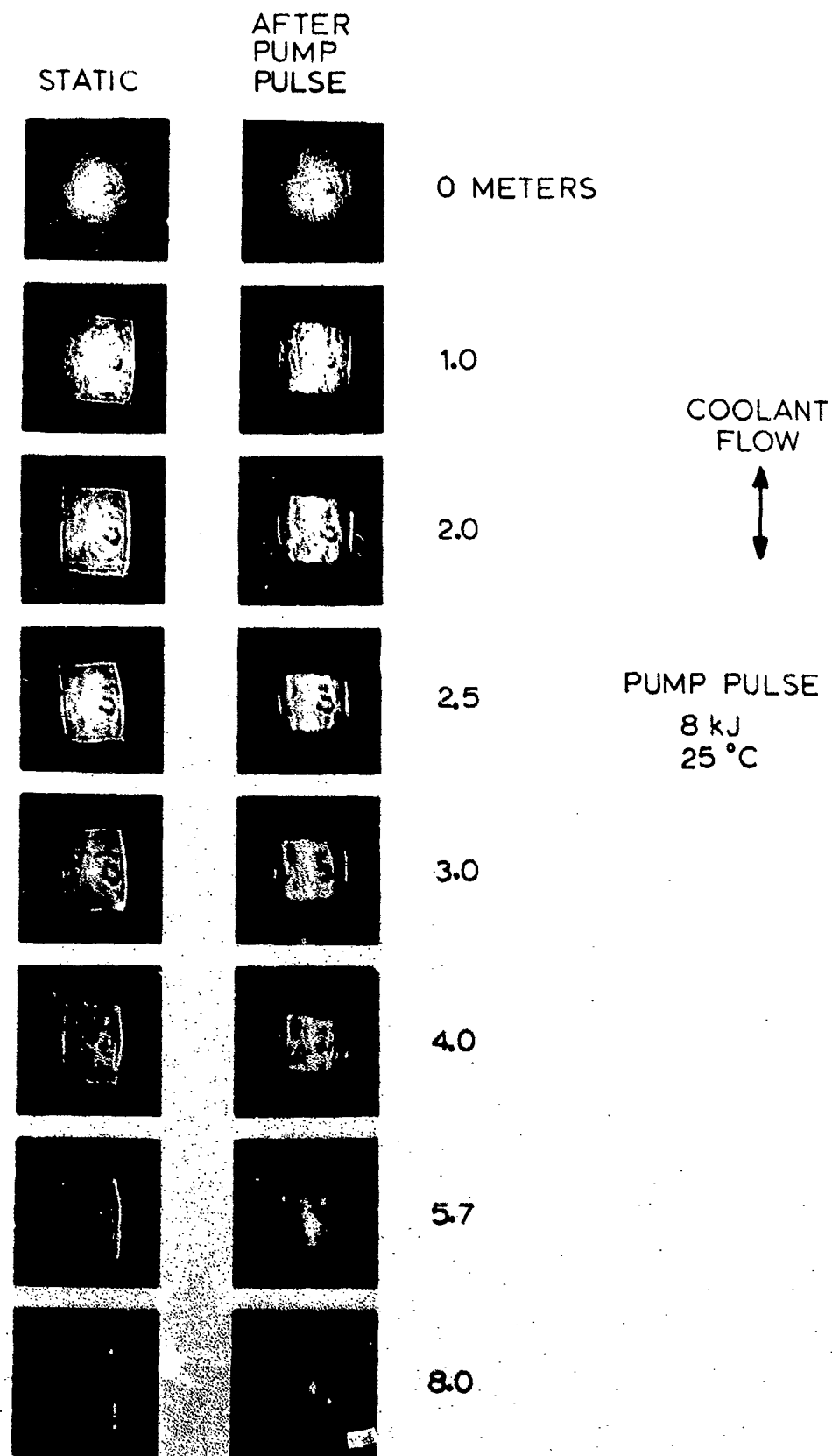


Fig. 20 Photographs of the probe beam before and just after the pump pulse at various distances from the output window of the B-2

Photographs of the probe beam transmitted through the N-2 for various conditions are shown in Fig. 21 taken at 0.5 and 8 m distance from the output window. The observed beam distortions just after the pump pulse were negligible at 7°C coolant temperature and just noticeable at 40°C in comparison to the distortions observed in the B-2 as shown in Fig. 20. Pictures taken 50 ms after the pump pulse show the beam distortions during the cooling cycle, where the transmitted signal of Fig. 17 reaches a minimum.

(d) Beamsteering and Thermal Lensing Measurements

During repetitively pulsed operation of the B-1, steering of the probe beam in the direction opposite to the coolant flow direction was observed at a rate of 0.13 mrad/kW. An estimate of the expected steering due to temperature gradients in the coolant and glass resulted in 0.11 mrad/kW as described in Ref. 13 and agreed well with the observed steering. However, there was no thermal lensing observed with the B-1, since the far field plane of the focused probe beam did not change within ± 0.05 diopter at 10 kW average input power.

During repetitively-pulsed operation of the N-1, thermal lensing was observed of about +0.15 diopter at 3.5 kW average input power as described in Ref. 13 and shown in Fig. 22. Estimates of the expected optical lensing depend strongly on the cooling situation as described in Section III.3. Assuming uniform heating of round discs and uniform cooling at all surfaces, an induced optical power of +0.15 diopter per kW input was estimated. However, with only axial cooling, the average induced optical power was practically zero. The experimental results are bracketed by these extreme cases, indicating a situation of principal axial cooling with partial radial cooling, which seems reasonable.

For comparison, the thermal lensing of a 3% Nd-doped rod was measured in the N-1 fixture as described in Ref. 16, with the results also shown in Fig. 22. The induced spherical power in the solid rod increases approximately linearly at 0.7 diopter/kW. From our estimates, for 6328Å wavelength and a thermal loading of 3.2 W/cm³, an induced optical power of +4.3 and +3.2 diopter for radial and tangential polarization, respectively, was calculated. Assuming 10 to 15% of the electrical input energy is absorbed in the laser rod, an average induced lensing of +1.0 to +1.5 diopter/kW was estimated.

In contrast, the thermally-induced spherical power of the N-1 increases at +0.06 diopter/kW which is more than an order of magnitude improvement.

0.5 m			8 m		
NO FLOW	1GPM		NO FLOW	1GPM	
7° C		40° C	7° C		40° C

BEFORE

AFTER
6ms

AFTER
50ms

Fig. 21 Photographs of the probe beam for various conditions of the N-2

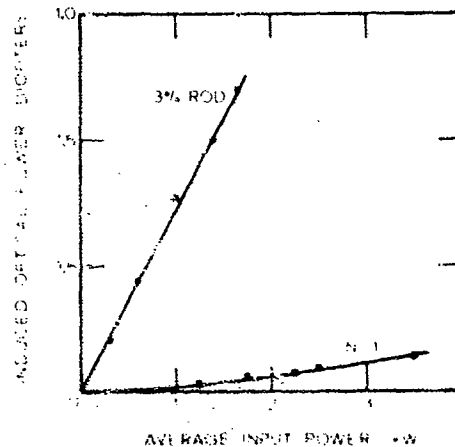


Fig. 22 Thermal lensing measured with a 6328Å probe beam

For the B-2, the thermally-induced lens power was not measurable, or less than ± 0.005 diopter/kW, which means thermal lensing was essentially eliminated for the B-2. However, for the initial B-2 design, beam steering was observed due to movement of the entrance and exit windows. This problem was corrected using shellac to cement the windows in the mounting rings in order to avoid softening of the wax observed during high repetition rate operation. In addition, the mounting rings were rigidly fastened to the bulkheads instead of being only supported by the silicon rubber "O" rings which provided the seals.

(e) Single-Pass Beamspread During Repetitively-Pulsed Operation

The single-pass beamspread was measured by focusing the probe beam on an aperture and recording the transmitted signal on a chart recorder during repetitively-pulsed operation of the device. A far field aperture was chosen which transmitted about 50% of the total probe beam intensity, after thermal equilibrium was reached for the device.

Typical chart recorder traces of the probe beam intensity at average input powers of 2.0 kW and 10 kW, to the B-2 are shown in Fig. 23. Trace A is the intensity of the emerging probe beam in a sufficiently large angle of acceptance to capture all of the output beam. The spikes in the trace are flashlamp pulses.

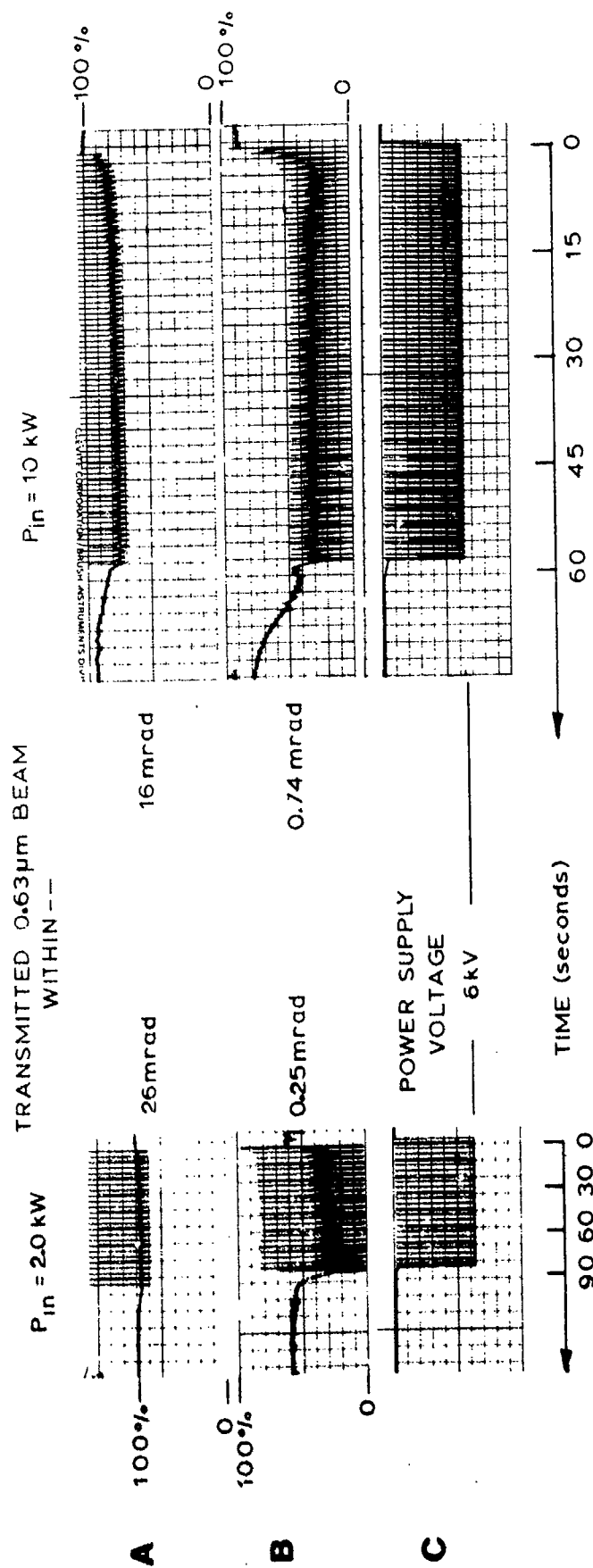


Fig. 23 Behavior of the signal from a probe beam transmitted through the B-2 and focused on an aperture at 8 kJ input and 1 GPM flow rate

After each flashlamp pulse, the intensity of the transmitted beam rapidly decreases, probably due to internal vignetting, bubbles, and depolarization losses. The intensity then slowly increases and in the case of an input power of 10 kW, another flashlamp pulse arrives before the loss is fully recovered. Increasing the angle of acceptance by almost a factor of two did not noticeably change the magnitude of the transmitted intensity.

Trace B is the output intensity of the probe beam within a cone angle selected to contain $\approx 50\%$ of the transmitted probe beam intensity at thermal equilibrium. The time constant for the decay of distortion after a 10 kW run measures about 5 seconds, which is close to the thermal decay rate for the discs.

Trace C is the output voltage of the power supply selected to yield an input energy of 8.0 kJ per pulse.

The beamspread of the emerging probe beam at thermal equilibrium was measured taking into account the loss in signal due to depolarization and vignette shown in Trace A. The final intensity ratio for the 2.0 kW and 10 kW average input power is 45% and 50%, respectively.

The results of these measurements at thermal equilibrium are shown in Fig. 24, and were taken at the best focus of the probe beam, correcting for beam steering and thermal lensing.

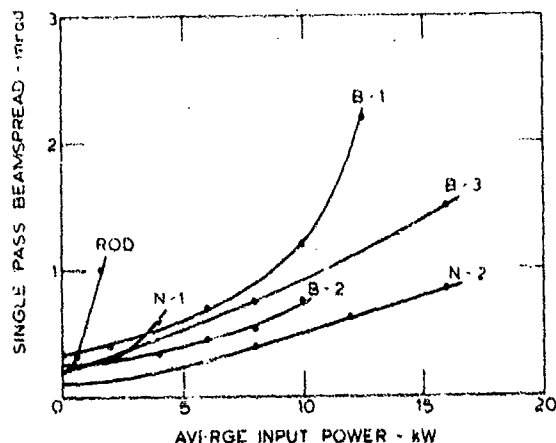


Fig. 24 Increase in single pass beamspread with average input power at 6328 Å wavelength

The beamspread of the solid rod increased above 500 W input power at a nearly linear rate of 0.6 mrad/kW. The maximum input power was limited to 1.6 kW to insure that the rod was not fractured and could be used for maximum output power measurements as described in Section VII.

In comparison to the rod, the B-1 showed little increase in beamspread up to 10 kW; however, above this input level, at repetition rates above 3 pps, a large increase in beamspread was measured, which could have been caused by thermal-optic distortions in the coolant, since the flow distribution of the B-1 was not very uniform.

The beamspread of the N-1 increased above 2 kW at a rate of about 0.2 mrad/kW, which could be caused in part by thermal-optic distortions in the discs, since thermal lensing was observed in the N-1 and one disc fractured at 6 kW average input power.

The change in single-pass beamspread for the B-2 as compared to that of the solid rod is about one order of magnitude lower. These data correspond to a potential improvement in amplifier radiance of over two orders of magnitude for the B-2 over the solid rod.

The single-pass beamspread of the B-3 was found to be larger than for the B-2, despite the improvements in the design and the lower single-shot beam distortions. However, only three flow reverser discs were used in the B-3 while the flow rate was maintained at 1 GPM, which could explain this difference in performance.

The single-pass beamspread of the N-2 was measured with an aperture of 16 x 12 mm in front of the N-2, to eliminate the transmission losses due to edge effects as described in the next section. A coolant flow rate of 1 GPM, a coolant temperature of 7°C and an input energy of 8 kJ per pulse were used for this measurement. The improvement in the single-pass beamspread in comparison to the other devices is probably due to the elimination of the edge effects and the lower coolant temperature. Time did not allow measurement of the single-pass beamspread of the N-3, which should be identical.

For the N-2, the single pass beamspread was also measured for different coolant flow rates as shown in Fig. 25. The results show a large reduction in beamspread with increasing flow rate up to about 1 GPM. Higher flow rates are only effective at high average input powers.

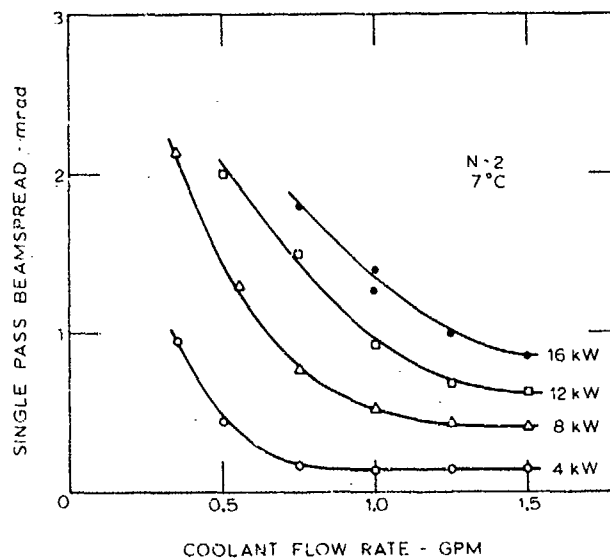


Fig. 25 Dependence of the single-pass beam-spread of the N-2 on coolant flow rate

At 4 kW input power a flow rate of 0.8 GPM is sufficient. At 8, 12 and 16 kW input, flow rates of about 1.0, 1.3 and 1.5 GPM, respectively, are required to keep distortions low. This behavior depends mainly on average input power and not on the combination of input energy and repetition rate chosen. However, the beamspread can be somewhat reduced at the same average input power level by increasing the energy input per shot and reducing the repetition rate.

In summary, the best performance of the N-2 at high average input powers can be obtained at maximum flow rate and energy input per shot, with minimum coolant temperature and repetition rate.

3. ACTIVE TRANSMISSION LOSSES

As discussed in the previous section, transmission losses were observed due to edge effects and depolarization.

The depolarization losses were measured with the disc lasers between parallel and crossed polarizers. The passive depolarization losses measured with the 6328Å probe beam were 0.14% and less than 0.2% for the B-1 and B-2, respectively.

Since the Brewster disc laser acts as its own partial analyzer, the transmitted depolarized intensity is only part of the total depolarized light generated in the device. Assuming a uniform contribution of depolarized light from each disc, the loss caused by the partial reflection within a Brewster disc laser can be estimated.

Defining ΔD as the fraction of depolarized light generated in each disc in respect to the incident parallel polarized light, the contribution ΔI_i^\perp of the i^{th} of n discs, counted from the output side, to the total depolarized output beam after being partially reflected at each successive interface with reflectivity R can be described by

$$\Delta I_i^\perp = \Delta D I_i^\parallel T^{i/n} (1 - R)^{2i} T_w \quad (77)$$

with
$$I_i^\parallel = I^\parallel T^{1-i/n} = I_0^\parallel / T^{i/n} \quad (78)$$

where I_i^\parallel = intensity of parallel polarized light incident on i^{th} disc.

I^\parallel = intensity of parallel polarized light incident on the Brewster disc laser.

I_0^\parallel = intensity of parallel polarized light emerging from the Brewster disc laser.

T = transmission of the Brewster disc laser in the low loss plane of polarization = $I_0^\parallel / I^\parallel$.

T_w = transmission of the output face of the Brewster window for the high loss plane of polarization $\approx 85\%$.

The total depolarized output I_0^\perp is then the summation for all n discs:

$$I_0^\perp = \sum_{i=1}^n \Delta I_i^\perp \approx \Delta D I_0^\parallel T_w \frac{1 - (1-R)^{2n}}{2R} \text{ for } R \ll 1 \quad (79)$$

The total amount of depolarized light generated in the device I^\perp is

$$I^\perp = \sum_{i=1}^n \Delta D I_i^\parallel = \Delta D I^\parallel \sum_{i=1}^n T^{1-i/n} \approx n \Delta D I^\parallel \text{ for } T \approx 1 \quad (80)$$

For $R = 1.5\%$, $n = 67$ and $T_w = 85\%$ the depolarization D of the B-2 is

$$n = \frac{I^\perp}{I^\parallel} \approx n \Delta D \approx 2.7 \frac{I_0^\perp}{I_0^\parallel} \quad (81)$$

which means the ratio I_0^\perp/I_0^\parallel , which was measured with a 6328 \AA probe beam and is independent of the absorption losses of the device, can be correlated to the depolarization D of the B-2 at $1.06 \text{ }\mu\text{m}$ using Eq. (81) above. However, the retardation at $1.06 \text{ }\mu\text{m}$ might be less than at 6328 \AA , which would reduce the expected depolarization at $1.06 \text{ }\mu\text{m}$.

For the B-2 with $T = 78\%$ only about 30% of the depolarized light generated in the device is transmitted while the rest is reflected and lost internally. This would increase the measured passive depolarization losses to about 0.5% which is still negligible.

After a single 8 kJ shot of the B-2, about 1.3% of the total probe beam intensity was found to be in the wrong plane of polarization, which corresponds in a total depolarization loss of about 3.5%. The relaxation time for the depolarization after a single pulse of about 3.5 seconds agrees well with the thermal decay rate for the discs of about 4 seconds as discussed in Section III.2.

The depolarized component of the transmitted probe beam was also measured under repetitively pulsed operation. A typical set of chart recorder traces is shown in Fig. 26 for two input powers of 5 and 10 kW into the B-1 with an energy input of 3.5 kJ per pulse. Trace A is the voltage of the power supply and Trace D the temperature difference between coolant outlet and inlet. Trace B, taken with the polarizing analyzer oriented in the preferred plane for the B-1, shows a decrease in signal of 15 and 20% at 5 and 10 kW input power, respectively. Trace B, taken with the polarizing analyzer oriented in the high loss plane of the

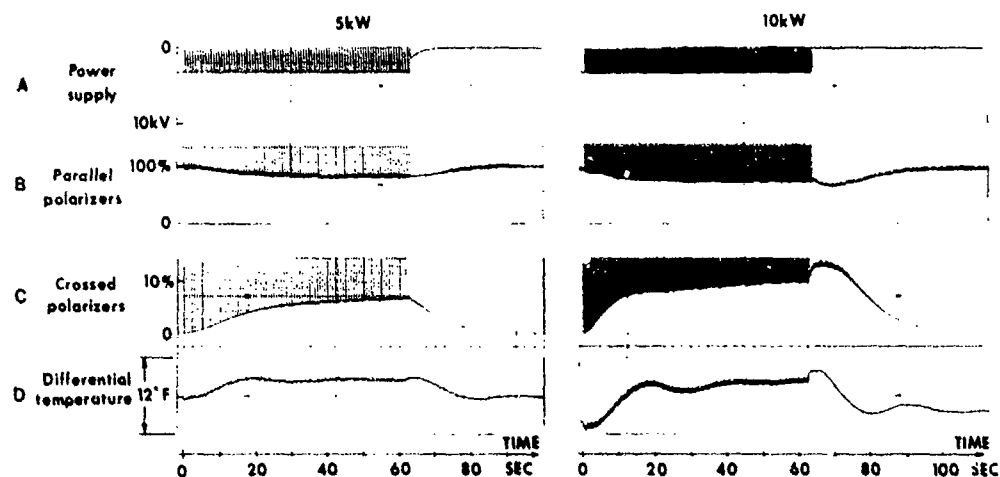


Fig. 26 Change in transmission through the B-1 with parallel and crossed polarizers for 6328Å probe beam due to depolarization at 5 and 10 kW average input power

B-1, shows increases of 8 and 12% at the same time. By using the calculations above, the depolarization D for the B-1 can be estimated by $D \approx 1.8 I_0 / I_0$ which results in a total depolarized light generated in the B-1 of 14 and 21% for 5 and 10 kW average input power respectively, which agrees well with the observed decrease in signal of Trace B. Without a polarizer in front of the detector, the relative transmission decreased by about 7% at 10 kW input, which comes close to the estimated loss of 9%.

The same measurements were taken with the B-2 and B-3, but at 8 kJ input energy per pulse. Since it was not possible to determine the total depolarized light generated in the Brewster disc lasers directly, because most of the depolarized light was lost internally, the depolarization loss of the N-2 was measured for comparison. The results of these measurements are shown in Fig. 27. The observed losses in relative transmission at 6328Å with parallel polarizers are almost the same for the different devices. The depolarization losses of the N-2 were measured at a flowrate of 1 GPM, a coolant temperature of 20°C an energy input of 8 kJ per pulse and with an 16 x 12 mm aperture in front of the N-2. Under these conditions and without an analyzer, the transmission of the 6328Å probe beam did not change with input power. The 16 x 12 mm aperture was necessary to eliminate

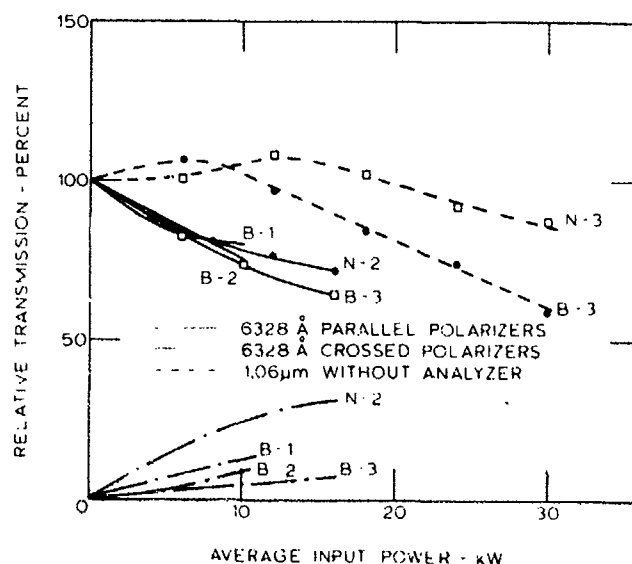


Fig. 27 Change in transmission of the disc lasers during repetitively pulsed operation

transmission losses due to edge effects, which were observed when the full aperture of the N-2 was illuminated by the 6328 Å probe beam.

The depolarization losses of the B-3 were taken with the full aperture, but otherwise under the same conditions as for the N-2. The somewhat higher losses for the B-3 could be caused by edge effects.

Changing the coolant flowrate and temperature of the N-2, while maintaining an input power at 8 kW resulted in increasing depolarization losses of 10, 19 and 23% for increasing flowrates of 0.5, 1.0 and 1.5 GPM respectively. In addition, the depolarization losses were found to increase for lower coolant temperatures. To reduce the depolarization losses, low coolant flowrates and high coolant temperatures are desirable, which is contrary to the requirement to reduce the beam distortions in the coolant. These opposing requirements have to be well balanced in an optimum Brewster disc design, while depolarization is of no concern in the normal incidence approach.

The transmitted intensity of the 6328 Å probe beam in the wrong place of polarization is also shown in Fig. 27. With crossed polarizers, the transmitted signal in the wrong place of

polarization increases with average input power as expected and equals the transmission loss measured with parallel polarizers in the case of the N-2. For the Brewster disc lasers, the depolarized light is only partially transmitted and is reduced by the factor in Eq. (81), which is 1.8, 2.7 and 4.1 for the B-1, B-2 and B-3, respectively. The difference in this factor for the B-3 in comparison to the B-2, is the higher reflectivity of 2.5% per disc surface for the B-3, because of the higher index of Ed-2 glass.

The change in transmission of the disc lasers was also indirectly measured with a $1.06\text{ }\mu\text{m}$ source, as the change in effective gain for single shot and repetitively pulsed operation. The results are also shown in Fig. 27 in the form of dashed curves. The initial increase in effective gain or transmission could not be explained, especially since the $1.06\text{ }\mu\text{m}$ probe beam was reduced in size to avoid the edges of the disc laser. The loss in effective gain at high average input power to the N-3 is probably due to beam distortions, because the acceptance angle of the thermopile used to measure the output energy was only about ± 20 mrad. The loss in effective gain for the B-3 at high average input powers is greater than for the N-3 as expected. However, the observed depolarization losses at $1.06\text{ }\mu\text{m}$ seem to be appreciably lower than at 6328 \AA , probably due to the difference in retardation.

4. AVERAGE RADIANCE MEASUREMENTS

The average radiance capability of the B-3 and N-3 was measured by amplifying a single laser pulse from a high radiance device, after thermal equilibrium was reached for the repetitively-pulsed disc lasers. This approach had to be taken since there was no high average power laser available with a sufficient low beam-spread, which could have been used as driver.

The $1.06\text{ }\mu\text{m}$ laser beam from the high radiance device was well collimated to about 0.5 mrad. An aperture in front of the disc laser was used to reduce the beam in size, just sufficient to avoid the edges of the discs. With this arrangement, the single pass beamspread of the B-3 and N-3 was measured and found to increase about linearly with input power from 0.6 mrad without pumping, to 3 mrad at 30 kW average input power. The measured beamspread for the B-3 and N-3 was the same within the accuracy of the measurement, but somewhat higher than expected from the measurement taken with the 6328 \AA probe beam. With the size of the $1.06\text{ }\mu\text{m}$ probe beam reduced to 11 mm in diameter, the beamspread of the N-3 was improved at 24 kW from 2.5 to 1.5 mrad over the central area, which again indicates appreciable edge effects. The passive beamspread of 0.6 mrad is mainly determined

by the probe beam. The beamsread during repetitively pulsed operation was also measured using a Q-switched probe beam, with identical results.

The small signal gain of the B-2 at 12 kJ input was measured at 16 dB, which corresponds to a stored energy of 0.5 J/cm^3 using the advertised OI specific gain coefficient of $0.18 \text{ cm}^2/\text{J}$. With a linearly polarized input beam of 30 J, a maximum energy of 100 J was extracted from the device within a beam cross-sectional area of 2 cm^2 . This corresponds to an average extracted energy of 1.2 J/cm^3 , which is much larger than the calculated stored energy available. Since the measurement was taken with a normal mode signal, repumping has to be considered, but does not explain the full difference. From other measurements on ED-2 and AO glass, a specific gain coefficient of about $0.1 \text{ cm}^2/\text{J}$ seems to be more reasonable, which would help to explain the discrepancy.

The Q-switched amplifier performance of the B-3 and N-3 was tested with 40 nsec Q-switched pulses from the high radiance device. With the B-3 pumped at 6 kJ, a 6 joule input signal was amplified to 30 joules in a 2 cm^2 beam. At this energy density of 15 J/cm^2 , the surface of the output window was severely damaged. Increasing the beam cross-sectional area to the full aperture and decreasing the output energy to 23 joules eliminated this problem. A maximum output power of 90 W was obtained with the B-3 pumped at 4 pps and 6 kJ energy input per pulse. These results correspond to an average radiance for Q-switched signals of about $5 \text{ MW/cm}^2\text{-sr}$.

With the N-3 pumped at 6 kJ, Q-switched pulses of 5 joules and 40 nsec duration were amplified to 22 joules. At a repetition rate of 5 pps an average Q-switched output power of 110 W was obtained. Higher average output power could be obtained for lower gain levels, which makes the meaning of average power or average radiance for an amplifier irrelevant without considering the effective gain.

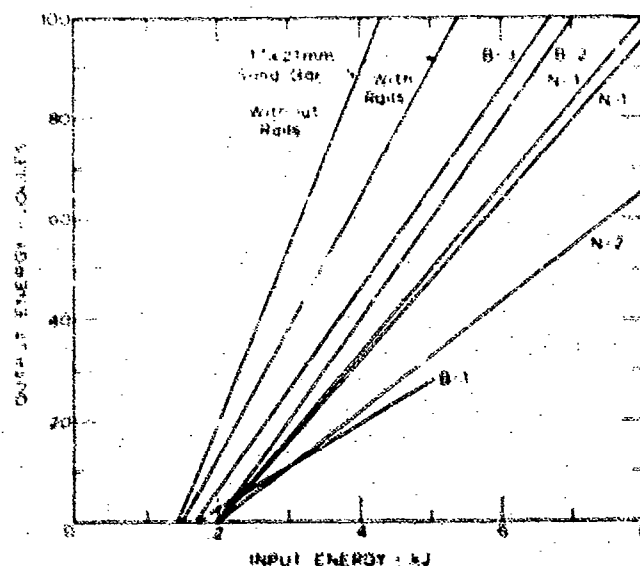
SECTION VII

OSCILLATOR PERFORMANCE

1. SINGLE SHOT DATA

The evaluation of a laser as an oscillator is the most critical test, since all imperfections and losses are magnified by the many round-trips of the laser beam inside the cavity. For the application of a disc laser as amplifier, the somewhat lower transmission and gain can be easily tolerated especially under repetitively pulsed operation, where the beam quality is greatly improved.

The initial output characteristics of the disc lasers operating as normal mode oscillators, are shown in Fig. 28.



Copy available to DDC does not permit fully legible reproduction

Fig. 28 Single shot oscillator performance under normal mode operation

Over extended periods of time and many shots, the performance of most disc lasers, except the B-3 and N-3 deteriorated slowly due to coolant contamination and solarization as discussed in Section IV. The results for the disc lasers were compared to those of equivalent solid rods in the same pump cavity. In all cases, the output reflectance was optimized for best overall performance.

For the B-1 a maximum slope efficiency of 0.85% with a threshold of 1.7 kJ was obtained, using an output reflectance of 59% and a pump-pulse of 0.83 msec duration. The single-shot beam-spread was measured to be 4 mrad at 2.4 kJ input. In comparison, a 2% Nd-doped, 2.54 cm diameter solid rod with normal ends, had a higher slope of 1.45% with a lower threshold of 1.4 kJ, using its optimum output reflectance of 45%.

For the N-1 with magnesium fluoride coated discs and an output reflectance of 28%, a slope efficiency of 1.6% and a threshold of 2 kJ was measured, using the 40 kW power supply, which provided a pump-pulse of 0.9 msec duration.

For comparison, a 2% Nd-doped solid rod 18 mm in diameter was installed in a fixture with the same pump geometry as for the N-1. The rod had a 5° bevel at one end and was completely immersed in water. The other face of the rod was normal to the optic axis and aligned to the output reflector. The maximum slope efficiency of this rod was 2.2% with a threshold of 2.3 kJ using an output reflectance of 10% and a pump-pulse of 0.64 msec duration.

Since an improvement in oscillator efficiency was observed in other measurements with higher Nd-doping than desirable for uniform gain in the amplifier mode, a 3% Nd-doped rod was tested in the N-1 fixture. To prevent solarization, the rod was totally immersed in a 10% aqueous sodium nitrite solution. With this rod, a 27% improvement in slope and threshold was measured, despite the use of a less desirable pump pulse of 0.9 msec duration with a long RC decay.

For the B-2 a maximum slope efficiency of 2% and a threshold of 2 kJ was measured using an output reflectance of 26% and a pump pulse of 0.6 msec duration.

To determine the efficiency of the B-2 pump geometry, a 3% Nd-doped rectangular bar measuring 17 x 21 mm, which is equivalent to the disc dimensions, was tested in the B-2 cavity. The results shown in Fig. 28 represent an average of the output characteristic of the rectangular bar, measured several times during this program for reference data to reflect any changes in the quality of the pump cavity. To investigate the discrepancy in performance between the B-2 and the solid bar, rails similar to the B-2 rails were installed to simulate the shading effect of the rails, which resulted in a 25% decrease in slope efficiency, while the threshold remained about the same. These results suggest that the use of a transparent material for the B-2 rails

would significantly enhance the B-2 performance. However, there are still significant differences in efficiency and threshold after taking into account the losses due to the rails. These differences are probably due to the differences in transmission, gain, vignette and beam distortions. The transmission losses of disc lasers are higher than for equivalent solid rods, because of absorption losses in the coolant as well as scattering and reflection losses on the disc surfaces. The gain in a disc laser is lower, because the active volume of laser glass is reduced and amplified spontaneous emission is increased due to the many internal reflections from the disc surfaces. The clear aperture of a disc laser is reduced because the tolerances required for ease in fabrication and assembly allow some displacement of the individual discs. In addition, vignette is caused by the beveled edges of the discs and the displacement of the laser beam in the Brewster disc array. Losses due to beam distortions in the coolant and bubbles generated during the pump pulse will also reduce the overall efficiency of a disc laser in comparison to a rod for single shot operation. More details about the measurements on the B-1 and N-1 are given in Ref. 13 and on the B-2 in Ref. 16.

The output performance of the N-2 was not reproducible, because of the imperfect coatings of the discs as discussed in Section IV.7. The many internal reflections contributed significantly to the output, depending upon how closely it was aligned to the optical axis. The reflections from the individual discs were all within an angle of ± 30 mrad. With the disc faces aligned to the optical axis, a slope efficiency of 1.1% with a threshold of 2.0 kJ was measured using an output reflectance of 30%. With the disc faces tilted with respect to the optical axis, about a 30% lower slope and a 10% higher threshold was observed. The internal reflections resulted also in a large beamspread of about 10 mrad in comparison to 4 mrad measured with the B-2. The beamspread of the N-2 was reduced to 6 mrad, with the disc faces tilted with respect to the optical axis, and with an optical correcting lens installed to compensate for the +0.1 diopter spherical power of the discs.

The N-2 was also operated as a Q-switched oscillator, utilizing a rotating prism to avoid polarization of the beam and the associated depolarization losses. The rotating prism also has the advantage of maintaining optical alignment in a similar manner to that of a retroreflector. However, the roof of the prism has to be well aligned to the centerline of the beam to avoid losses due to vignette. The clear aperture of the prism is 27 x 21 mm, which should be adequate for the 21 x 27 mm aperture of the N-2. The rotating prism was statically and dynamically

balanced and operated up to 400 Hz without any difficulties. The normal mode performance of the N-2 with the prism stationary was found to be the same as with the 100% mirror. However, under Q-switched operation, a slope efficiency of only 0.35% was measured with a threshold of 1.9 kJ using a 30% output reflector. At 8 kJ input a maximum output energy of 15 joules was obtained in a pulse of 100 nsec duration. The poor performance of the N-2 under Q-switched operation is probably caused by amplified spontaneous emission within the device due to the imperfect coatings. At 8 kJ input prelasing was observed even with the rotating prism blocked, which amounted to an output energy of about 2 joules. With the output mirror removed, the N-2 was still Q-switching off the internal reflections at an input of 8 kJ. From these results it became apparent that better coatings are essential for Q-switched operation of the N-2.

The B-3 provided the best overall efficiency so far with a slope of 2% and a threshold of 1.7 kJ, using an output reflectance of 30% and a pump pulse of 0.66 msec duration. This improvement is probably due to the higher transmission and gain of this device in comparison to the B-2. The single-shot beam-spread of this device was 2.4 mrad which compares favorably with the 4 mrad measured for the B-2. This improvement is in part due to the lower operating temperature of about 7°C for the B-3 in comparison to 20°C for the B-2, because of the seasonal variations in the temperature of the cooling water.

The B-3 was also Q-switched with a Pockels cell, consisting of a 25.4 mm cube KD*P crystal, providing a clear aperture of 19 mm x 16 mm. The B-3 served as the polarizer providing about 10 dB loss in the high-loss plane of polarization. The insertion loss of the Pockels cell was negligible since the normal-mode output was essentially the same as with the 100% mirror. Since the B-3 had to be operated below 10 J Q-switched output to prevent damage to the device, the power supply was changed, reducing the capacitance and increasing the voltage to provide easier triggering of the flashlamps. With the resulting shorter pump pulse of about 0.45 msec duration, the threshold was reduced to 1.0 kJ with slope efficiencies of 1.3 and 0.9% for long pulse and Q-switched operation, respectively. During Q-switched operation at 10 joules output with a pulse duration of 30 nsec, the 30% output reflector and the KD*P crystal was damaged. To avoid damage to the output reflector, a sapphire flat was installed. This change, plus the damage in the crystal, increased the threshold to 1.5 kJ with slope efficiencies of 1.4% and 1.0% for long pulse and Q-switched operation respectively.

With a new KD*P crystal, a 15% higher threshold was measured. This might be due to increased loss in the new crystal which was only 90% deuterated, while the first crystal was 99% deuterated. The B-3 was Q-switched up to the 10 joule output level without any damage to the KD*P crystal. However, under repetitively-pulsed operation, the 100% mirror deteriorated, which seems to be the final output-limiting component for Q-switched operation.

The slope efficiency and threshold energy of the N-3 were measured using different output reflectors. The best overall performance was obtained with a 20% output reflector, which resulted in a threshold energy of 2 kJ and a slope efficiency of 1.65% at a pump pulse of 0.66 msec duration. The difference in performance of the N-3 in comparison to the B-3 could only be caused by the difference in passive transmission of 71% and 84% respectively, since all other conditions were essentially the same for both devices. The 15% higher loss in the N-3 agrees quite well with the expected and observed change in threshold and slope efficiency.

The single-shot beamspread of the N-3 was measured to be 5.5 mrad at 10 kJ input and 123 J output energy. This single-shot beamspread is about twice as high as measured for the B-3, which might be caused by the many weak reflections within the N-3.

2. REPETITIVELY-PULSED OPERATION

The average output power and beamspread of the different lasers during repetitively-pulsed operation were measured with two calibrated photodiodes. The integration time constant of these photodetectors was chosen long in comparison to the output pulse duration of about 0.5 msec, but short in comparison to the pulse interval at a repetition rate of a few pps. This arrangement made it possible to record the energy per pulse on a recorder with a fast response time. The deflection on the recorder was found to be linear with output energy from the laser and was calibrated, using a ballistic thermopile. The beamspread was measured by focusing part of the output beam onto an aperture which transmitted about 50% of the beam energy after thermal equilibrium was reached.

Typical chart recorder traces for the B-2, the 3% Nd-doped 18 mm OD solid rod, and the N-3 are shown in Fig. 29, 30 and 31 respectively. Trace 29A shows the total output energy per pulse for the B-2. The output energy for the first pulse of

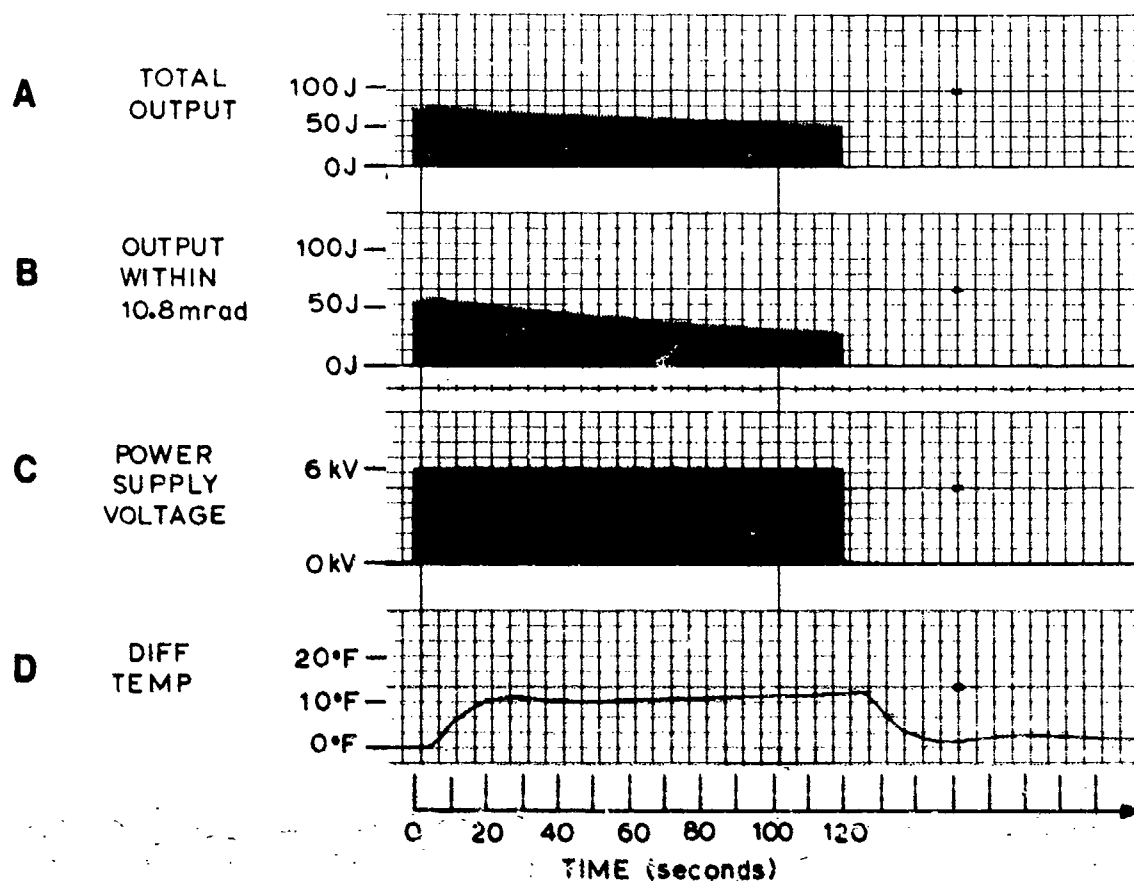


Fig. 29 Oscillator performance of the B-2 at 1 pps and 8 kJ input per pulse

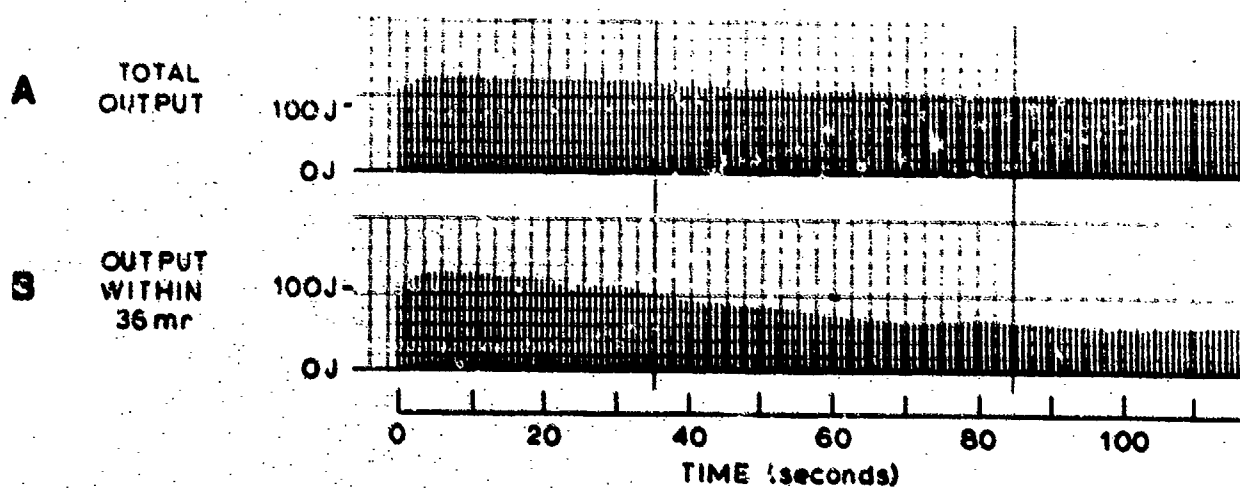


Fig. 30 Oscillator performance of the 3% Nd-doped 18 mm OD solid rod at 1.2 pps and 7 kJ input per pulse

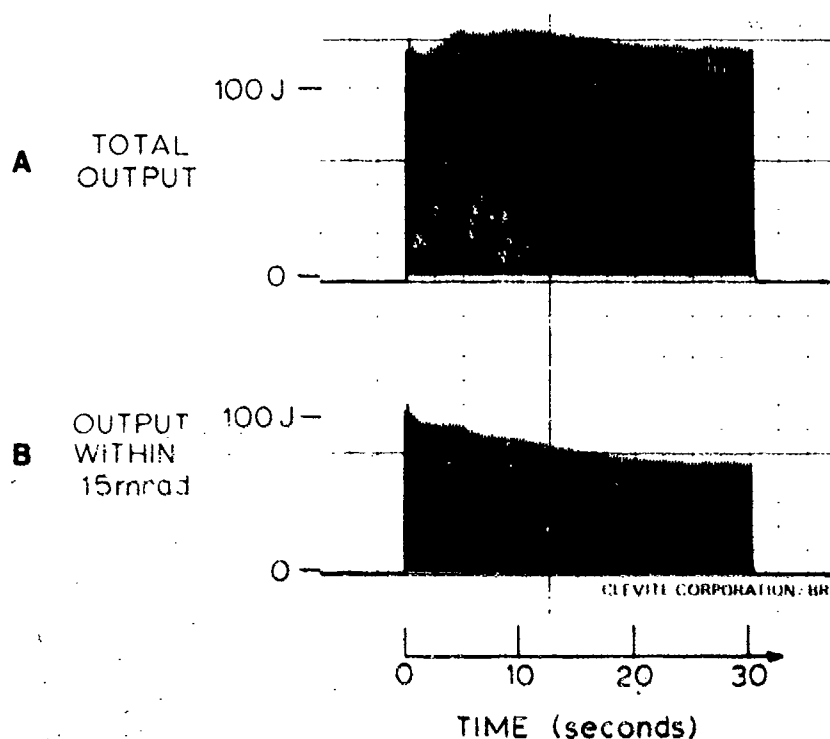


Fig. 31 Oscillator performance of the N-3 at 3.5 pps and 10kJ per pulse

70 J is low in comparison to the initial results taken with the B-2 due to solarization and contaminated disc surfaces, as already discussed in Section IV. Thermal equilibrium should be reached after about 19 seconds as indicated by the differential temperature (Trace D); however, the output continuously decreases due to the end windows moving in their holders, causing the cavity to misalign. This is evidenced by the 1 to 2 mrad of permanent mirror misalignment at the end of this series of measurements.

Trace 29B shows the amount of the output energy within an angle of 10.8 mrad, which was selected to show $\approx 50\%$ of the output energy at the end of the 2.0 min run. Initially, 78% of the total output energy is within the angle of acceptance of 10.8 mrad. For the first 20 seconds the beamspread is essentially constant but later, the beamspread becomes continuously greater as evidenced by a steeper slope of Trace B as compared to Trace A. This increase in beamspread is probably also caused by the steering of the beam due to window movement. Stabilizing the windows should

greatly reduce the observed increase in beamspread and loss in output energy.

Trace 29C shows the output voltage on the power supply capacitors of 5.94 kV which corresponds to 8.0 kJ input per pulse.

Trace 29D shows the differential temperature, which after reducing the data, indicates that about 15% of the flash-lamp pump input is dissipated into the water. This agrees with previous results obtained for the B-1 and N-1 as described in Ref. 13. The observed time required to reach thermal equilibrium of about 15 to 20 seconds agrees reasonably well with the estimates in Section III.2.

The radiance measurement for the 3% Nd-doped solid rod was taken with the rod mounted in a close-coupled fixture, which resulted in a slope-efficiency of 3.6% and a threshold of 1.9 kJ using an output reflectance of 17% and a pump-pulse of 0.9 msec duration. The maximum input energy per pulse was limited to 7 kJ to avoid damage to the output reflector above 170 J output. After repetitively-pulsed operation for an extended period of time, the output performance of the rod deteriorated from 170 J to 122 J per pulse. After the 8.4 kW run shown in Fig. 30, the rod had a permanent optical distortion of about -0.12 diopter, which along with solarization of the rod and the Supremex water jackets, caused the slope efficiency to drop off 30% to 2.5% with little change in threshold.

Trace 30A shows the total output energy, which increases for the first few pulses, but remains in general quite steady, while the radiance decreases during the first 60 seconds as evidenced by the loss in the angular-limited output signal in Trace 30B.

The performance of the N-3 at 35 kW average input power is shown in Fig. 31. The total output power remained essentially constant at about 120 J per pulse, while the radiance decreased during the first 20 seconds as shown in Trace 31A and B. At thermal equilibrium, about 60% of the total output energy of the N-3 was within 15 mrad, which corresponds to a beamspread of 18 mrad.

The results of these measurements of average output power, solid angle beamspread and average radiance are shown in Fig. 32, 33 and 34 respectively. The 3% Nd-doped solid rod provided the highest overall efficiency as expected, with a maximum of 150 W average output power. Since the solid angle beamspread

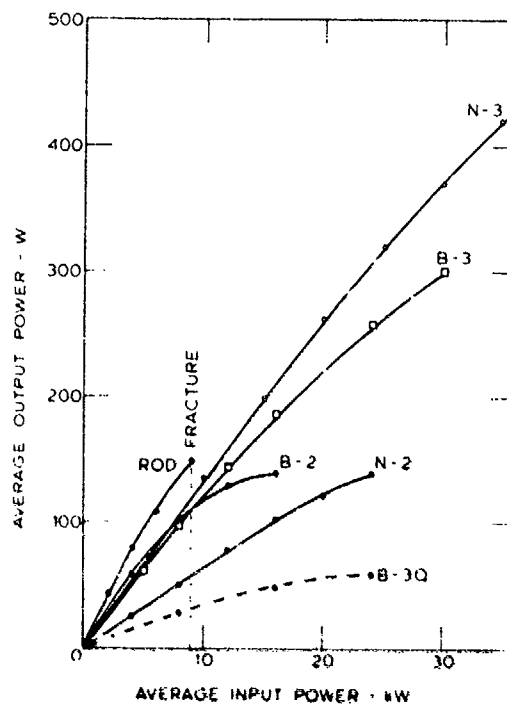


Fig. 32 Repetitively pulsed oscillator performance of the different disc lasers and the solid rod

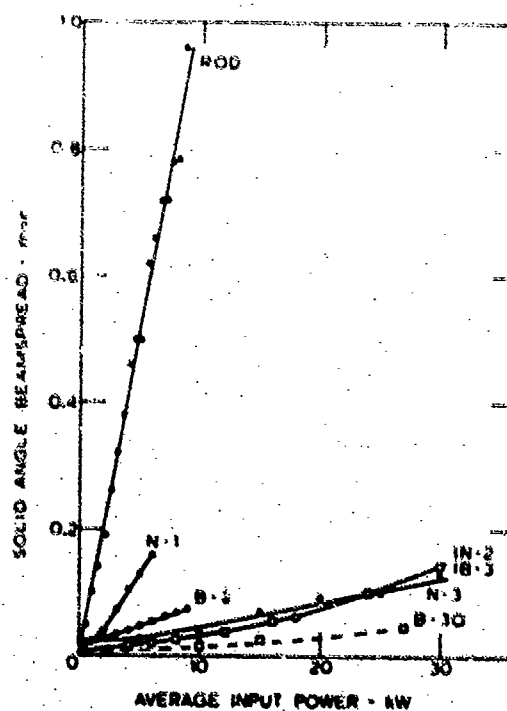


Fig. 33 Solid angle beamspread of the disc lasers and the solid rod during repetitively pulsed operation

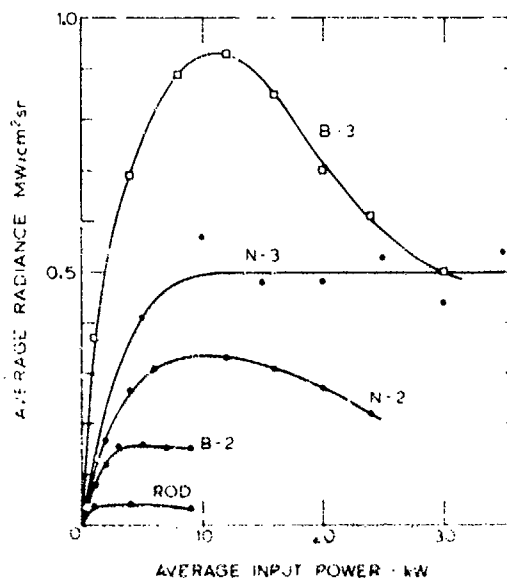


Fig. 34 Average output radiance for the disc lasers and the solid rod under normal mode operation

increased about linearly with input power at a rate of $105 \mu\text{sr/kW}$, the radiance of the 3% Nd rod was found to be about constant at $34 \text{ kW/cm}^2 \text{ sr}$. At 9 kW average input power, the 3% Nd rod fractured due to thermal stress. The maximum tensile stress on the surface of the rod was estimated with Eq. (5) at 18,000 psi, assuming 15% of the input power is absorbed in the rod.

By comparison, the 2% Nd-doped solid rod, evaluated previously, had a lower output radiance of $13 \text{ kW/cm}^2 \text{ sr}$, which was the result of about an equal increase in solid angle beam-spread with input power of $83 \mu\text{sr/kW}$; however, the output power was significantly lower due primarily to operation closer to threshold and a poorer pumping geometry. This rod fractured at 3.5 kW average input power, which corresponds to a maximum stress of 7,000 psi, and indicates the large variations of the tensile strength from the average value of about 12,000 psi for rough-sided laser rods.

The maximum output power measured for the 2% Nd-doped rod and the N-1 of about 17 W and 30 W respectively, is poor because a low input energy close to threshold was chosen, which reduced the overall efficiency and does not allow a fair comparison to all the other devices. For the N-1 an average radiance of

approximately $40 \text{ kW/cm}^2\text{-sr}$ was measured, which is about three times higher than for the 2% Nd-doped rod in the N-1 pump cavity.

At 6 kW average input power to the N-1, one disc fractured. From the calculation in Section III.3 a maximum tensile stress of about 3,000 psi was determined for an average power input of 2.2 kW. Since the calculations also showed a linear relationship between stress and thermal loading, a maximum tensile stress of about 8,000 psi was estimated for 6 kW input. This value is again within the variations for the tensile strength of laser glass.

The initial data taken with the B-2 resulted in a maximum output power of 140 W at 16 kW input power. Higher input powers did not increase the average output power, probably because of the imperfections of the initial design described in Section V.3. During the radiance measurements, the average output power at 9 kW was found to be only 56 W instead of the initial 104 W. This loss in output power was primarily due to solarization of the discs and coolant contaminations. Despite this loss in output power, the radiance of the B-2 was approximately constant at $170 \text{ kW/cm}^2\text{-sr}$, because of about an order of magnitude improvement in the solid-angle beamsread in comparison to that of the solid rods.

The overall efficiency of the N-2 was relatively poor because of the imperfect coatings. However, the beamsread did not increase appreciably with input power, which resulted in an average radiance of $300 \text{ MW/cm}^2\text{-sr}$ at 12 kW input.

For the B-3, the overall efficiency was about twice as high as for the N-2, while the beamsread of the B-3 and N-2 was essentially the same. With the beam cross-sectional area of the B-3 being 1.5 times smaller than for the N-2, because of the Brewster windows, about a 3 times higher radiance results. At 12 kW average input power with 8 kJ input and 97 J output per pulse, a beamsread of 6.9 mrad was measured which corresponds to an average radiance of $930 \text{ kW/cm}^2\text{-sr}$. At higher average input powers, the radiance falls off because the solid-angle beamsread increases faster than the average output power. At 30 kW average input, an output of 100 joules at 3 pps was obtained. The beamsread of the 300 W output beam was 13.5 mrad. In comparison, the solid rod fractured at 150 W average output power at a 27 times lower radiance.

The average output power and beamsread of the B-3 was also measured under repetitively Q-switched operation. The B-3 was operated at the 10 joule Q-switched output level up to 6 pps as shown in the dashed curve of Fig. 32. To maintain a constant

output level, the input energy was increased from 2.5 kJ single shot to 3.8 kJ at 6 pps. After several thousand shots, no damage other than the bulk damage in the crystal was observed. The beam-spread measured under Q-switched operation was found to be appreciably lower than for normal mode operation as shown in the dashed curve of Fig. 33. This reduction in beamspread could be caused by the lower input energy per pulse. With a new KD*P crystal, prelasing and after-pulsing were observed at 24 kW average input power. This is probably due to depolarization in the B-3, which does not provide sufficient polarization at high average input powers to prevent prelasing. To prevent after-pulsing, a pulse-forming network should be incorporated which provides a 0.5 μ sec square pulse to the Pockels cell instead of the voltage step applied. With these changes, and a more durable mirror, the full capability of the B-3 should be realized.

The overall efficiency of the N-3 remained essentially constant at 1.3 % up to 25 kW average input power. A maximum average output power of 420 W was measured with an input energy of 10 kJ per pulse and a repetition rate of 3.5 pps. The increase in solid-angle beamspread was measured to be about linear with average input power at a rate of 4.3 μ sr/kW, which is comparable with the results obtained for the N-2 and B-3. Since the average output power and the solid angle beamspread was found to be essentially linear with input power, the radiance of the N-3 was about constant from 5 to 35 kW input power with a value of 0.5 MW/cm²-sr.

SECTION VIII

CONCLUSIONS AND RECOMMENDATIONS

The average radiance of the disc lasers has been at least tripled every year during this program. The disc lasers have been developed to the point where efficiencies close to that of solid rods can be obtained, especially for amplifier applications. The devices operate reliably over many hundred thousand shots. Earlier problems such as uniform flashlamp pumping, mechanical stability, coolant contamination, solarization protection, disc holding technique, and uniform flow distribution have been solved. Simplicity in design allows relatively loose tolerances, ease in fabrication, assembly and maintenance.

From the data presented, a reasonably good understanding of the behavior of the disc laser was gained. The experimental results agreed well, in general, with our estimates and allowed us to predict the performance of disc and solid rod lasers for different geometries and laser materials.

Present limitations of the disc lasers are the thermal-optic distortions in the coolant and at the edges of the discs, losses due to depolarization or imperfect coatings for the Brewster or normal incidence approach respectively, as well as losses in pump light due to the opaque rails.

To reduce the thermal-optic distortions in the coolant, the D_2O should be cooled close to its freezing point, where the thermal index coefficient becomes negligibly small. In addition, a short disc laser with a high-gain material like YAG would greatly improve the flow rate and decrease the thermal-optic distortions in the coolant.

To reduce the edge effects, which presently reduce the useful aperture to about one half of the total pumped cross section, thinner or clad discs should be considered to provide a better radial-to-axial cooling ratio.

Thinner discs should also reduce the depolarization losses in Brewster disc lasers, while better monitoring of the coatings should provide a better transmission for the normal-incidence disc laser. Excellent coatings on YAG have been produced which match well with heavy water as coolant.

A short YAG disc laser would also allow use of rails made from transparent materials, which would also help to improve

the overall efficiency. Rails made of Fiberglass or other transparent or translucent materials should be investigated.

The average radiance capability of solid rods for CW or normal-mode operation can be increased by reducing the cross-sectional area of the rod, which is difficult for the disc approach. However, in the cases where a large cross-sectional area is required due to damage limitations at high normal mode or Q-switched output energies, the disc laser provides the ideal solution.

REFERENCES

1. M. Born and E. Wolf, "Principles of Optics," The Maxmillion Co., New York 1959, p. 180
2. F. Kreith, "Principles of Heat Transfer," Int. Textbook Co., Scranton, 1959, p. 44
3. S. Timoshenko and J. N. Goodier, "Theory of Elasticity," McGraw Hill Book Co., New York 1951, p. 410
4. S. E. Miller, Bell System Technical Journal 44, 1965, p. 2017
5. J. D. Foster and L. M. Osterink: JAP 41 (9) 1970, p. 3656;
W. Koechner: Applied Optics 9 (11) 1970, p. 2548;
I. J. Barton and D. W. Goodwin: J. Phys. D; Appl. Phys. 5, 1972, p. 228; D. Findlay and A. F. Fray: Opto Electronics 2, 1970, p. 51; G. A. Massey: IEEE QE-8(7) 1972, p. 669
6. M. Jakob, "Heat Transfer," J. Wiley and Sons, Inc., New York, 1949, Vol. I, p. 434 and p. 262
7. Perry's Chem. Eng. Handbook, 4th. Edition, McGraw Hill Book Co., New York, p. 5-30
8. H. Welling and C. J. Bickart: JOSA 56 (5) 1966, p. 611
9. F. W. Quelle, Appl. Opt. 5, 1966, p. 633
10. C. J. Koester, "Optical Inhomogeneities in Pumped Lasers," American Optical Corp., Contract No. Nonr 4875(00), Final Report, May 1967
11. W. F. Hagen, et al, "Research in Glass Laser System Technology," American Optical Corp., Contract No. DA-AH01-67-C-2343, Final Report, April 1969
12. H. S. Carslaw and J. C. Jaeger, "Conduction of Heat in Solids," Oxford University Press, London, 2nd Ed., 1959
13. W. F. Hagen, et al, "Segmented Glass Laser Investigation," Technical Report, AFAL-TR-69-363, Feb. 1970
14. L. W. Tilton and J. K. Taylor, "Refractive Index and Dispersion of Distilled Water for Visible Radiation, at Temperatures 0 to 60°C," Nat. Bur. Stand. J. Res., 20, 419-477 (1938).

REFERENCES

15. Fainberg and Miller, "Molar Refractivity in Fluorine Containing Perhalo Compounds," J. of Org. Chem. 30, 864, (1965)
16. W. F. Hagen, et al, "Segmented Nd Glass Laser," Technical Report, AFAL-TR-71-303, Feb. 1972

UNCLASSIFIED

Security Classification

DOCUMENT CONTROL DATA - R & D

(Security classification of title, body of abstract and indexing annotation must be entered when the overall report is classified)

1. ORIGINATING ACTIVITY (Corporate author) American Optical Corporation Laser Products Dept., Research Division Southbridge, MA 01550		2a. REPORT SECURITY CLASSIFICATION Unclassified	
		2b. GROUP N/A	
3. REPORT TITLE THERMAL-OPTIC DISTORTION-FREE SOLID LASER TECHNOLOGY			
4. DESCRIPTIVE NOTES (Type of report and inclusive dates) Final Report 70 Nov. 30 - 72 Sept. 30			
5. AUTHOR(S) (First name, middle initial, last name) Wilhem F. Hagen			
6. REPORT DATE July 1973		7a. TOTAL NO. OF PAGES 98	7b. NO. OF REFS 16
8a. CONTRACT OR GRANT NO. F33615-71-C-1137		9a. ORIGINATOR'S REPORT NUMBER(S) TR-617-F	
8b. PROJECT NO. 5237		9b. OTHER REPORT NO(S) (Any other numbers that may be assigned this report) AFAL-TR-73-111	
8c. Task No. 10			
10. DISTRIBUTION STATEMENT "Distribution is limited to U.S. Government agencies only by reason of inclusion of test and evaluation data; applied June 1973. Other requests for this document must be referred to AFAL/TEO, Wright Patterson AFB, Ohio 45433."			
11. SUPPLEMENTARY NOTES		12. SPONSORING MILITARY ACTIVITY Air Force Avionics Laboratory (TEO) Air Force Systems Command, USAF Wright-Patterson AFB, Ohio 45433	
13. ABSTRACT This report summarizes the design considerations and experimental results obtained from four different disc lasers. These devices were successfully operated as amplifiers and oscillators at high average powers. The results were compared with the performance of solid rods of both circular and rectangular cross section. The thermal lensing, which limits the performance of solid rods, especially under Q-switched operation, was essentially eliminated with the disc approach. With the disc amplifier, transmission and gain values very close to those of solid rods have been measured. The single pass distortions were reduced by over one order of magnitude, which corresponds to an improvement in amplifier radiance of about two orders of magnitude for the disc laser in comparison to an equivalent solid rod. For Q-switched pulses, an average output power of 110 W was obtained with the disc amplifier operating at 5 pps. With the disc laser operating as normal mode oscillator, an average output power of 420 W was measured with an improvement in average radiance by a factor of 27 over that of an equivalent solid rod at its fracture point. The performance of disc lasers is limited by thermal-optic distortions in the coolant and by depolarization losses observed in Brewster disc lasers. The depolarization losses can be avoided with the normal incidence disc approach. To reduce the thermal-optic distortions in the coolant requires careful design of the flow channels and a coolant with a low thermal index coefficient. Initial problems such as disc holding techniques, mechanical and chemical stability, uniform flashlamp pumping, coolant contamination, solarization protection and uniform flow distribution have been solved, providing reliable performance of the present devices over many hundred thousand shots.			

DD FORM 1473
1 NOV 66

UNCLASSIFIED

Security Classification

UNCLASSIFIED

Security Classification

14. KEY WORDS	LINK A		LINK B		LINK C	
	ROLE	WT	ROLE	WT	ROLE	WT
Lasers						
Disc Lasers						
Solid Lasers						
Glass Lasers						
Thermal-Optic Distortion						
Segmented Lasers						
Coolants, Laser						
Long-Pulse Lasers						
Q-switched Lasers						
High Power Lasers						

UNCLASSIFIED